AD-A202 738

Fracture Toughness Testing of a
Ceramic Matrix Composite at
Elevated Temperatures

THESIS

John H. Mol
Major, USAF

AFIT/GAE/AA/88D-26

DEPARTMENT OF THE AIR FORCE

AIR UNIVERSITY

AIR FORCE INSTITUTE OF TECHNOLOGY

Wright-Patterson Air Force Base, Ohio

89 1 17 180

AFIT/GAE/AA/88D-26

Fracture Toughness Testing of a
Ceramic Matrix Composite at
Elevated Temperatures

THESIS

John H. Mol
Major, USAF

AFIT/GAE/AA/88D-26

DTIC
SELECTED
1 7 JAN 1989
E

FRACTURE TOUGHNESS TESTING OF A

CERAMIC MATRIX COMPOSITE AT

ELEVATED TEMPERATURES

THESIS

Presented to the Faculty of the School of Engineering

of the Air Force Institute of Technology

Air University

In Partial Fulfillment of the

Requirements for the Degree of

Master of Science

John H. Mol, B.S.

Major, USAF

December 1988

Accession For	
NTIS GRA&I	☒
DTIC TAB	☐
Unannounced	☐
Justification	

By		
Distribution/		
Availability Codes		
Dist	Avail and/or Special	
A-1		

Approved for public release, distribution unlimited

Preface

The purpose of this study was to determine the Mode II fracture toughness of Corning 1723 Glass composite. This required the design and construction of a load fixture and technique for testing small ceramic composites at elevated temperatures. Any tests requiring three point or four point bend at temperatures less than 1300 degrees Fahrenheit should be able to make use of this load fixture and techniques.

Table of Contents

iv

List of Figures

List of Tables

AFIT/GAE/AA/88D-26

Abstact

The need for a load fixture and technique for determining the fracture toughness in fiber reinforced ceramic composites at elevated temperatures was identified. A technique for pre-cracking end notched flexure specimens of ceramic glass was developed to accommodate this need. Next, a three point bend load fixture capable of withstanding temperatures up to 1000 degrees Fahrenheit and providing accurate, repeatable results was designed and constructed. A test procedure for finding compliance and critical load at room and elevated temperatures was developed. Specimens were tested at varying crack lengths at room temperature, 600 degrees Fahrenheit, and 1000 degrees Fahrenheit. Second order, third order and truncated third order curve fits were fitted to the compliance data to determine the best compliance-crack length relationship (that which produced the narrowest band of fracture toughnesses) and compared with the results from a theoretical compliance-crack length relationship. The critical load for a given crack length was found by loading a specimen until its compliance changed. Finally, the Mode II critical strain energy release rate, or fracture toughness, was calculated at each temperature. The fracture toughness for room temperature was slightly higher than the

fracture toughness for 600° F. The fracture toughness for 1000° F was more than three times that for room temperature. Postmortem examination was done on specimens for each temperature. Specimens tested at 600° F had smoother Mode II fracture surfaces than the room temperature specimens indicating a more brittle fracture and supporting the experimental results. The specimens tested at 1000° F had a rougher Mode II fracture surface with fiber pull-out and small matrix fragments attached to the fibers, indicating a more ductile failure and therefore increasing the fracture toughness. A color change from black to dark gray and the presence of crystals on the Mode I fracture surface of the 1000° F specimens indicated a chemical change in the specimens. The apparent chemical change and significantly higher fracture toughness in the 1000° F specimens indicates that much more study is required of this material at elevated temperatures. Sample X-Y plotter results, load fixture drawings, and spread sheets for data reduction are included at the end of this report.

I. Introduction

Problem

"Improved methods of producing and processing tougher, cheaper ceramics have increased their potential aerospace applications, particularly in engines" (1). Because new technologies are pushing materials to their physical limits, fracture mechanics has become an integral part of the design process. The durability of a part or structure is often directly related to a material's resistance to crack initiation and growth. By accurately predicting crack growth behavior, the usable life of a component can also be predicted. This aids the engineer in selection of materials during design and maintenance scheduling once the material is part of an operating structure.

Griffith (2,3) provided the basic concepts of fracture mechanics in the 1920's and Irwin (4) and others followed on his work in the 1940's and 1950's. The early work was done with homogeneous isotropic materials, first with glass and then with metals (5). In recent years, composites have received an increasing amount of attention. Any analysis of composites is difficult due to their non-homogeneous and anisotropic nature (6).

With the high temperature requirement for new engines, new materials are needed. Researchers have sought to develop tough ceramics whose performance characteristics retain the best properties of their parent ceramics and have the additional quality of not being susceptible to fracture (7-10). The development of fiber

1

reinforced glass-ceramic matrix composites is one of the best examples in this direction.

Since the motivation for developing these ceramic composites is to utilize their improved toughness in structural applications, an accurate fracture toughness measurement technique is needed. There is a standard procedure recommended by the American Society for Testing and Materials (ASTM) for finding the fracture toughness for metals at room temperature (11). No such procedure exists for fiber reinforced ceramic composites.

According to Jenkins (12), "Fracture testing of structural ceramics is complicated by the lack of an accurate technique for measuring the small crack opening displacement. This is further complicated by the small crack sizes which are associated with specimens at failure". Furthermore, the composite specimens available for testing are small due to the limited availability of material. In addition, fracture testing at very high temperatures is required since these ceramic composites are being developed for high temperature applications.

With composites, fracture due to crack growth in shear sliding Mode II or Mixed Mode I and II is of a potentially greater significance. This is particularly true with unidirectional fiber reinforced composites. The composite fibers serve as obstructions to Mode I fractures perpendicular to the fiber direction. However, cracks oriented parallel to the fibers can propagate and fail catastrophically in Mode II. To model the Mode II fracture, a three point bend configuration is used. The end-notch flexure (ENF)

2

specimen has been successfully used to measure G_{IIc}, the critical strain energy release rate of interlaminar delamination growth in composites (13).

The flexure specimen is a beam with a crack located on the neutral plane at one end. The beam is subjected to three-point bending. Mall (14), used this type of beam when he investigated Mode II failure of composites using a finite element technique. Giare (15) measured Mode II fracture toughness using a clip gauge to measure relative displacement of a crack surface on a end-notch flexure specimen. He was able to apply Linear Elastic Fracture Mechanics (LEFM) to a unidirectional glass fiber reinforced composite material in Mode II. A good technique is still needed that can accurately predict Mode II fracture at a wide range of operating temperatures.

Objective

The objective of this study was to measure the compliance and critical load of a small glass-ceramic composite specimen at different temperatures up to 1000°F and varying crack lengths in order to find the effect of temperature on G_{IIc}, the Mode II fracture toughness.

Approach

This study involved several intermediate goals. First, it required the design, construction, and validation of a three point bend load fixture capable of withstanding 1000°F and giving accurate reliable results. It would measure the load, the midpoint displacements, and protect the instruments from excessive heat. Next, a technique to measure compliance and critical load in small

composite specimens was developed. Finally, the Mode II fracture of a unidirectional glass matrix composite was investigated, using the technique and hardware that was developed by using the end-notch flexure specimen.

The composite used was a 1723 Corning glass matrix with silicon carbon yarn as reinforcing fibers. This ceramic composite is currently being developed and studied by engineers at the Air Force Materials Laboratories. The results of this study provide an accurate experimental tool to perform fracture toughness testing of many structural composites under a shear loading condition at elevated temperatures.

II. Background

Griffith developed one of the basic theories of fracture mechanics in the early 1920's (2,3). Griffith used brittle glasses to derive equations for crack propagation. His equations were based on the idea of critical energy release rate. He stated that "crack propagation will occur if the energy released upon the crack growth is sufficient to provide all the energy that is required for crack growth (5)".

The field of fracture mechanics took on greater importance in the 1940's and 1950's with the increased use of high strength materials. Irwin (4) applied fracture mechanics to metals. He did extensive studies on the effects of stress on the crack tip and the crack tip plastic zone size. Broek (5) presents a good history of the basic problems and concepts of Linear Elastic Fracture Mechanics in his book. The bulk of these works, however, deal with homogeneous isotropic materials such as metals and simple glasses.

Composites are non-homogeneous and anisotropic in nature. This complicates any analysis of composite materials. The basic mechanics of composite materials are described by Jones (6). Many of the new composites are being developed for high temperature applications in today's engines.

One of the areas of study for these applications is tough ceramic composites. The toughening mechanisms for ceramic composites were described by Jelinek (16). Jelinek lists three methods of toughening ceramic composites: 1) increase the local

5

driving force necessary to propagate cracks to failure, 2) locally increase the mechanical energy consumed per unit area of propagation of any crack, or 3) decrease the local strain by cracking, which reduces the stress concentration. Jelinek also lists six ceramic matrix composite toughening concepts.

The Ceramic Bulletin (17) provided information on processing techniques for fiber-reinforced ceramic matrix composites. The article deals with properties and processing of several composites, but concentrates mainly on silicon carbide reinforced glasses and composites. The article discusses processing from the initial slurry, through hot pressing, and includes information on future needs and directions.

The Naval Research Laboratory has done work on refractory-ceramic fiber composites (18). The engineers at the Research Laboratory present the significant opportunities, problems, and possible solutions associated with ceramic fiber composites. Processing, mechanical properties, and limitations of the composites were all discussed.

Hasselman (19-21) did extensive work in ceramic composites. His works concentrated in the areas of thermal shock and thermal stress fracture and dealt with the use of non-continuous fibers. He stated that tailoring of material properties could be achieved to improve resistance to fracture initiation and resistance to crack propagation. This was achieved by adding substances to the matrix of a composite.

Kelly (22) used Hasselman's theories to study the influence of the addition of silicon carbide whiskers and zirconia on the material properties of a parent ceramic. Valentine (23) also followed some of Hasselman's techniques in the study of strength and thermal shock behavior of a ceramic composite. Valentine compared results based on varying compositions of a particulate and varying temperatures up to 1500°C. Both Kelly and Valentine characterized the microstructures of the composites that resulted from their experimentation.

One of the acknowledged experts in the area of glass-ceramic matrix composites is Dr. Karl Prewo. He has done extensive research at the United Technologies Research Center and he has published numerous articles on reinforced glass matrix composites and glass ceramic matrix composites (8-10, 24-32).

Prewo has completed a series of reports for the National Aeronautics and Space Administration of Research on Graphite Reinforced Glass Matrix Composites. In these reports, Prewo describes composite fabrication procedures, composite characterization procedures, and the results and discussion of those procedures.

Prewo described three point flexural strength, creep and fatigue tests for several glasses, including aluminasilicate glass composites. He found that the glass and glass-ceramic matrix composites to show great promise for high temperature applications. He did not, however, do any Mode II testing with end-notch flexure specimens.

Prewo did a range of tests and property studies at high temperatures up to about 1000°C. He noted, "The predominant mode of failure from room temperature to 600°C is local delamination of the composite along the fiber direction, indicative of a weak bond at the fiber matrix interface" (29).

Additional fabrication information was provided by Mr. Larry Zawada of AFWAL/MLLN (33). Mr. Zawada has been experimentally preparing small samples of the 1723 glass matrix composite. He has also been involved with mechanical property testing of this ceramic composite.

There are several sources which deal with fracture toughness testing. The American Society for Testing and Materials (ASTM) has several sources for metallic materials (11,34). ASTM also published guidelines for flexural tests of plastic and electrical insulating materials (35).

Kobayashi has detailed experimental techniques in fracture mechanics (36, 37). He describes compliance measurements, testing systems and instrumentation, mixed-mode stress intensity factors, laser interferometry, and many other fracture mechanics testing techniques.

According to Jones (6), the effect of a transverse shear may be more important for laminated composites than for isotropic materials. This view is strongly supported by Giare (15). Giare studied Mode II failure of reinforced composites. He used clip gauges to measure the crack mouth opening displacements versus load. These measurements led to the measurement of critical Mode

II stress intensity factor. Giare showed that the crack growth resistance curve is a material property and that linear elastic fracture mechanics applies well to unidirectional glass fiber reinforced composite materials in Mode II fracture.

Mall (14) applied a finite element analysis to an end-notch flexure specimen in Mode II. He investigated the effects of overhang on the Mode II strain energy release rate.

Once all the testing has been completed, the fractures must be examined and understood. Wiederhorn (38) investigated brittle fracture in ceramics. He stated that the fracture behavior of metals and ceramics were different. Fracture in ceramics was controlled by the microstructure on the crack tip. Lankford (39) completed a report on damage mechanisms in ceramic composites. Lankford tested glass-ceramic matrix composites reinforced with silicon carbide fiber. He tested unidirectional and multiaxial reinforced composites in compression. His damage characterization goes to the microscopic level. Marshall (40) studied failures during both tensile and flexural loading.

Vozzola (41) studied the fabrication of glass-ceramic matrix composites and then developed a test for Mode II fracture toughness. He used an ENF specimen in a three point bend fixture and a laser based interferometric technique to determine the instant of crack initiation. This was used to determine G_{IIc}.

This study applied Vozzola's technique to evaluate the same glass-ceramic matrix composite again at room temperature, and then at 600°F and 1000°F. It used the change in compliance instead of the

laser based interferometric technique to determine the instant of crack growth.

III. Test Setup and Validation

This study required the design and construction of a load fixture capable of withstanding temperatures up to 1000°F. This load fixture was then incorporated into a test setup that could utilize an Instron load machine, a linear variable differential transformer (LVDT), and four heat lamps. The basic ideas for the design came from Vozzola's setup (41) and conversations with Zawada (33). Drawings of some parts of the test setup, which required local fabrication, are included in Appendix E for future reference.

Design

The major constraint on the load fixture was that it must withstand temperatures up to 1000°F. This required that the structure either be able to withstand up to 1000°F and not be adversely affected, or it must be protected by insulation or cooling. Referring to Figure 1, the following discussion will explain the reasons for the design of each part of the load fixture.

Test Fixture

The heart of the load fixture was the three point bend fixture. This was made up of a base, top, and three rollers. Since the three point bend fixture would be in contact with the specimen, it would also reach the same temperature as the specimen. Therefore, the three point bend fixture parts were made of Inconel 718 which could withstand 1000°F. Holes were put in the base for pins which would
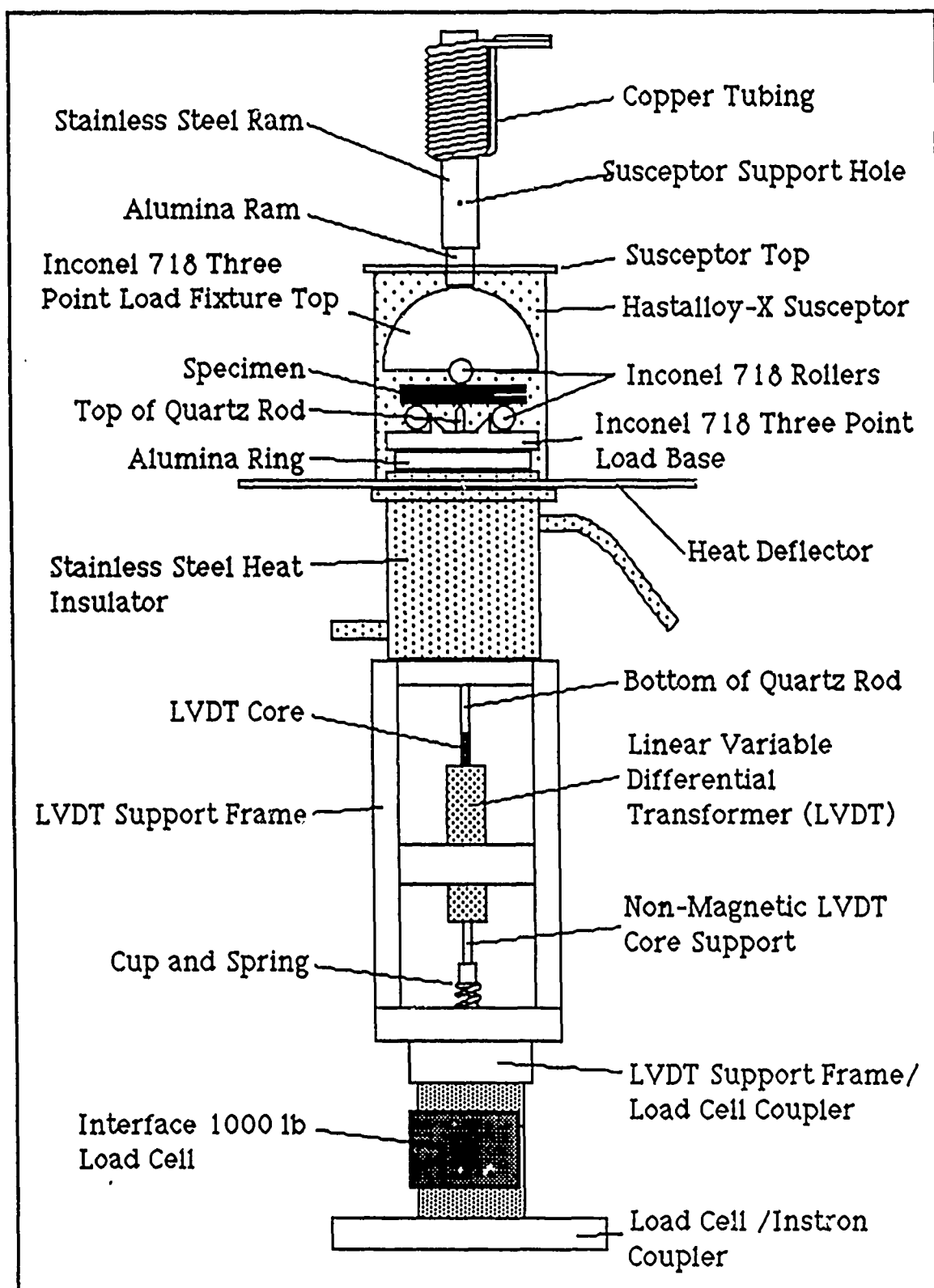
Figure 1. Load Fixture
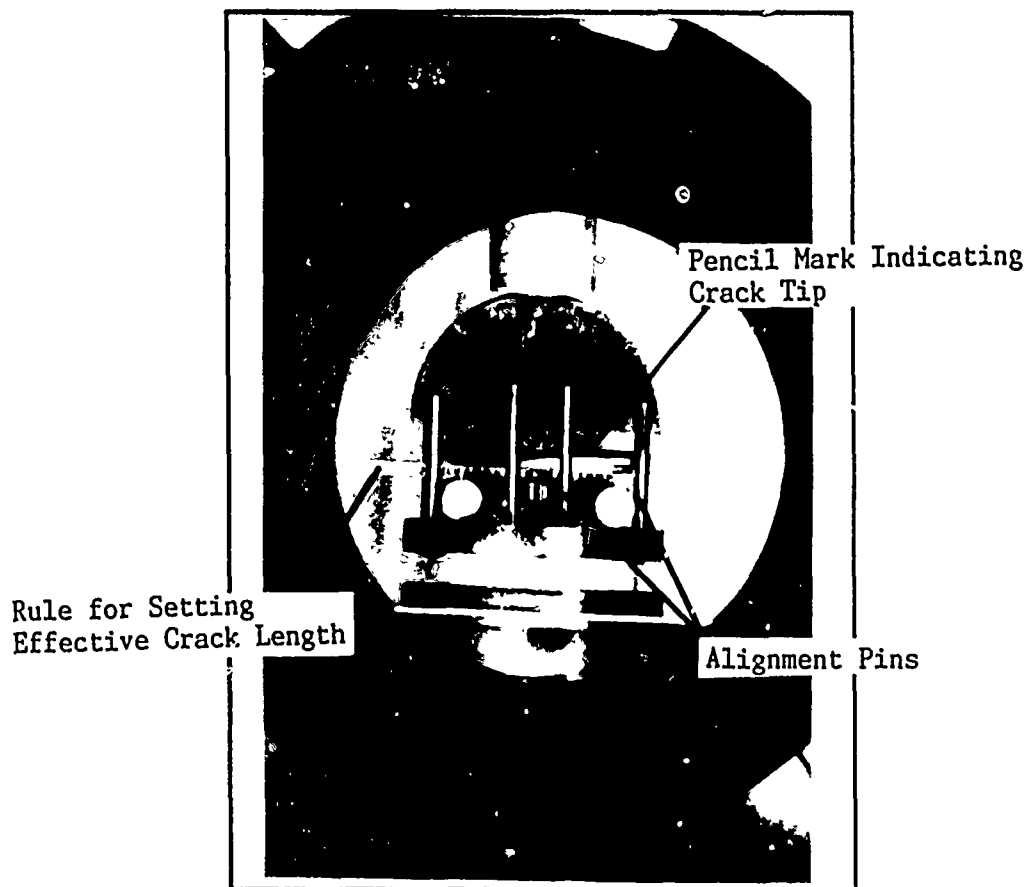
Figure 2.   Three Point Load Fixture with Alignment Pins Installed

hold the top in place during pre-loading (see Figure 2 and Appendix
E).   Since these pins would be removed before testing, they were
made from common steel rod.   The base design was modified from
Military Standard 1942 (MR) on Flexure Strength of High
Performance Ceramics at Ambient Temperature (42).   The base was
designed to set the span at the top of the rollers to L=1.5 inches
±0.001, and it allowed the rollers to move due to surface forces on
the specimen during loading.   The top was designed so that the
distance from the top surface to the bottom of the inserted roller was

the same (±0.001 inches) for slight angles from the perpendicular (see Figure 3). This would minimize any side forces that might occur from this misalignment.
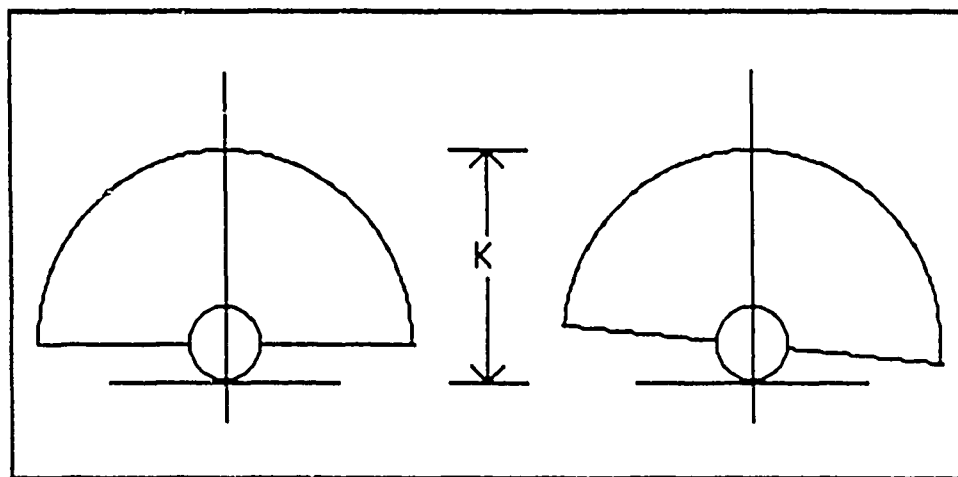
Figure 3. Three Point Bend Fixture Top Unaffected by
Slight Alignment Differences

Directly above the three point load fixture was the alumina and stainless steel ram. The alumina was chosen for its low thermal conductivity (0.070 cal/cm^2/cm/°C/sec) to prevent heat loss. The entire ram could have been made from the alumina, but a piece of the required size was not available; therefore, the alumina ram was extended with a stainless steel ram. The two were connected by a tight fitting sleeve drilled into the stainless steel. The stainless steel ram also had a small hole drilled through it at about half its length. A pin was put through the hole to support a susceptor when it was not in use. Finally, to protect the Instron from any heat carried through the rams, copper tubing was wrapped around the stainless steel ram and water circulated through it to carry away any conducted heat.

To keep the heat concentrated and even around the specimen, a susceptor was constructed from a rolled sheet of a super steel alloy, Hastalloy-X. This was of a cylindrical shape, enclosing the three point bend fixture and it functioned as a small oven around the specimen. It had a two- piece top that fit tightly around the alumina ram and the susceptor had a narrow notch near its bottom to allow room for the thermocouple wires to get inside.

Directly beneath the three point bend base there was a ring of alumina approximately 0.4 inches thick. This originally was not in the plan but was required because the heat insulator below it took away too much heat from the inside of the susceptor and the heat lamps were not able to heat the specimen to the desired temperature. The stainless steel heat insulator served several functions. Its most important function was to keep the heat even around the load fixture and protecting the LVDT below it from heat. It also supported the heat deflector which kept radiant heat from the lamps away from the LVDT. The stainless steel heat insulator was hollow except for a tube running from top to bottom through its center (see Appendix E). Water was run through the hollow portion from bottom to top to carry away heat and the tube allowed a quartz rod to reach the specimen from the LVDT.

A Robinson-Halpern 225A-300 LVDT was used to measure the midpoint displacement of the specimen. The input of the LVDT was an alternating current on its center coil. Two output coils picked up the magnetic coupling between themselves and the core. This output voltage was then calibrated to a known displacement as described in

Chapter 4. The top of the core was connected to a quartz rod. Quartz was chosen for its very low coefficient of thermal expansion (0.54 μin/in/°C) since it would be exposed to the same temperatures as the specimen and would affect the LVDT output if it changed length. The bottom of the core was connected to a wood support which in turn was held in place by a spring. The spring at the bottom of the LVDT support frame held the quartz rod so it always touched the midpoint of the specimen with a very low force (~0.5 lb). The LVDT was held in place by a support frame which, with the help of set screws, allowed the LVDT to slide up or down to put the LVDT core in the correct position and the frame transferred the load to the load cell below.

Test Setup

The test fixture was incorporated into an experimental setup, as shown in Figure 4. This consisted of an Instron TTD tension/compression tester, instrumentation for operating the LVDT, and a Microcon Digital Controller that operated the four heat lamps to heat the specimen. Figure 5. shows the equipment required to operate the LVDT. The output of the LVDT was fed into the X-axis of the X-Y plotter. The load cell was an Interface SM-1000. It measured the load that the Instron cross-head put on the specimen and its voltage output was plotted on the Y-axis of the X-Y plotter. Range and accuracy for the LVDT and load cell are shown in Table 1.
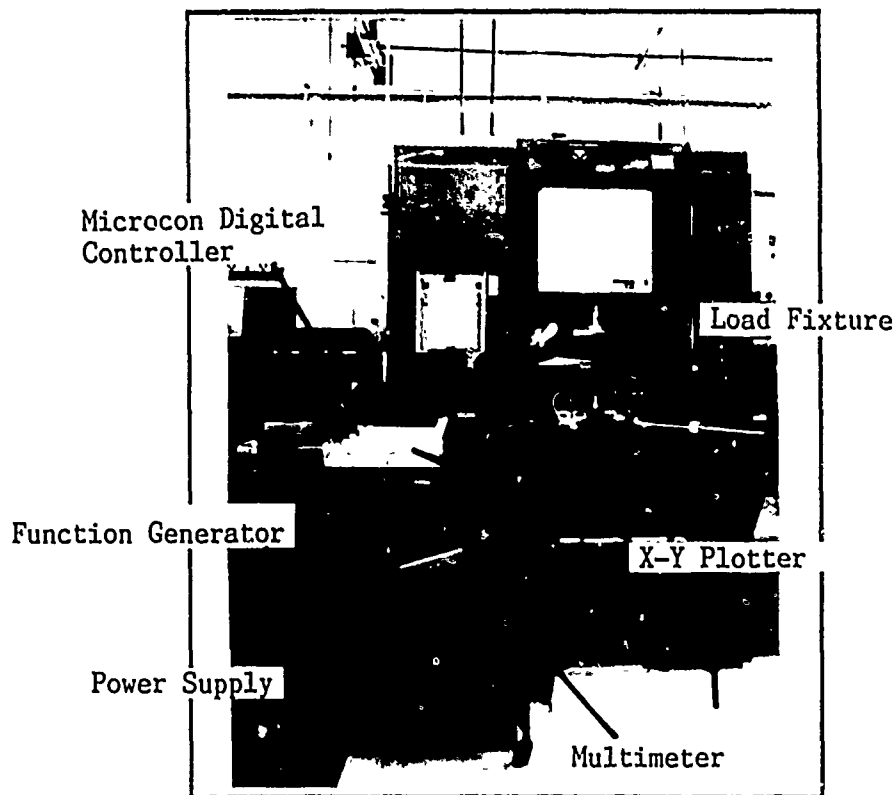
Figure 4.   Experimental Setup
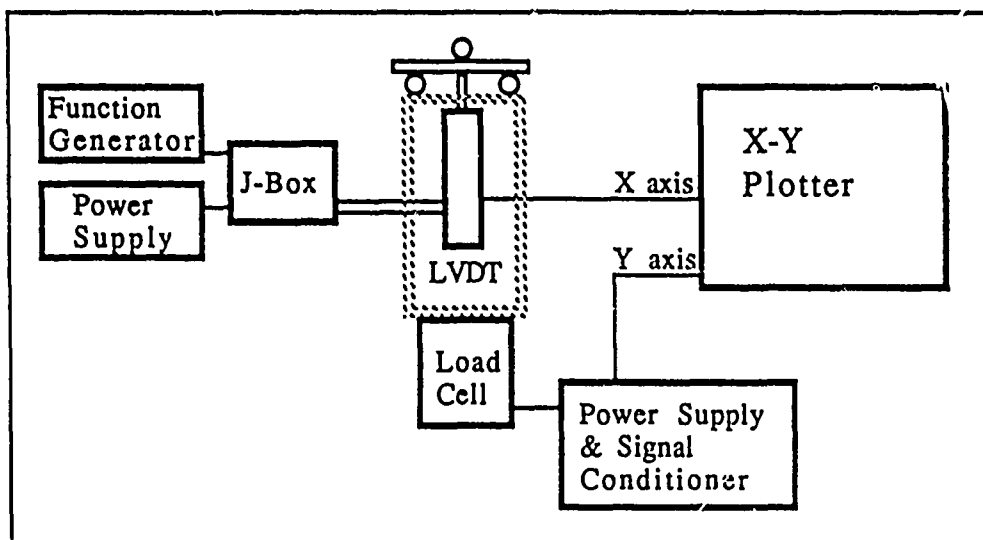
Figure 5.   LVDT and Load Cell Equipment Setup

To provide the heat for the specimen, a Microcon Digital Controller ran four power supplies to two line heaters and two variable strip heaters. Each heater had a thermocouple as feedback to the controller. The thermocouple controlling a particular lamp had to be the closest thermocouple to that lamp or else there would be feedback that would cause one lamp to run "hot" and another to run "cool", thus preventing the final desired temperature from being reached (see Figure 6).
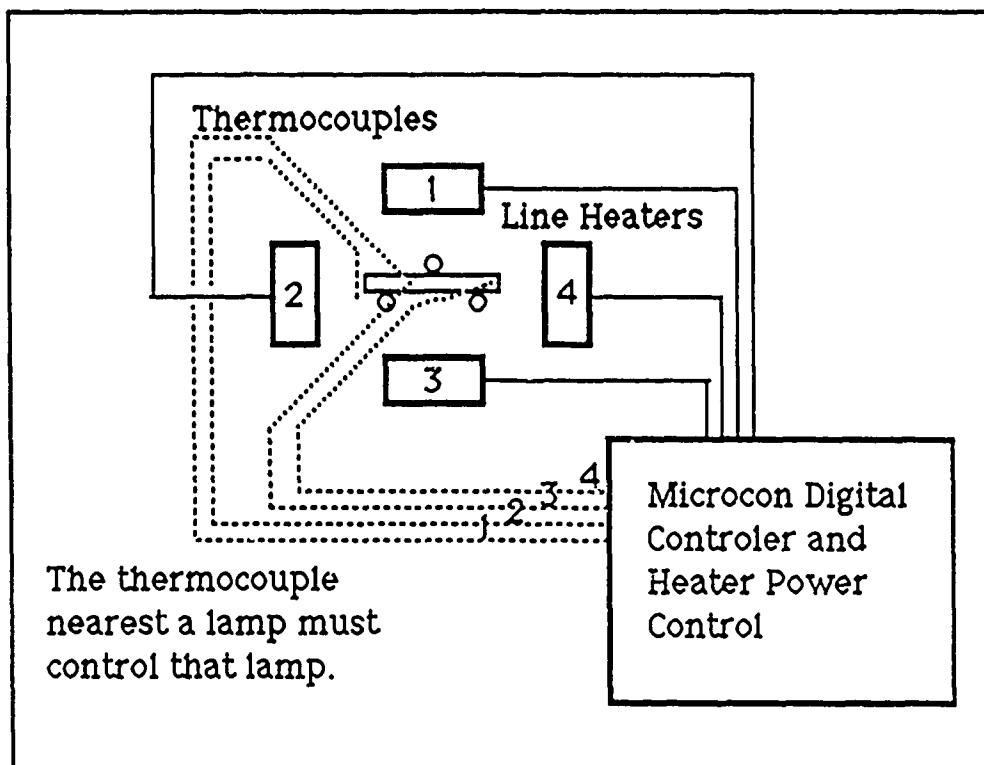
Figure 6. Microcon/Thermocouple Layout

Table 1

Equipment Listing

Unit/Model	Range	Accuracy
1. Robinson-Halpern 225A-300 Linear Variable Differential Transformer (LVDT)		
2. Power-Ten 3130A-2000 Power Supply		
3. Adjustable Amplifier/ Rectifier ("J-Box")	±0.3 in	±0.0002 in (calibrated)
4. Hewlett Packard 3312A Function Generator		
5. Instron TTD Tension/ Compression Tester		
6. Interface SM-1000 Load Cell	0-1000 lbs	±0.3 lbs
7. Endevco 4225 Power Supply and 4423 Signal Conditioner		
8. Hewlett Packard 3466A Digital Multimeter (DVM)	±20.0 volts	
9. Hewlett Packard 7045B X-Y Plotter	variable	
10. Research Inc. Microcon 823 Digital Controller		
11. Research Inc. Power Control Series 663 (4)		

Table I cont.

Equipment Listing

Unit/Model	Range	Accuracy
12. Research Inc. Model 5193 Line Heaters (2)		
13. Research Inc. Model 5305 Parabolic Strip Heaters (2)		
14. Mitutoyo Calibrating Micrometer	0.0-1.0 inch	±0.00005 inch

Validation

To validate the test setup, a three point bend specimen of known material properties was used to measure the compliance from the fabricated fixture and then compare it with the theoretical value. Aluminum 6061-T6 was used since its Young's Modulus was almost of the same order as that of the ceramic composite (41). This specimen was also of the same size as the ceramic composite. Its nominal dimensions were 0.3 inches high, 0.2 inches wide, and slightly longer than 1.5 inches. A simple strength of materials solution was assumed,

$$\delta = \frac{PL^3}{48EI} \tag{1}$$

where P is the applied load, L the distance between the bottom rollers, E Young's Modulus, I the moment of inertia, and δ the midpoint displacement. Several tests were run using the procedure in Chapter 4. The answer was consistently 20% short of the correct displacement. The simple strength of materials solution (i.e., Equation 1) ignores the shear affect. Adding this, in addition to the above components already defined, the deflection with shear effect included. is

$$\delta = \frac{PL^3}{48EI}\left(1 + \frac{12\alpha_S EI}{GAL^2}\right) \tag{2}$$

where α_S equals 1.5 for rectangular cross sections, G is the shear modulus, and A is the cross sectional area. When the shear term was used, the theoretical results were between 8 and 10% less than the experimental values. To provide a more accurate displacement, Dr. Torvik (43) suggested that the compliance of the load fixture be included by adding $\delta = P/K$ to Equation 2 as shown below.

$$\delta = P\left[\frac{L^3}{48EI}\left(1 + \frac{12\alpha_S EI}{GAL^2}\right) + \frac{1}{K}\right]$$ (3)

By adding K, the load fixture stiffness, to the displacement equation and running two tests, one with the specimen standing (depth 0.3 and width 0.2) and one with the specimen laying flat (depth 0.2 and width 0.3), there were two equations and two unknowns and K was found. This was good only if K was constant. To see if K was constant, a steel bar with an EI approximately 150 times that of the aluminum specimen was placed in the load fixture. The bar was assumed to be rigid so that any displacements measured during loading would be the displacement of the load fixture. The load fixture displaced non-linearly. Three runs were made with the output being plotted on the X-Y plotter. The average of these three runs was then plotted and a curve was fitted to it. This resulted in a second order polynomial with "Y" being the load and "X" the displacement. To find the displacement of the fixture for a given load, the polynomial was solved for "X" using MACSYMA on the AFIT csc computer. When this was included in Equation 3, the percent

error between the measured and the theoretical values was reduced to ±1%. The same procedure was followed for both 600°F and 1000°F to determine the stiffness of the test fixture for those temperatures. For all tests of the composite specimens, the appropriate amount of load fixture displacement for a given temperature at the corresponding load was then subtracted from the experimental displacements to determine the compliance of each specimen. One percent error was considered reasonable for the present investigation.

IV. Experimental Procedure

The following sections describe the procedure used in obtaining the data required for determining fracture toughness of an end notched flexure specimen made from a plate of 1723 Corning glass composite. The procedure will start with specimen preparation since small ceramic composites are sensitive to their manufacturing technique. Next, the pre-cracking will be explained, to include the design and use of a pre-cracking jig. How the specimens were placed in the load apparatus and what precautions were taken to prevent specimen/test fixture damage and to ensure consistent results will be explained. Then the process for acquiring room temperature compliance followed by the process for critical load will be described. Finally, any changes to the above procedures for testing specimens at elevated temperature will be listed.

Specimen Preparation

The end notched flexure specimens were cut from a plate of 1723 Corning glass matrix (see Table II) provided by and manufactured by AFWAL/MLLN. The fiber orientation of the silicon carbide yarn and lay up within the plate (88C10) was $[0]_{24}$. The specimens were cut from the plate as shown in Figure 7. The nominal dimensions of each specimen were 2.0 inches long, 0.3 inches high, and 0.2 inches thick, shown in Figure 8. There was a small ripple in the surface of the plate running its length, so the specimens were taken avoiding this area. A water cooled diamond wheel saw was used to manufacture the specimens. Specimens

88C1001 through 88C1004 were each notched on the end near the midplane. These specimens were later polished on the top and bottom using a 40 micron diamond wheel to put the notch closer to the midplane. Since tests had already been done before they were

TABLE II
Properties of Corning 1723 Glass

Constituents	Nominal Composition (% Wt.)
SiO_2	56.8
$B2O_3$	4.3
Al_2O_3	15.5
CaO	10.0
BaO	6.0
MgO	6.9
As_2O_3	0.5

Strain point	665°C	1229°F
Annealing point	710°C	1310°F
Softening point	908°C	1666°F
Working point	1168°C	2134°F
Melting point	1550°C	2822°F

polished, the newly sized specimens were designated 88C1001A, etc.
Specimens 88C1005 through 88C1008 and 88C1009 through
88C1012 were clamped together in sets and also notched and
polished simultaneously to make them more uniform. All end
notches were made from the same diamond wheel saw and were
approximately 0.1 inch long and 0.0015 inches wide. Finally, using a
micrometer, all specimens were measured both on the notched end
and the opposite end for height and thickness and the average of
each was used for all calculations.
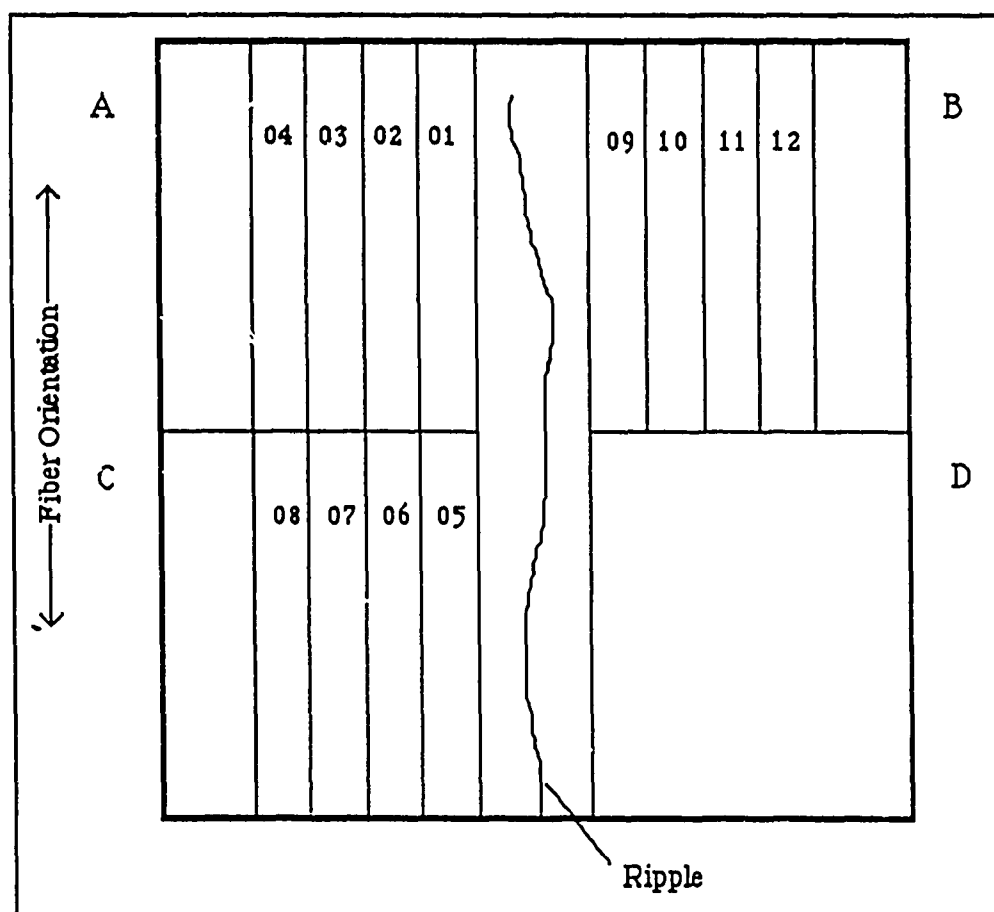
Figure 7. Specime. Location Within 1723 Corning Glass Plate 88C10
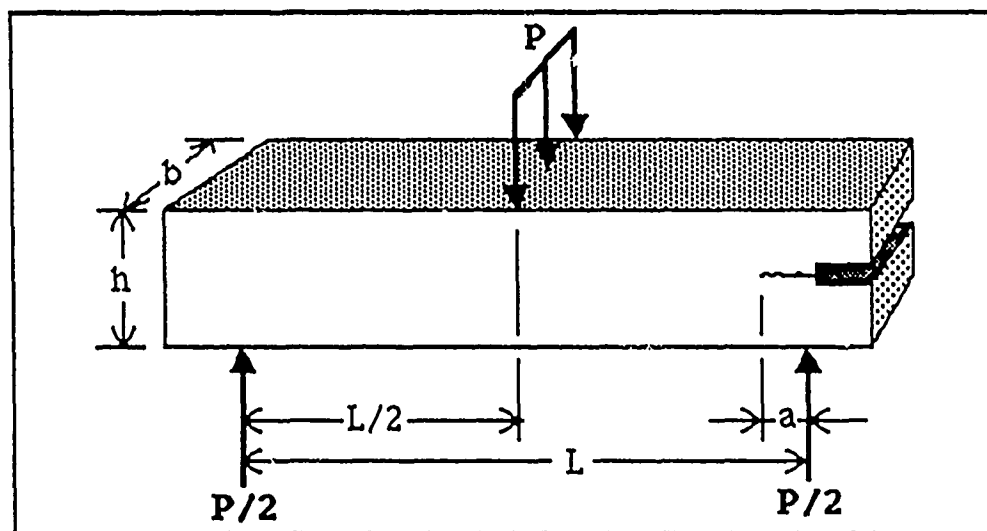
Figure 8. Specimen Dimensions

Pre-cracking

Pre-cracking of the specimen is necessary to provide a location for natural crack growth along the ...idplane. Much of the technique used in Vozzola's work (41) was used for this experiment. Each specimen was painted white on one side, designated the front, from the notch to the middle with typing correction fluid. This was done to make the crack more visible against the specimen's normally black surface. Next, a straight razor was used to saw a crack initiation point in the center of the notch. To help the arrest of crack growth, two flat pieces of Aluminum were clamped with a small C-clamp to either side of the specimen as in Figure 9 at the point of the desired pre-crack length. Pre-crack lengths varied from 0.0 inches to slightly over 0.6 inches. The pre-crack lengths were chosen so as to not have a roller within 0.1 inches of the end of a specimen and not to have a roller beneath the pre-crack notch. At this point, the procedure departs from Vozzola's procedure (41).
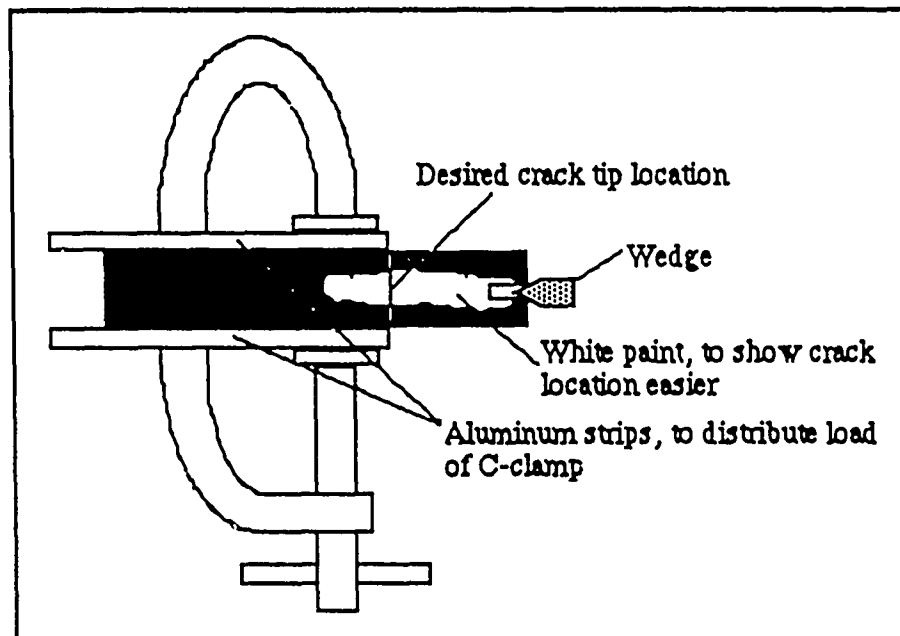
Figure 9. C-clamp for Arresting Crack Growth

Conversation with Vozzola (44), indicated that he had some difficulty applying a measured amount of force to a small wedge placed in the notch to cause the crack to grow. Because of this, a jig was constructed (see Figure 9) that could hold the specimen in a vise which in turn could be used to apply the necessary pressure to drive the wedge into the notch of the specimen. The jig and vise were
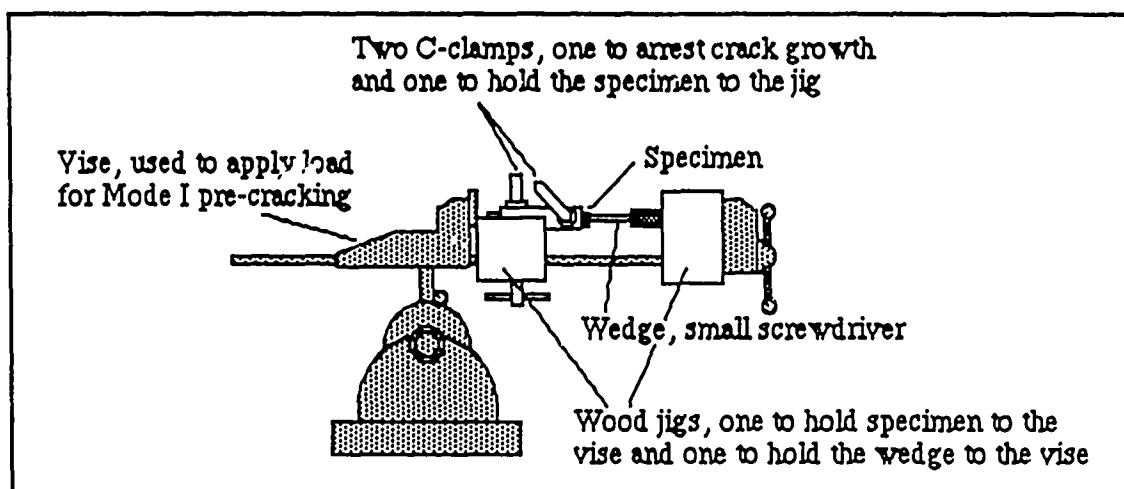
Figure 10. Pre-cracking Vise and Jigs

placed under a traveling microscope so the crack growth could be monitored. Once the crack was grown to the desired length, the crack tip was marked with a line from a pencil.

Loading Apparatus and Test Setup

To obtain consistent results throughout the experiment, the load and measuring apparatus had to be set the same way for each test. This included equipment warm-up, instrument settings, load cell preparation, and specimen placement.
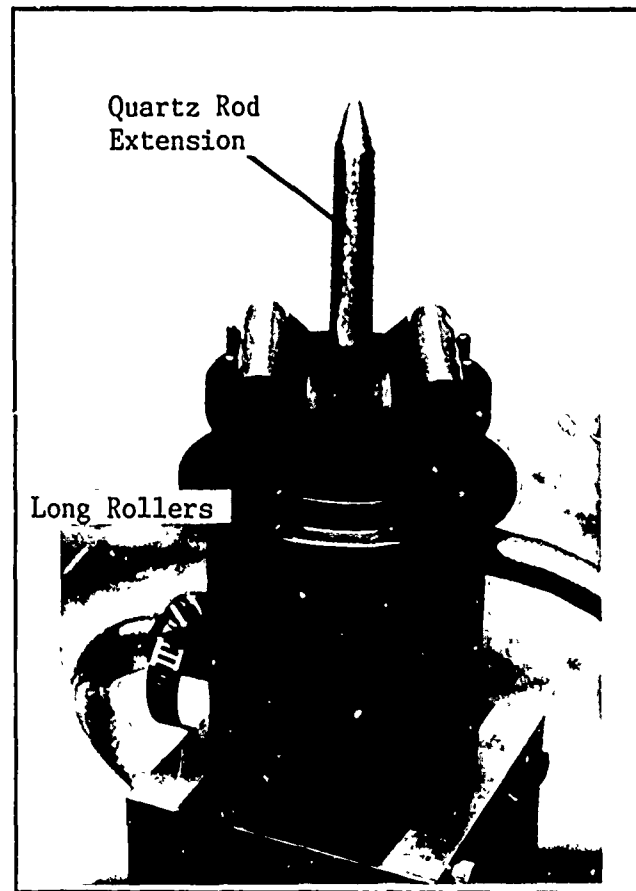
Figure 11. Three Point Bend Base Set for LVDT Calibration

All electrical equipment was allowed to warm up for half an hour. In this time LVDT and load cell readings stabilized. Once stabilized, the LVDT would be calibrated. The LVDT calibration involved putting short pins in the three point bend base and long rollers. This provided the most stable base for the Mitutoyo Calibrating Micrometer (see Figure 11). A rigid flat bar was placed on the fixture to obtain a no displacement reading. If the LVDT read too high or low, greater than ±250 mv, it was reset to near zero millivolts. The micrometer's design required an extension to the end of the LVDT's quartz rod (see Figure 12). With the extension in place,
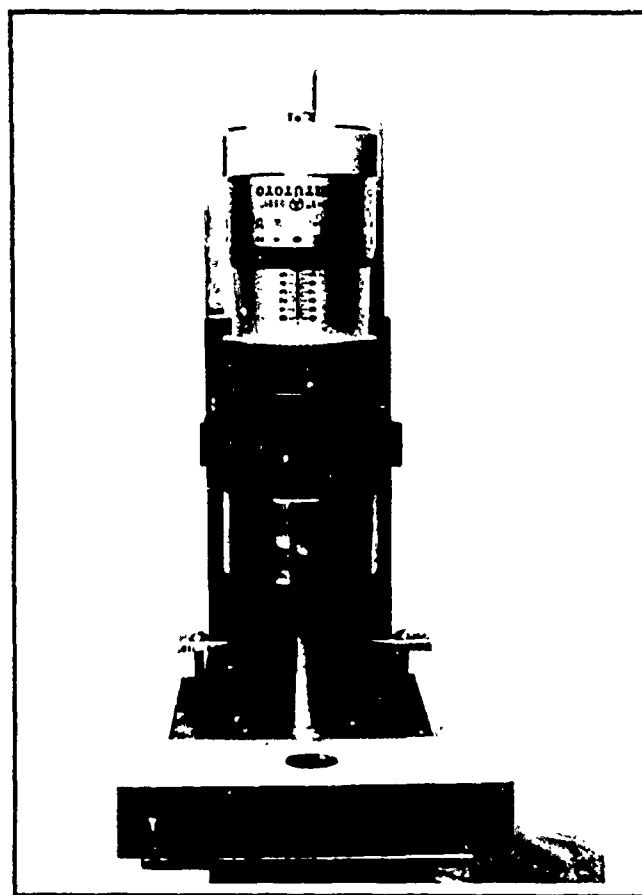
Figure 12. LVDT Calibration Setup

the micrometer was set to have a reading equal to that of the flat bar. From this point, a reading was taken every 0.0005" for a total of 0.0075". This amount exceeded the displacement during any test. The readings from the calibration were then plotted and fitted with a straight line (see Appendix A). The slope of the straight line fit represented the millivolt output per inch of the LVDT. Due to small drift in the LVDT output and early reservations of the LVDT's consistency, the LVDT was again calibrated at the end of testing for each day. With the local time of each calibration recorded, the LVDT output was interpolated for each test as shown in the spread sheets for compliance and critical load (see Appendix B).

In accordance with standard practice, the load cell was operated three times before testing started for the day. The amount of load used during the load cell warm-up exceeded the amount expected during any tests for the day.

The small size of the specimens made placement in the load fixture critical for consistent test results. First, long pins were placed in the base of the three point bend fixture. These would hold the bottom rollers in place while setting up the specimen and hold the top of the three point bend fixture directly in the center during pre-loading. Having placed the prepared specimen on the bottom rollers, a thin ruler graduated in 10ths of inches was placed in front of the specimen to allow the setting of an effective crack length. The ruler was also used, laid flat, to check that the specimen was perpendicular to the rollers. Next, after placing the three point bend fixture top on the specimen, a pre-load of approximately 10 lbs was applied (see

Figure 13). With the pre-load on the specimen, it was still possible to move the specimen side to side to obtain the desired effective crack length. Having placed the specimen in the desired position, the pins were removed to allow the rollers to move if necessary. The LVDT rod was flicked several times to ensure it was free to move, it rested against the specimen, and it assumed a neutral (no rotation) position. All tests for compliance and critical load started from this position with a few modifications made for testing at elevated temperatures that will be discussed later.
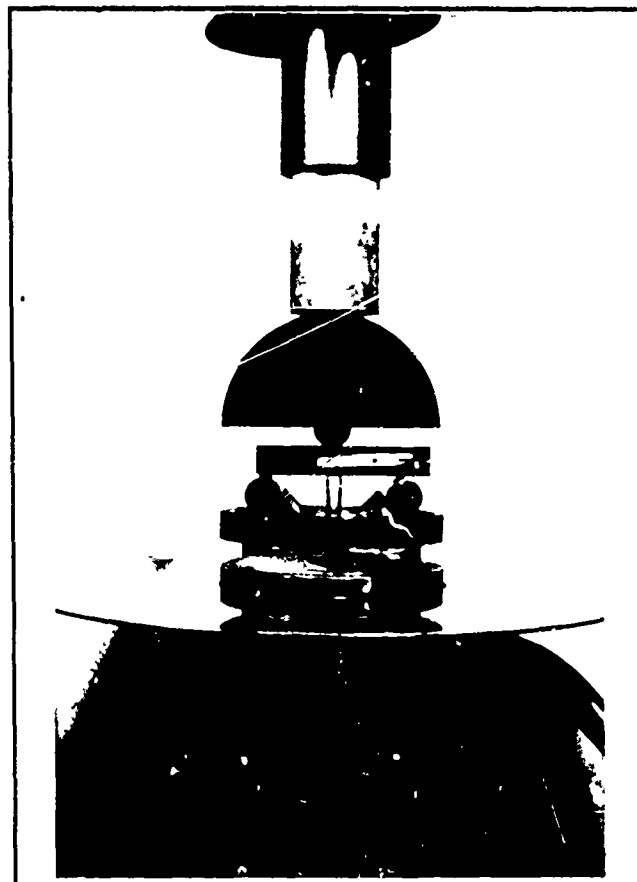
Figure 13. Specimen in Three Point Bend Fixture

Compliance Measurement at Room Temperature

Each specimen was tested at the desired crack length in four positions at room temperature for compliance. The specimen was rotated first right to left, then front to back, and finally left to right (see Figure 14). This was done to account for any differences in compliance due to the position of the crack in relation to the midplane and for any asymmetry in the load fixture. The average of the four runs was used as the compliance for that particular crack length. Using the critical loads found in Vozzola's work as a guide (41), each specimen was loaded to between 50 and 75 percent of its critical load. A loading rate of 0.005 inches per minute gave a smooth plot at a manageable speed. The X-Y plotter recorded the load versus displacement. Once the tests were run, a straight edge
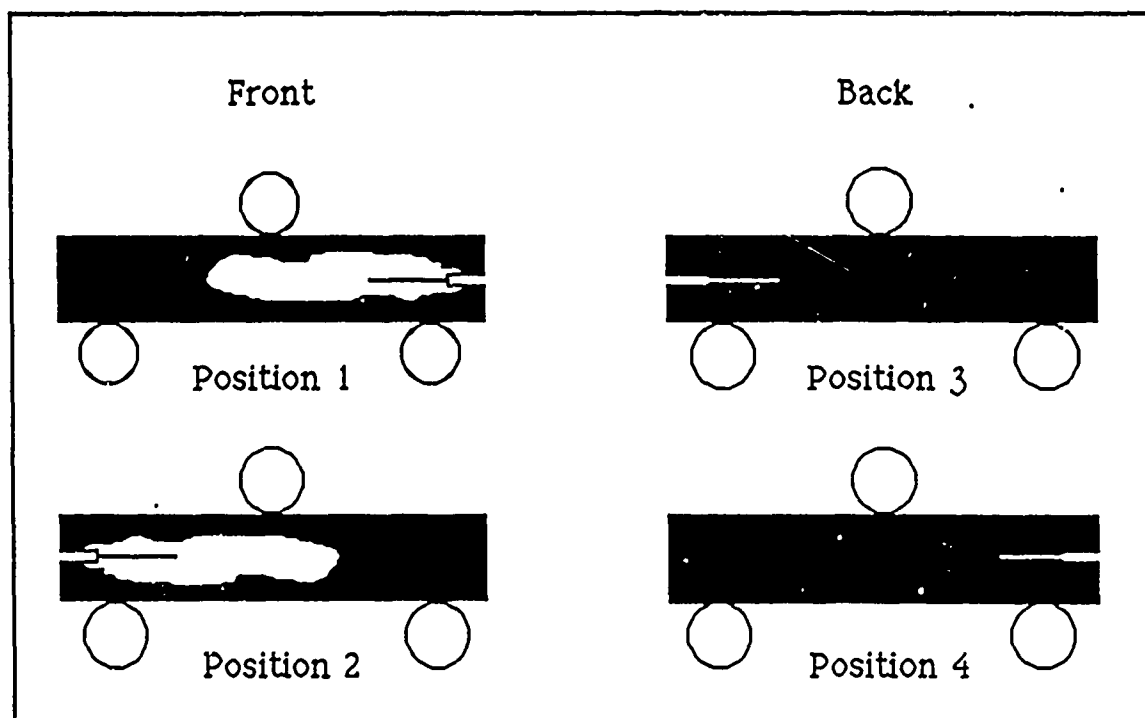
Figure 14. Specimen Positions for Room Temperature Compliance

was fit to the later portion of the load versus displacement curve to obtain the compliance. The beginning of the curve was nonlinear due to reasons discussed in Chapter 3 and therefore not used. This procedure was repeated for crack lengths between 0.0 and 0.6 inches. Because the critical load was not reached in these tests, the specimen could be moved left or right in the three point load fixture and used for measuring the compliance of a new crack length. If the pre-crack length permitted, overlapping tests were done with two different specimens. This would show if one particular specimen was overly sensitive to load.

Critical Load Measurement at Room Temperature

The critical load was found for crack lengths from 0.3 to 0.6 inches because there was a limited number of specimens to test and the compliance curve was well behaved in this range. Specimens were modified by inserting a 0.002 inch thick Nichrome shim just inside the pre-crack to reduce fiber locking which will be discussed later in Chapter 5. To get the shim into the specimen it was necessary to put the specimen into the pre-cracking jig and opening the pre-crack up. While in the jig, the pre-crack length was remeasured and marked.

Again using the results of Vozzola's work as a guide, the X-Y plotter's scale was adjusted to allow for greater loads and displacements. The X-Y plotter's pen was set at the position corresponding to the pre-load's voltage output. To give an early indication if the test was being done properly, a point on the curve

from a previous compliance test for the specific crack length was translated to the new X-Y plotter scale and plotted. The Instron load machine was allowed to load the specimen until the load-displacement curve began to flatten out indicating the critical load had been reached and the crack had grown.

Testing at Elevated Temperatures

By increasing the temperature of the specimen, the test procedure difficulties are also increased. During the 600°F tests, two heat lamps were used. These lamps were controlled by the thermocouples that were glued to the specimen's front and back. The thermocouples were placed far enough to one side to avoid inhibiting crack growth during the critical load testing.
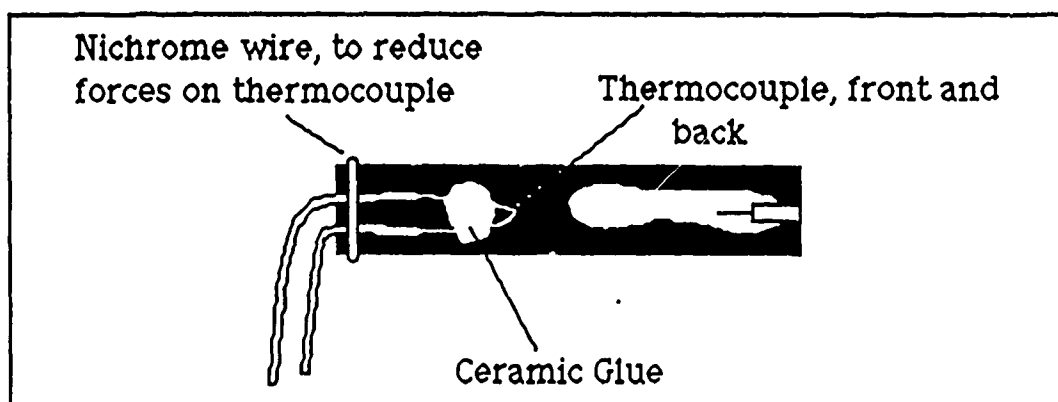
Figure 15. Thermocouple on Specimen

The specimens had a non-porous surface which did not allow for a sufficiently strong bond of the glue. To help alleviate some of the forces on the glue, a small Nichrome wire was wrapped around the thermocouples on the end of the specimen (see Figure 15). Two

additional thermocouples were used to monitor temperatures in the susceptor for 600° F tests. One thermocouple was placed in the pre-crack notch and the other was positioned just under the specimen at the opposite end from the notch as shown in Figure 16. For the tests at 1000°F, four lamps were used and all thermocouples controlled lamps. To even the temperature of the specimen, all tests were run with the specimen enclosed in a susceptor.
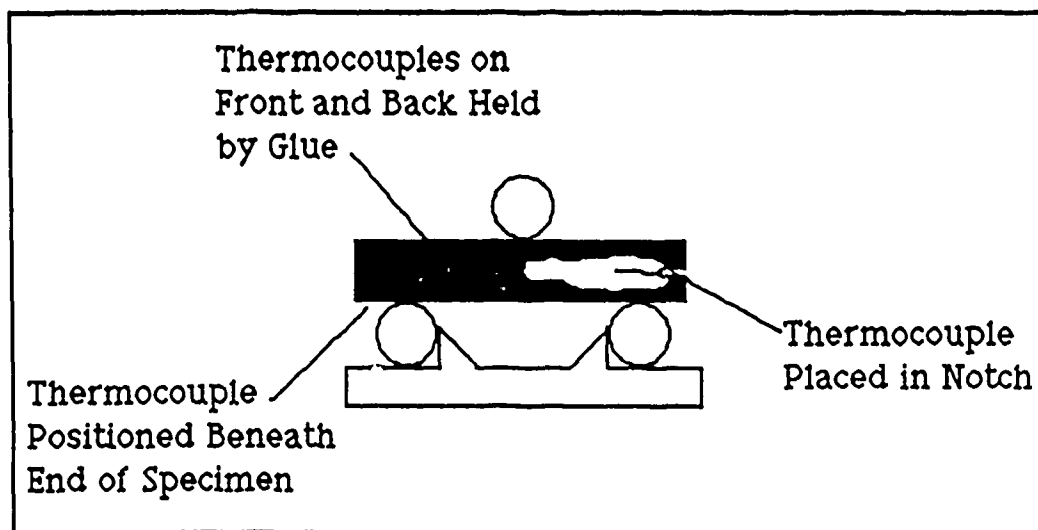
Figure 16. Thermocouple Positions

Despite several design considerations for thermal expansion of the load fixture, it was still necessary to unload the specimen during heat soaking. Starting with a pre-load of 20 mv (12.42 lbs) the lamps were turned on. The lamps were programed, using the Microcon controller, to reach 600°F and 1000°F in 6 and 12 minutes respectively. This allowed the lamps to gradually build up, preventing overloads and lamp burn out, and it provided time to unload the Instron to keep between 20 and 40 mv pre-load on the specimen. It was possible to keep the pre-load within limits using

the lowest cross-head speed of 0.002 in/min. Once the thermocouples reached the desired temperature, the specimens were heat soaked for 20 minutes. During the first compliance tests at 600°F and 1000°F, the compliances were tested after 20 minutes and later after 50 minutes of heat soaking. There was less than 4% difference in compliance between the two different times for each temperature (see Appendix C). Therefore, 20 minutes was used as the standard heat soaking time.

V. Results and Discussion

In order to determine the fracture toughness of a material, it was necessary to first find the compliance for a range of crack lengths to determine a compliance-crack length relationship. Next, the critical load for a particular crack length was needed. These data would be required for room temperature, 600° F and 1000° F for this study. Once found, the data would be used to calculate experimental values for fracture toughness for each temperature and compare them with theoretical values, thereby indicating the affects of elevated temperatures on a ceramic glass matrix composite fracture toughness.

Compliance

Four ENF specimens were tested at each temperature to determine a compliance-crack length relationship. Each specimen was used for several crack lengths by sliding the specimen right or left on the two lower support rollers changing the amount of overhang, thus varying the effective crack length. The compliance was calculated using the following equation below,

$$C = \frac{\delta}{P} \tag{4}$$

where C was the compliance, δ the midpoint displacement, and P the load. The midpoint displacement was modified by subtracting the

displacement of the load fixture for the particular load as mentioned earlier in Chapter 3.

Since the specimens varied in height and width (see Table 3), the compliances found were normalized to the nominal dimensions by modifying the experimental compliance as in Equation 5. The first four specimens were

$$C_{Normalized} = C_{Experimental}\left(\frac{b}{0.2}\right)\left(\frac{h}{0.3}\right)^3 \tag{5}$$

resized after testing had begun to make the specimen dimensions more uniform. The modified specimens are indicated by an "A" following their designator. The crack lengths were non-dimensionalized by dividing with the half span length (0.75 inches).

Table III. Specimen Dimensions

Specimen Number	Length (±0.016 inches)	Average Height (±0.0005 inches)	Average Thickness (±0.0005 inches)
88C1001	1.922	0.3078	0.1828
88C1002	1.922	0.3012	0.1885
88C1003	1.922	0.3096	0.1920
88C1004	1.922	0.3156	0.1958
88C1001A	1.922	0.2978	0.1828
88C1002A	1.922	0.2954	0.1885
88C1003A	1.922	0.2974	0.1920
88C1004A	1.922	0.2990	0.1958
88C1005	1.984	0.2610	0.1812
88C1006	1.984	0.2628	0.1872
88C1007	1.969	0.2636	0.1906
88C1008	2.000	0.2633	0.1938
88C1009	1.984	0.2820	0.1723
88C1010	1.984	0.2992	0.1763
88C1011	1.984	0.3004	0.1776
88C1012	2.000	0.2994	0.1774

Following the procedure for determining compliance, 32 tests were run at room temperature (see Table IV). Each specimen was tested four times for a particular crack length, once in each of the positions discussed

earlier. This was assumed necessary to account for the crack not being on the neutral axis and any load fixture alignment errors. The average of the four tests for that particular crack length was taken as the compliance . Appendix C shows a sample of the results of the X-Y plotter and Appendix B shows a sample of how the data was reduced using a spreadsheet.

As mentioned in Chapter 2, ENF specimens have been used extensively to determine fracture toughness of laminated polymer based composites. Russell (13) developed a theoretical relationship for compliance of this specimen as given below.

$$C = \frac{1 + 1.5\left(\frac{2a}{L}\right)^3}{4E_{11}b\left(\frac{h}{L}\right)^3} \qquad (6)$$

This analytical relationship was developed using simple linear beam theory. To calculate theoretical compliances using Russell's equation, a value for Young's Modulus, E_{11}, was needed. By solving Russell's equation for E_{11} and using the average value of no crack compliance found experimentally to be 9.4E-06 in/lbs (see Figure 17), E_{11} was calculated to be 1.6622E+07 lbs/in^2. This is within 12% of the average experimental E_{11} value, 1.878E+07 lbs/in^2, found in tensile

tests by Zawada (33). Once E_{11} was found, compliances could be found for different crack lengths from Equation 6.

Figures 17, 18, and 19 show the average compliance for a given crack length at room temperature compared with theoretical values for compliance. Figure 17 has a second order polynomial curve fit to the experimental compliances and Figure 18 has a third order polynomial curve fit. Figure 19 uses a straight line fit with compliance versus $(2a/L)^3$ as used by Chai and Mall (45). This gives a modified cubic curve fit that is more similar to Russell's theoretical equation. All of the curves fit relatively well (R, the sum of the squares of the residuals equal to 0.99 in all cases) with the experimental values for compliance, but deviate from the theoretical values for non-dimensionalized crack lengths greater than 0.5. For a non-dimensional crack length of 0.8 there was a 22% difference between experimental and theoretical compliance. The difference between the experimental and theoretical compliances could have been caused by the small specimen size or the limits of simple linear beam theory. A more accurate theoretical model needs to be found for use with small composite specimens. All three curve fits for the experimental values of compliance were used in this study.

Table IV. Experimental Compliance at Room Temperature

Run		Specimen	Position	Crack Length (in)	Experimental Compliance (in/lbs)	Average Compliance (in/lbs)
1	Sep/1255	88C1004A	1	0.0	8.44E-06	
1	Sep/1300	88C1004A	2	0.0	8.22E-06	
1	Sep/1307	88C1004A	3	0.0	1.17E-05	
1	Sep/1316	88C1004A	4	0.0	1.03E-05	9.68E-06
1	Sep/1355	88C1001A	1	0.075	9.20E-06	
1	Sep/1343	88C1001A	2	0.075	9.42E-06	
1	Sep/1358	88C1001A	3	0.075	9.27E-06	
1	Sep/1410	88C1001A	4	0.075	9.12E-06	9.26E-06
1	Sep/1518	88C1003A	1	0.225	9.79E-06	
1	Sep/1527	88C1003A	2	0.225	1.10E-05	
1	Sep/1536	88C1003A	3	0.225	8.18E-06	
1	Sep/1544	88C1003A	4	0.225	8.98E-06	9.48E-06
1	Sep/1420	88C1001A	1	0.3	1.01E-05	
1	Sep/1428	88C1001A	2	0.3	1.10E-05	
1	Sep/1436	88C1001A	3	0.3	9.44E-06	
1	Sep/1448	88C1001A	4	0.3	1.01E-05	1.02E-05
1	Sep/1552	88C1003A	1	0.375	1.04E-05	
1	Sep/1600	88C1003A	2	0.375	1.05E-05	
1	Sep/1609	88C1003A	3	0.375	9.30E-06	
1	Sep/1619	88C1003A	4	0.375	9.87E-06	1.00E-05
1	Sep/1718	88C1002A	1	0.45	1.09E-05	
1	Sep/1726	88C1002A	2	0.45	1.17E-05	
1	Sep/1736	88C1002A	3	0.45	9.66E-06	
1	Sep/1748	88C1002A	4	0.45	1.06E-05	1.07E-05
1	Sep/1628	88C1003A	1	0.525	1.26E-05	
1	Sep/1639	88C1003A	2	0.525	1.16E-05	
1	Sep/1646	88C1003A	3	0.525	1.10E-05	
1	Sep/1702	88C1003A	4	0.525	1.13E-05	1.16E-05
1	Sep/1759	88C1002A	1	0.6	1.18E-05	
1	Sep/1809	88C1002A	2	0.6	1.40E-05	
1	Sep/1817	88C1002A	3	0.6	1.15E-05	
1	Sep/1828	88C1002A	4	0.6	1.38E-05	1.28E-05

$$y = 0.9623 - 0.3069x + 0.8607x^2 \quad R = 0.99$$
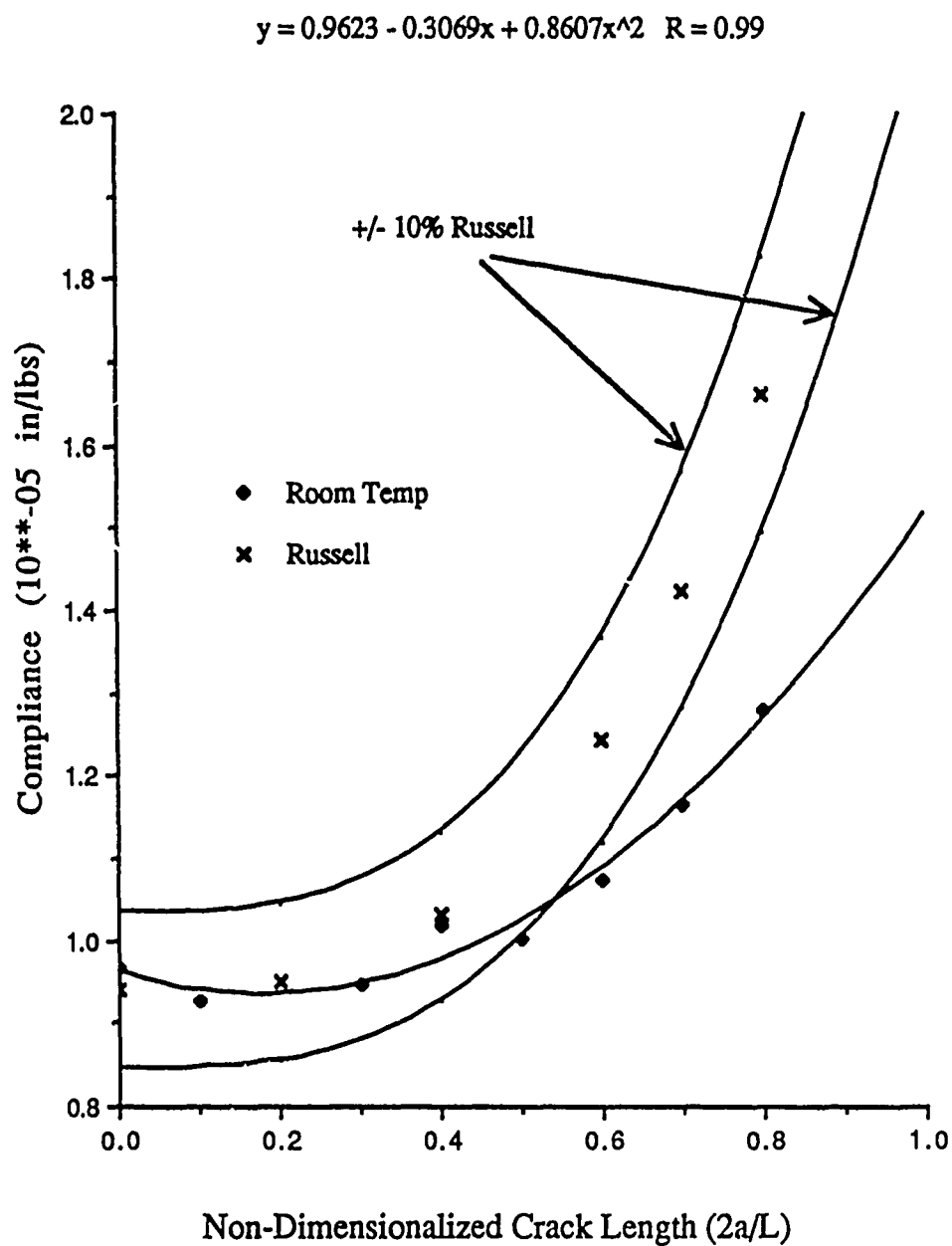
Figure 17. Room Temperature Compliance with Second Order Curve Fit Compared with Russell's Theoretical Compliance

43
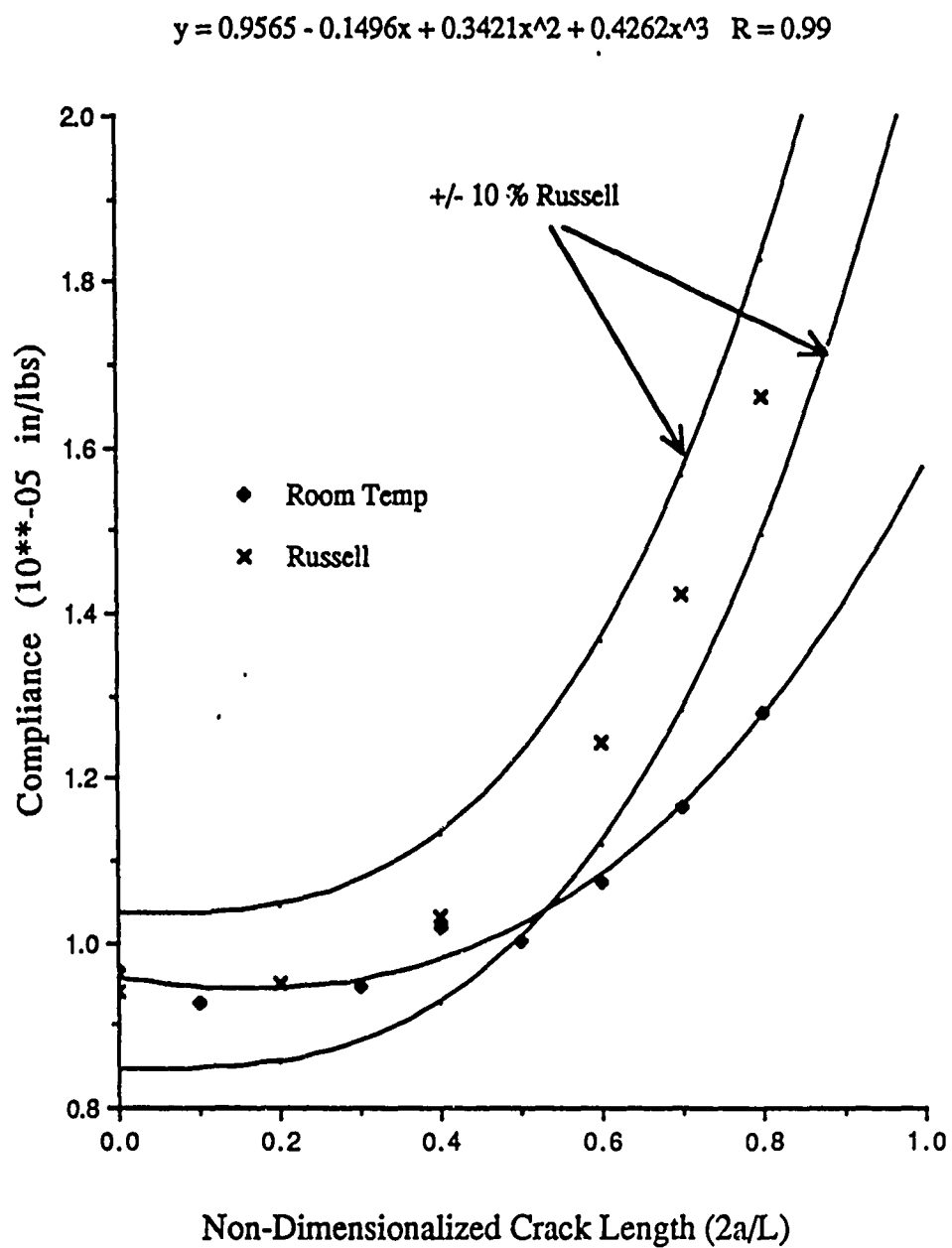
Figure 18. Room Temperature Compliance with Third Order Curve Fit
Compared with Russell's Theoretical Compliance

$$y = 0.9436 + 0.6431x \quad R = 0.99$$
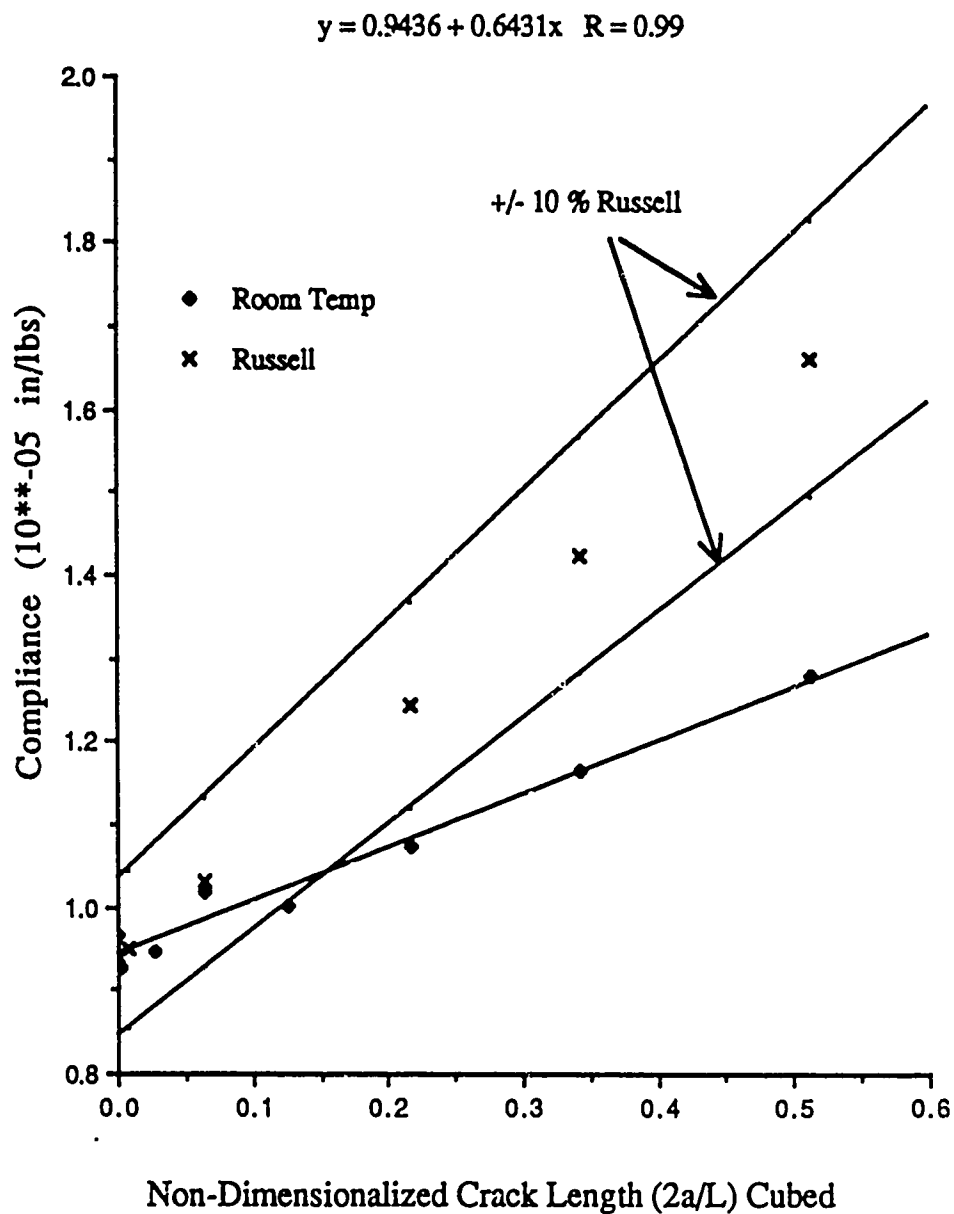
Figure 19. Room Temperature Compliance with Straight Line Curve Fit Compared with Russell's Theoretical Compliance

Once the compliance-crack length relationships for room temperature were developed, it was necessary to repeat the experiment for both 600° F and 1000° F. The experimental procedure modified for elevated temperatures discussed in Chapter 4 was used. A total of 22 compliance tests were run at 600° F (see Table V). Due to the results from the room temperature tests, only two tests per crack length were run. The results indicated there was a difference in compliance due to the position of the neutral axis with respect to the crack location, but they showed no compliance sensitivity to load fixture alignment problems. The average of the two tests per crack length was used as the compliance for that specimen at that particular crack length. Each crack length was tested a minimum of two times using different specimens. The results of these tests are shown in Figures 20, 21, and 22. The 600° F compliances are shown and compared with the room temperature compliances along with ±10% of a second order curve fit, a third order curve fit, and a straight line curve fit for $(2a/L)^3$ in Figures 17, 18, and 19, respectively. Because nearly all of the 600° F temperature compliances fall within the ±10% of room temperature compliance results, it is reasonable to assume that this is an experimental scatter and the compliance was not affected at 600° F. Further, this is expected since there is no change in the Young's modulus of the present ceramic composite at 600° F from room temperature. Therefore, the 600° F compliance averages for a particular crack length (two runs per specimen per crack length) were averaged with the room temperature compliance averages

Table V. Experimental Compliance at 600° Fahrenheit

Run		Specimen	Position	Crack Length (in)	Experimental Compliance (in/lbs)	Average Compliance (in/lbs)
13	Oct/1340	88C1005	1	0.0	1.00E-05	
13	Oct/1735	88C1005	2	0.0	9.73E-06	9.89E-06
20	Oct/1341	88C1005	1	0.0	9.42E-06	
20	Oct/1510	88C1005	2	0.0	9.59E-06	9.50E-06
20	Oct/1425	88C1005	1	0.15	9.38E-06	
20	Oct/1637	88C1005	2	0.15	9.46E-06	9.42E-06
13	Oct/1516	88C1005	1	0.15	1.05E-05	
13	Oct/1727	88C1005	2	0.15	1.00E-05	1.02E-05
18	Oct/1245	88C1006	1	0.3	1.05E-05	
18	Oct/1710	88C1006	2	0.3	8.69E-06	9.62E-06
19	Oct/1644	88C1008	1	0.3	9.83E-06	
20	Oct/1129	88C1008	2	0.3	9.50E-06	9.67E-06
19	Oct/1735	88C1008	1	0.45	1.12E-05	
20	Oct/1217	88C1008	2	0.45	1.05E-05	1.08E05
15	Oct/1632	88C1006	1	0.45	1.21E-05	
15	Oct/1529	88C1006	2	0.45	1.01E-05	1.11E-05
18	Oct/1330	88C1006	1	0.45	1.08E-05	
18	Oct/1806	88C1006	2	0.45	9.37E-06	1.01E-05
15	Oct/1735	88C1005	1	0.6	1.12E-05	
15	Oct/1835	88C1005	2	0.6	1.12E-05	1.12E-05
21	Oct/1623	88C1007	1	0.6	1.25E-05	
21	Oct/1724	88C1007	2	0.6	1.20E-05	1.22E-05

47
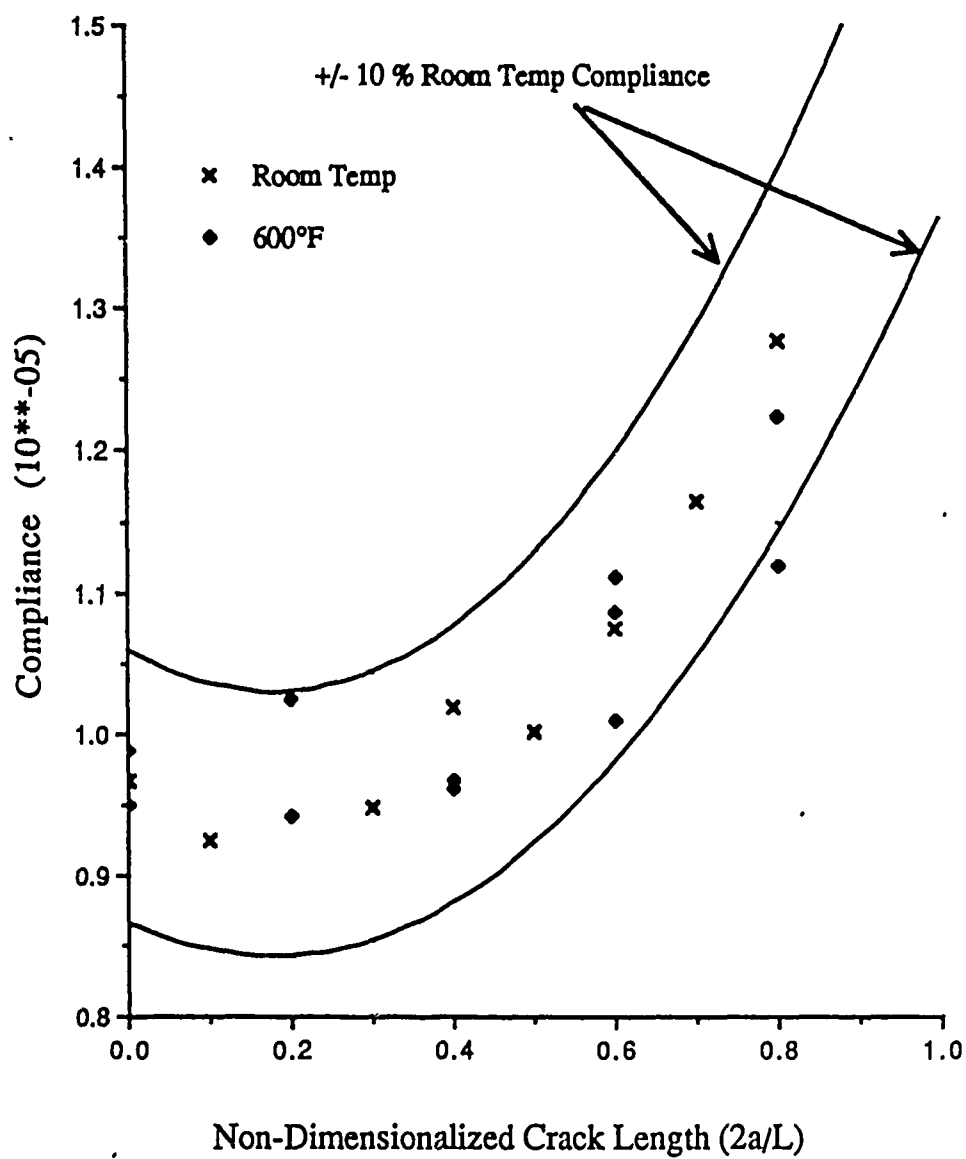
Figure 20.   600° F Compliances Compared with Room Temperature
Compliances (Second Order Polynomial Curve Fit)
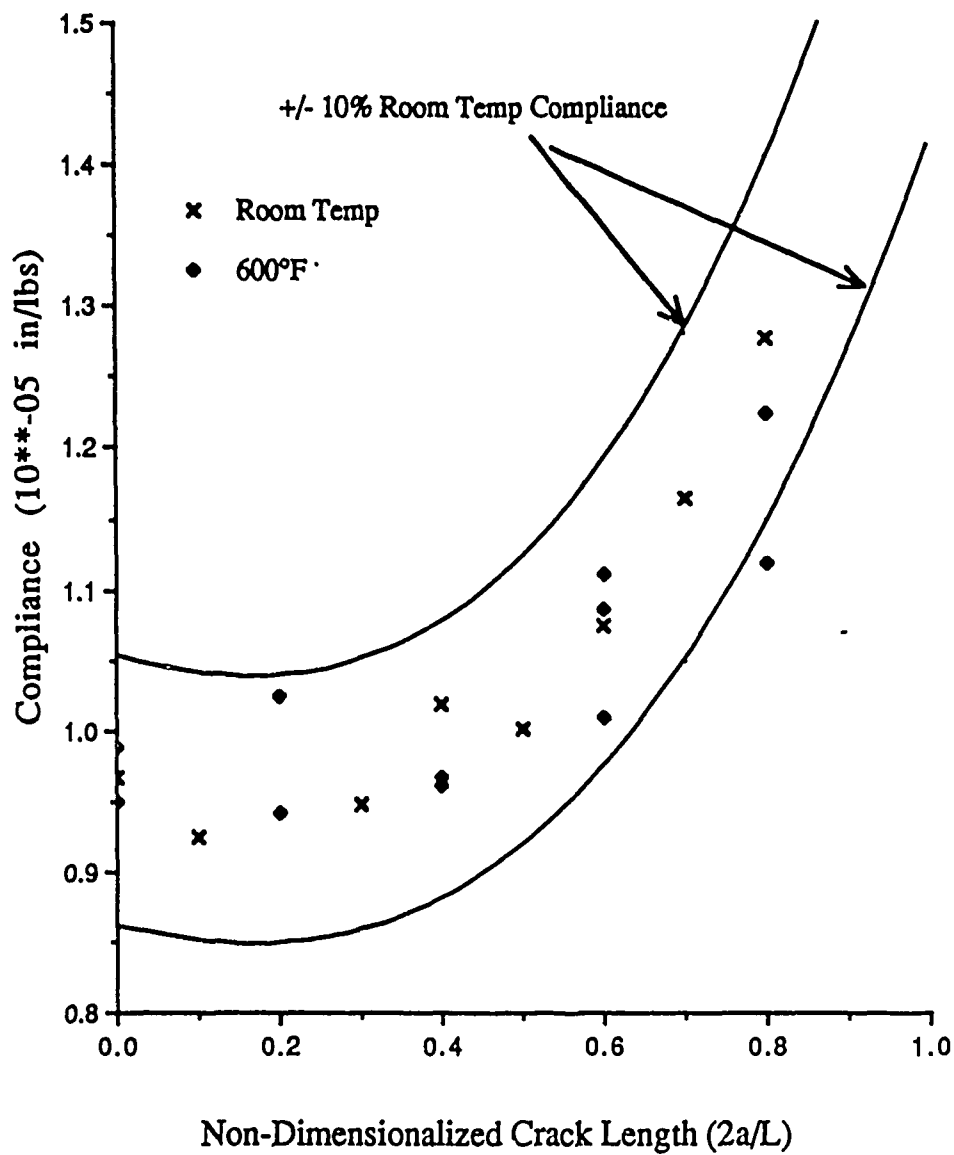
Figure 21. 600° F Compliances Compared with Room Temperature Compliances (Third Order Polynomial Curve Fit)
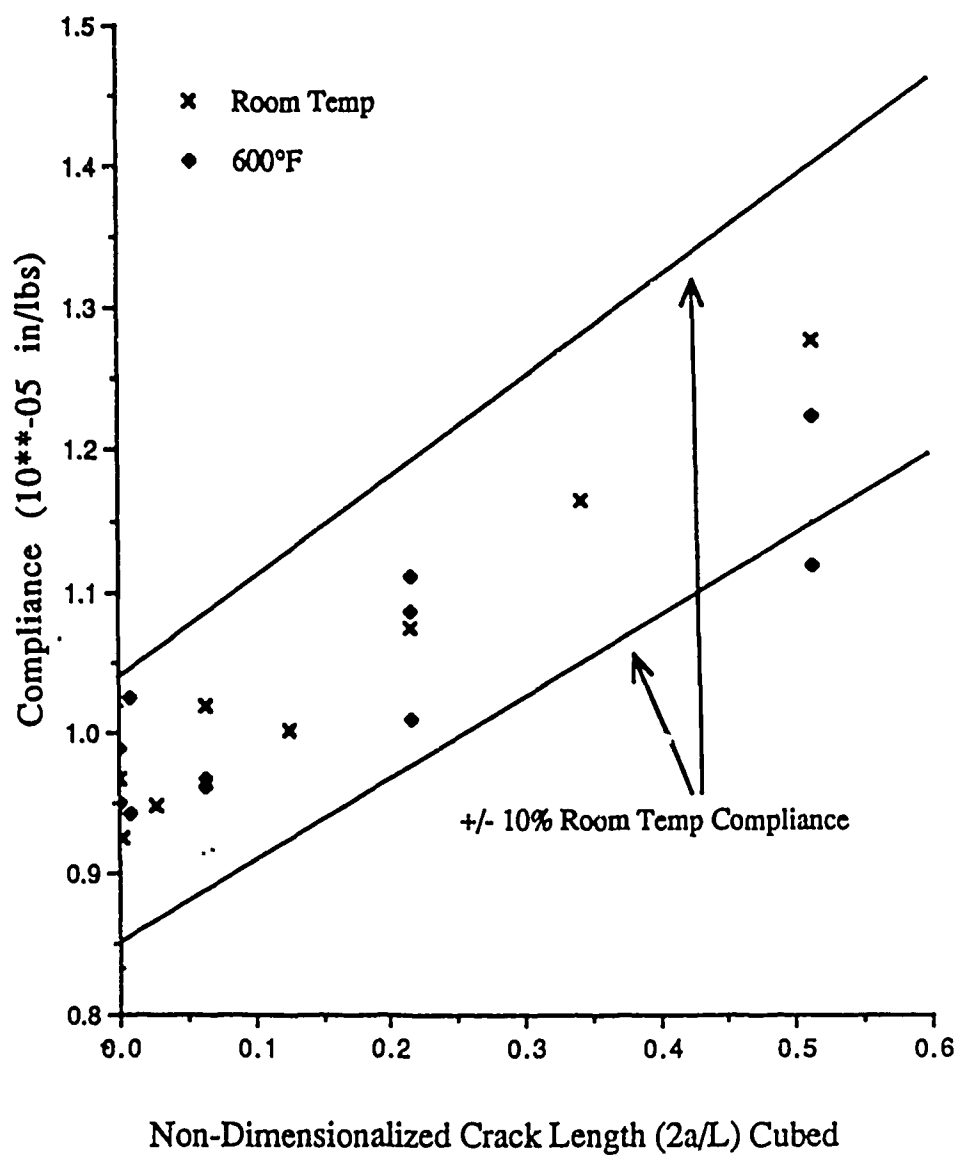
Figure 22. 600° F Compliances Compared with Room Temperature Compliances (Straight Line Curve Fit to $(2a/L)^3$)

50

(four runs per specimen per crack length). The resulting total compliance-crack length relations (using the average of room temperature and 600° F compliances for a given crack length) were fit with a second order curve fit to create Equation 7, a third order curve fit to make Equation 8, and a truncated cubic fit by comparing compliance versus $(2a/L)^3$ to develop Equation 9. Figures 23, 24, and 25 show the curve fits and equations where y is the compliance and x is equal to $(2a/L)$ of the total compliance-crack length data.

$$C = 0.9655 - 0.2344\left(\frac{2a}{L}\right) + 0.6882\left(\frac{2a}{L}\right)^2 \tag{7}$$

$$C = 0.9645 - 0.2139\left(\frac{2a}{L}\right) + 0.6202\left(\frac{2a}{L}\right)^2 + 0.0567\left(\frac{2a}{L}\right)^3 \tag{8}$$

$$C = 0.9509 + 0.5337\left(\frac{2a}{L}\right)^3 \tag{9}$$

To determine the compliance-crack length relations for 1000° F and to save some test time (each test run at an elevated temperature took approximately one hour and fifteen minutes), a combination was used of strictly compliance tests and the compliances from critical load tests. A total of 12 runs were accomplished with the

51

$$y = 0.9655 - 0.2344x + 0.6882x^2 \quad R = 0.98$$
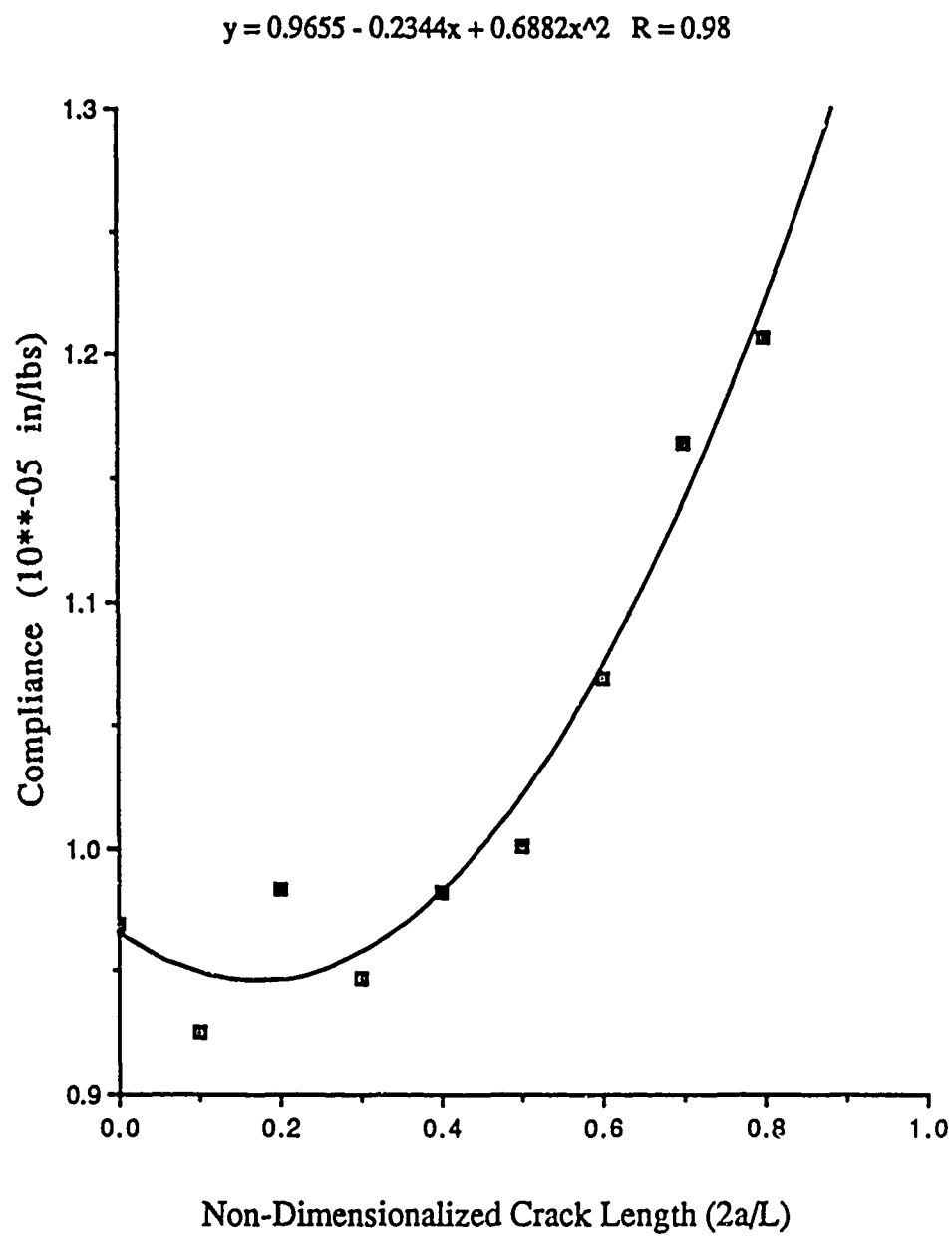
Figure 23. Total Compliance (Room Temperature and 600° F) with Second Order Polynomial Curve Fit

52

$$y = 0.9645 - 0.2139x + 0.6202x^2 + 0.0567x^3 \quad R = 0.98$$
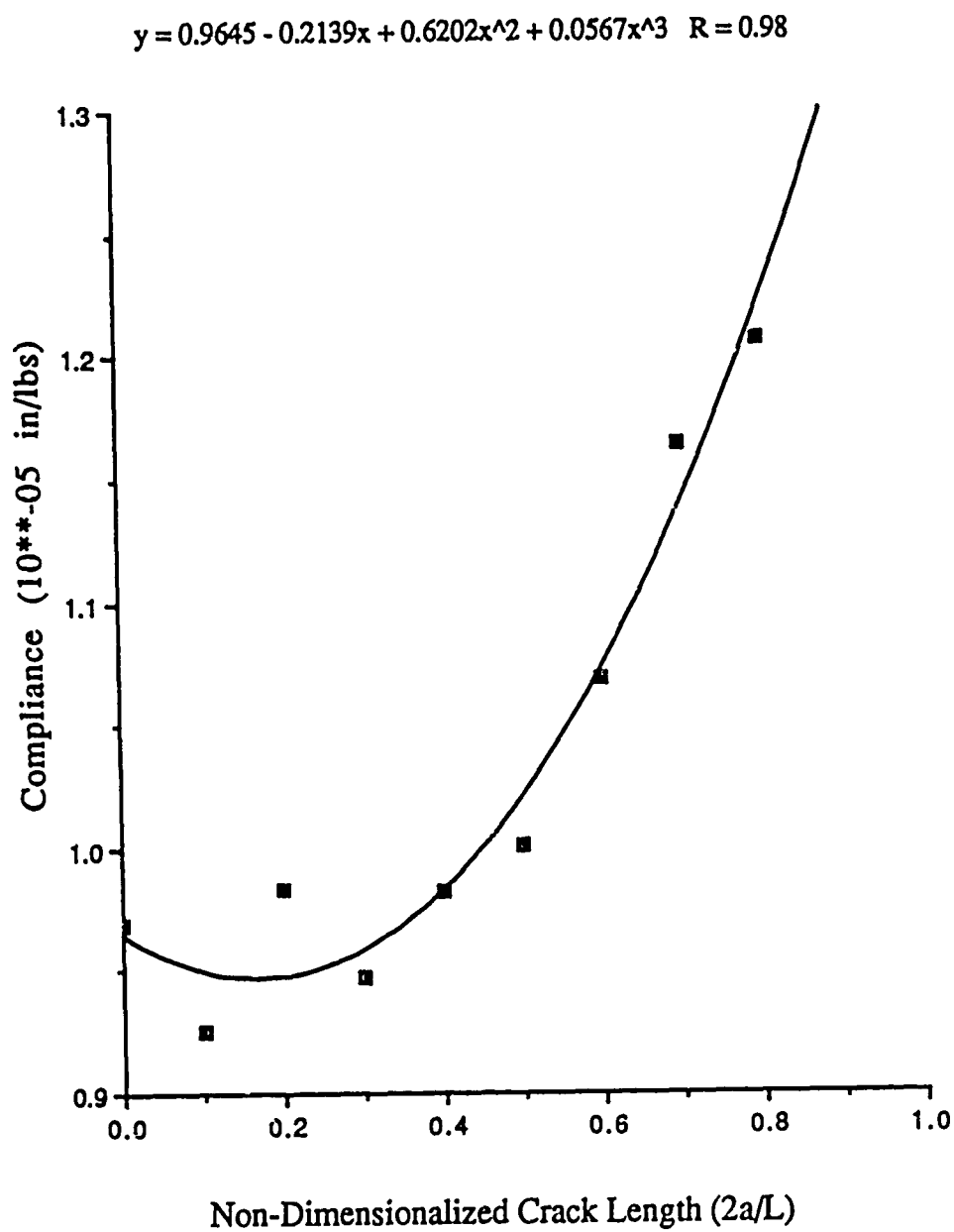
Figure 24. Total Compliance (Room Temperature and 600° F) with Third Order Polynomial Curve Fit

$$y = 0.9509 + 0.5337x \quad R = 0.98$$
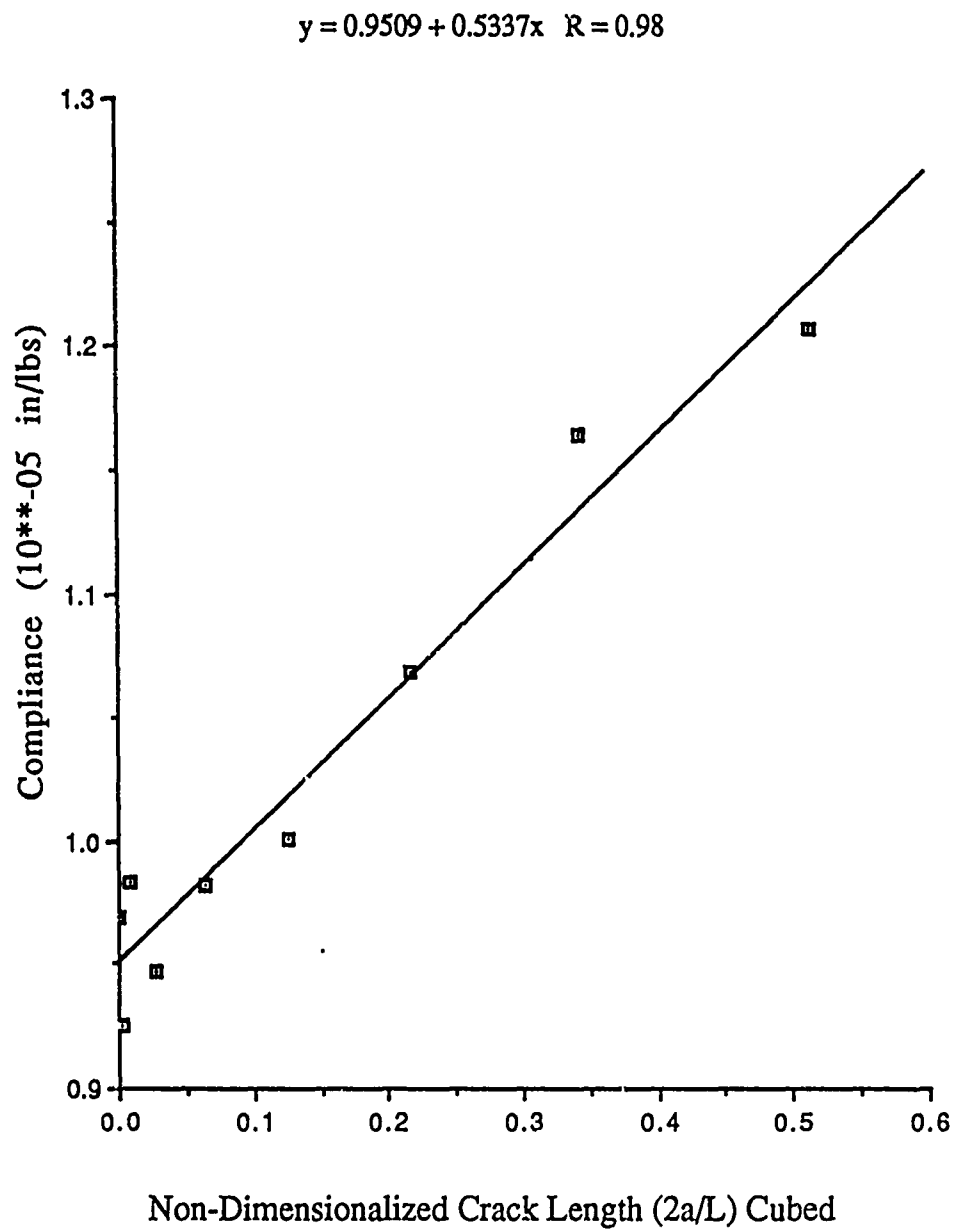
Figure 25. Total Compliance (Room Temperature and 600° F) with Straight Line Curve Fit versus $(2a/L)^3$

results shown in Table VI. As in the 600° F tests, when a specimen was tested in position 1 and position 2 for a given crack length, the average of the two tests was used. These compliances were plotted and compared with the room temperature and 600° F compliance-crack length curve fits in Figures 26, 27, and 28, again using a second order, a third order, and a truncated third order curve fit, respectively. In generating the curve fits, an artificial compliance value was used for zero crack length since the experimental value was higher than the larger crack length compliances near it and this is an impossiblity. These figures show that for the 1000° F tests, there was a slight increase (≈10%) in compliance for short crack lengths, but then the compliance increased rapidly for longer crack lengths. New curves were fit to the averages of the 1000° F compliances and are shown below in Equation 10 for the second order curve fit, Equation 11 for the third order curve fit, and Equation 12 for the truncated cubic.

$$C = 0.973 - 0.272\left(\frac{2a}{L}\right) + 1.158\left(\frac{2a}{L}\right)^2 \tag{10}$$

$$C = 0.9717 - 0.2152\left(\frac{2a}{L}\right) + 0.9411\left(\frac{2a}{L}\right)^2 + 0.2031\left(\frac{2a}{L}\right)^3 \tag{11}$$

$$C = 0.9722 + 1.1348\left(\frac{2a}{L}\right)^3 \tag{12}$$

Table VI. Experimental Compliance at 1000° Fahrenheit

Run	Specimen	Position	Crack Length (in)	Experimental Compliance (in/lbs)	Average Compliance (in/lbs)
13 Nov/1031	88C1012	1	0.0	1.09E-05	1.08E-05
11 Nov/1735	88C1011	1	0.15	9.74E-06	
11 Nov/2028	88C1011	2	0.15	9.74E-06	9.74E-06
11 Nov/2130	88C1011	2	0.3	1.01E-05	1.01E-05
13 Nov/1430	88C1011	1	0.3	1.08E-05	1.01E-05
13 Nov/2000	88C1011	1	0.375	1.11E-05	1.11E-05
12 Nov/1035	88C1010	1	0.45	1.29E-05	
12 Nov/1135	88C1010	2	0.45	1.43E-05	1.37E-05
13 Nov/1315	88C1009	1	0.45	1.22E-05	1.22E-05
13 Nov/1630	88C1010	1	0.45	1.24E-05	1.24E-05
13 Nov/1130	88C1010	1	0.45	1.17E-05	1.17E-05
13 Nov/1815	88C1012	1	0.525	1.34E-05	1.34E-05

$$y = 0.973 - 0.272x + 1.158x^2 \quad R = 1.00$$
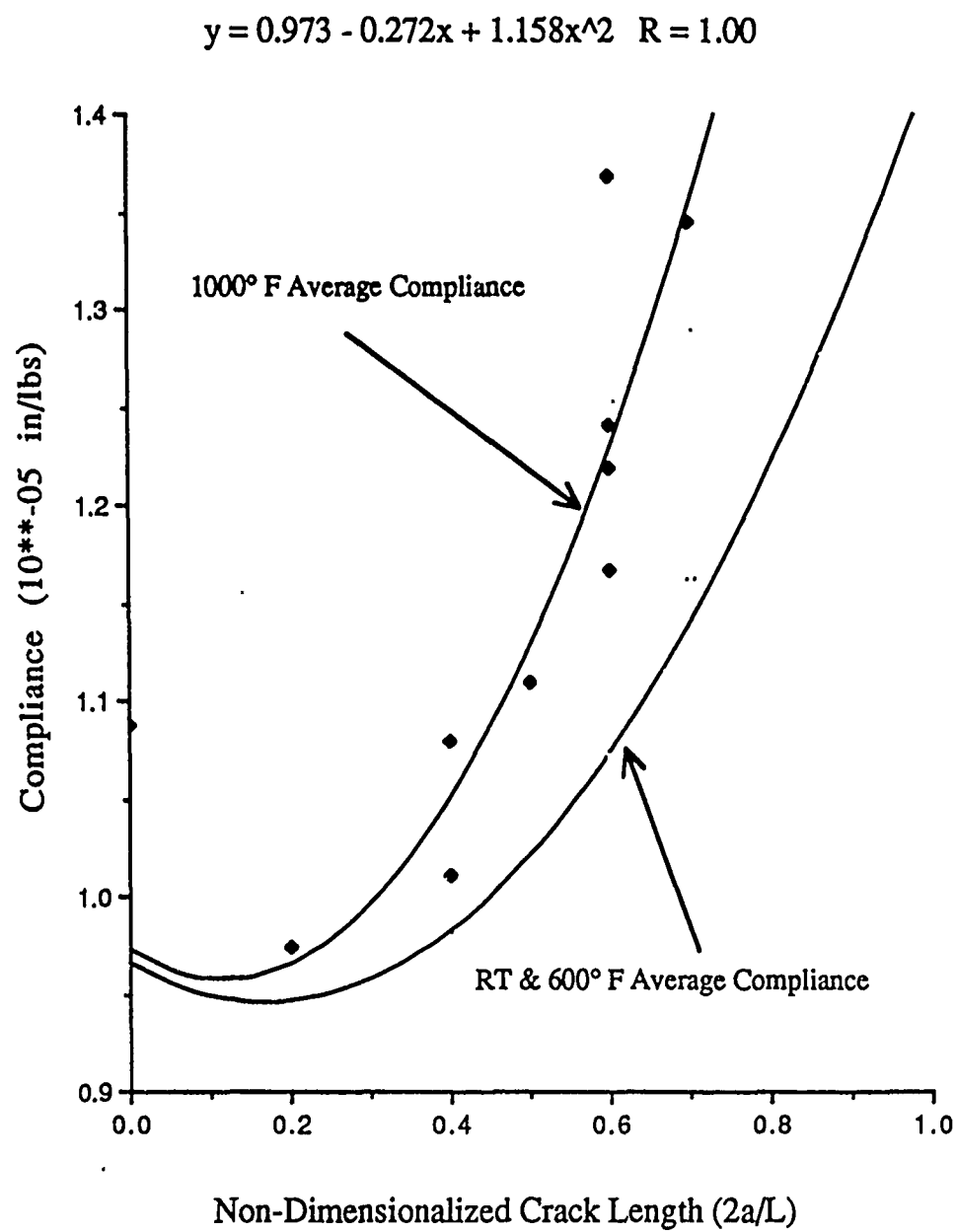
Figure 26. Compliance for 1000° F with Second Order Curve Fit

$$y \approx 0.9717 - 0.2152x + 0.9411x^2 + 0.2031x^3 \quad R = 1.00$$
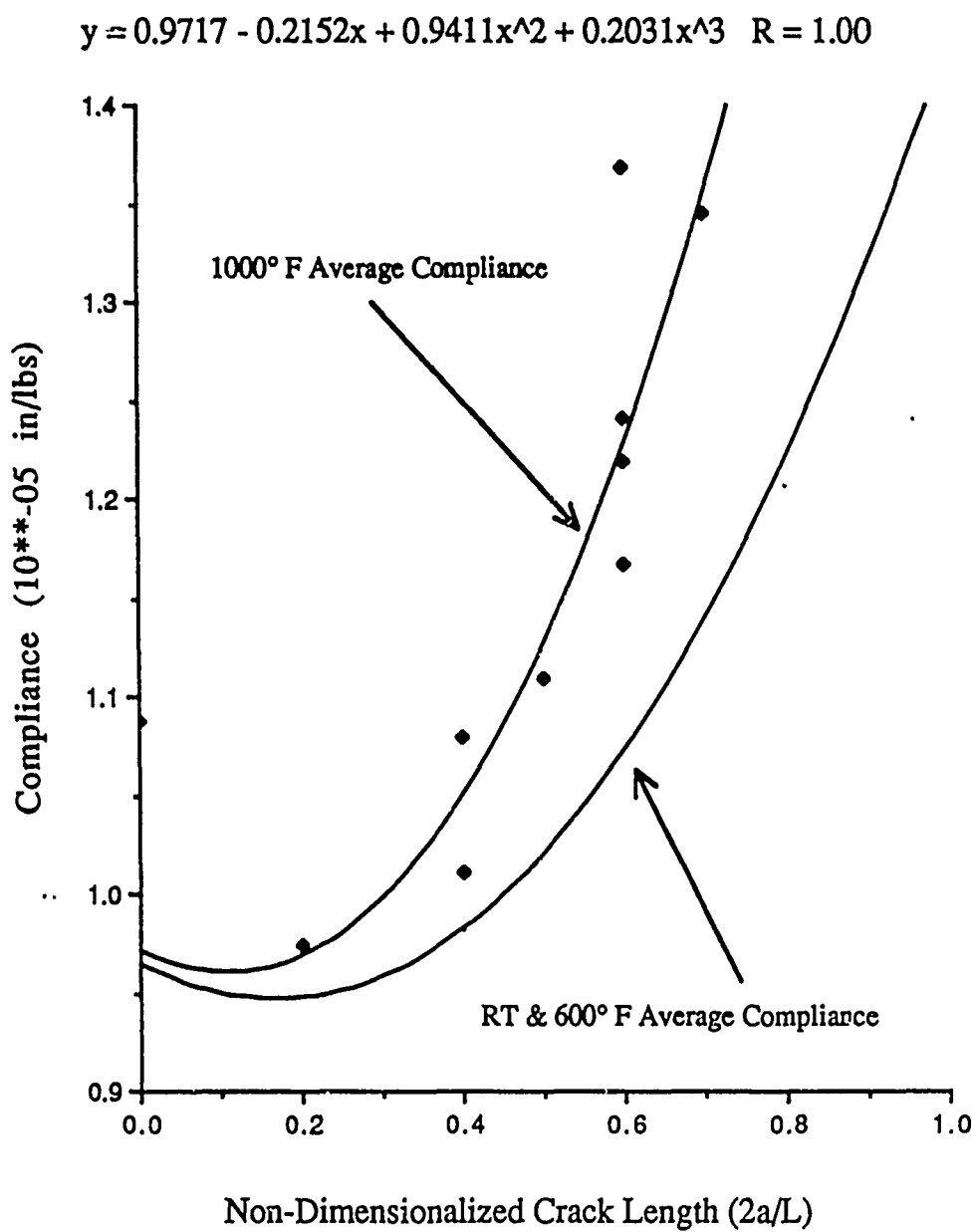
Figure 27. Compliance for 1000° F with Third Order Curve Fit

$$y = 0.9722 + 1.1348x \quad R = 0.99$$
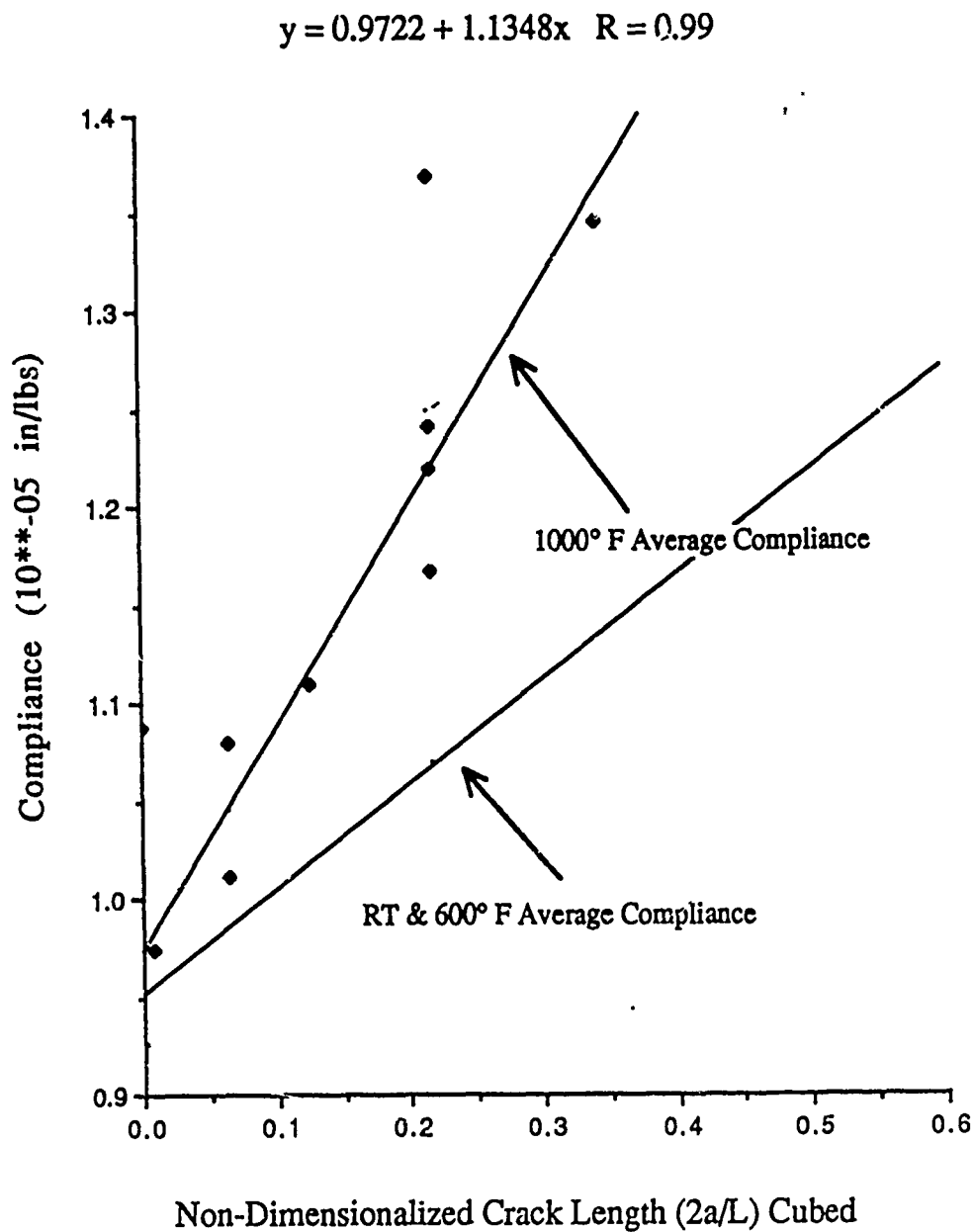
Figure 28.   Compliance for 1000° F with Straight Line Curve Fit for Compliance versus $(2a/L)^3$

Critical Load

The critical load, or the load required for a crack to grow, for a given crack length was required for calculating the fracture toughness. Unlike Vozzola's work where he used laser interferomentry to measure crack growth initiation (41), this study would use a change in the specimen's compliance.

To find the critical load of a specimen for a given crack length, the procedures described in Chapter IV were used. The specimens were loaded until the compliance increased indicated by a change of the slope on the X-Y plotter (see Appendix D). It was desirable not to destroy the specimen by testing it until if failed catastrophically since the new crack growth could be measured, then marked with a pencil and the specimen tested again.

During early experiments, specimens were loaded until their compliance changed indicating crack growth, and unloaded. They were then loaded again, without removing them from the load fixture, to see if they assumed the compliance of the new longer crack. They did not. Apparently, the surfaces of the inside of the crack were not entirely free of each other, causing locking. This locking could be caused by the fibers of one side of the crack, although fractured, protruding into the opposite crack surface, preventing it to unload or recover its original configuration. To prevent this locking, a 0.002 inch Nichrome shim was inserted into the notched end of the crack. This shim produced a small Mode I force which was used to separate the two fracture surfaces allowing them to unload fully. Specimens with the shim installed assumed

their new compliance once the critical load was reached and the crack grown. Shims were installed in all specimens before testing for the critical load.

After a test had been completed, a straight line was fit manually to the linear portion of the curve generated by the X-Y plotter (see Appendix D). The early non-linearity of the curve was due to settling and was ignored in the curve fitting. Another straight line was fit to the upper portion of the curve where the crack had grown. The intersection of the two lines was used as the critical load. For some tests, it was difficult to discern where the upper straight line should be drawn, allowing for some judgement. On other tests, it was possible to see where the specimen had reached its critical load and the crack grown, indicated by a new slope or compliance, and then with continued loading, cracked again showing another change in compliance.

Because the compliance curve was well behaved towards its middle, crack lengths from 0.3 to 0.6 inches were examined. The results of the room temperature, 600° F, and 1000° F critical load tests are shown in Table VII, Table VIII, and Table IX, respectively, and Figure 29. Although the specimens were not all identical in size, two trends can be seen. First, the longer the crack, the smaller the critical load as expected. Secondly, the critical loads measured at 600° F were lower than the room temperature tests for the same crack length, but more importantly the critical loads for the 1000° F tests were higher. This indicated that the tested ceramic composite

behaved more brittle when heated to 600° F but acted more ductile at 1000° F.

Table VII. Critical Loads at Room Temperature (Position 1)

Run		Specimen	Crack Length (in)	Experimental Compliance (in/lbs)	Critical Load (lbs)
3	Oct/1725	88C1003A	0.3	9.63E-06	351.04
3	Oct/1834	88C1001A	0.375	1.03E-05	305.50
3	Oct/1803	88C1003A	0.45	1.03E-05	274.62
4	Oct/0850	88C1002A	0.57	1.20E-05	231.10
3	Oct/1821	88C1003A	0.6	1.16E-05	241.69
4	Oct/0920	88C1004A	0.6	1.40E-05	241.38

Table VIII. Critical Loads at 600° Fahrenheit (Position 1)

Run		Specimen	Crack Length (in)	Experimental Compliance (in/lbs)	Critical Load (lbs)
22	Oct/1741	88C1006	0.3	9.77E-06	290.68
22	Oct/1635	88C1008	0.3	9.90E-06	248.45
22	Oct/1835	88C1007	0.45	1.07E-05	222.36
22	Oct/2133	88C1008	0.525	1.09E-05	206.75
22	Oct/2038	88C1007	0.6	1.43E-05	152.17

Table IX. Critical Loads at 1000° Fahrenheit (Position 1)

Run		Specimen	Crack Length (in)	Experimental Compliance (in/lbs)	Critical Load (lbs)
13	Nov/1430	88C1011	0.3	1.08E-05	465.83
13	Nov/2000	88C1011	0.375	1.11E-05	427.95
13	Nov/1315	88C1009	0.45	1.21E-05	283.85
13	Nov/1630	88C1010	0.45	1.24E-05	345.96
13	Nov/1815	88C1012	0.525	1.34E-05	273.29
13	Nov/2120	88C1012	0.6	2.52E-05	250.93
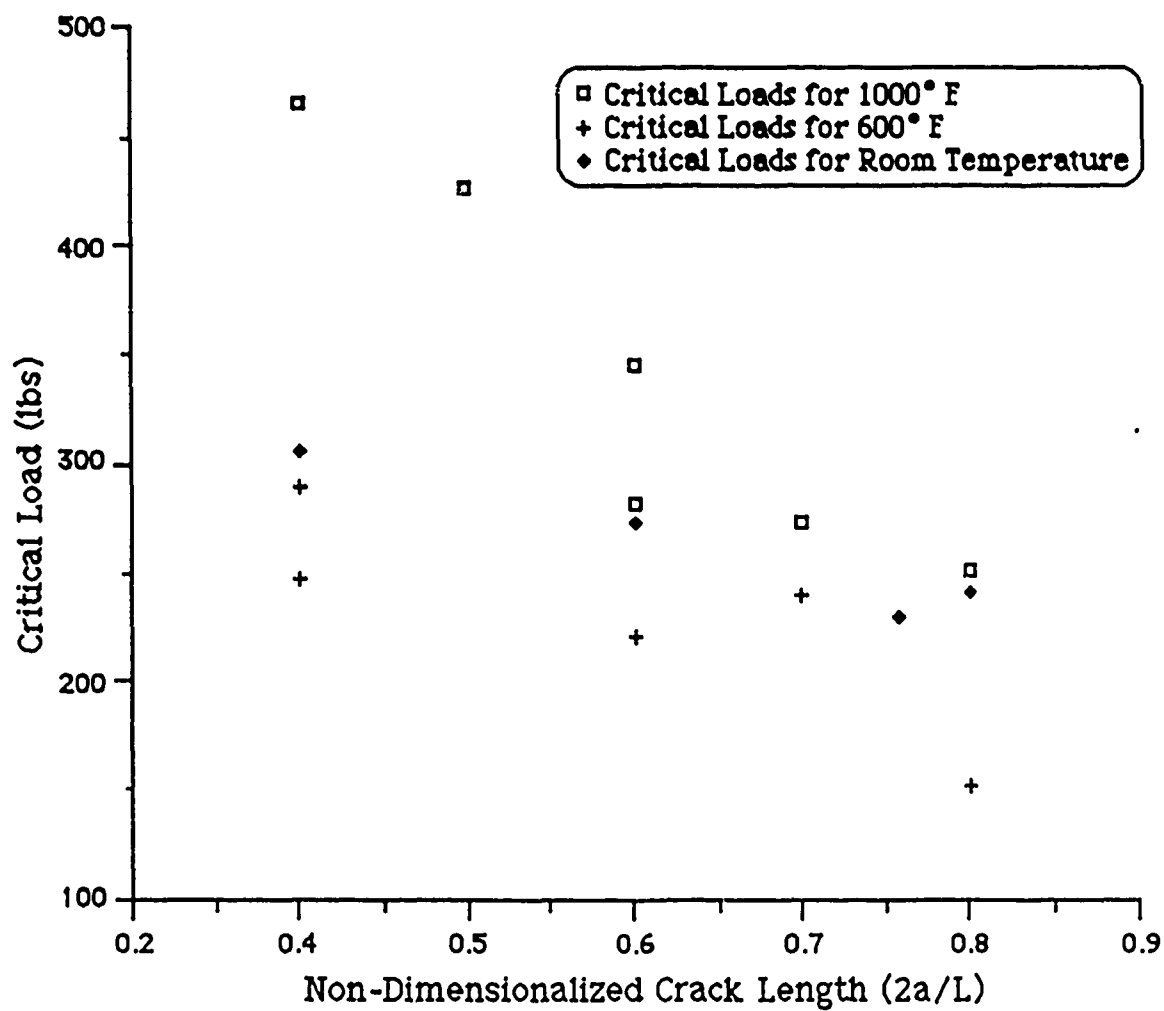
Figure 29. Critical Loads Found at Room Temperature, 600°, and 1000° Fahrenheit

Fracture Toughness

The objective of this study was to develop a method for finding the Mode II fracture toughness of a ceramic glass matrix composite at elevated temperatures. Once the method was developed, it would be used to measure the G_{IIc} of Corning 1723 glass ceramic matrix composite.

To determine the experimental fracture toughness of a specimen, it was necessary to know the slope of the compliance curve. This could be simply found by taking the derivative of the compliance-crack length relationship with respect to "a", the effective crack length, and applying it for a given crack length. The derivative would be taken for each compliance-crack length relationship, Equation 7, Equation 8, and Equation 9 for room temperature and 600° F tests and Equations 10, 11, and 12 for the 1000° F tests. These numbers were then un-normalized by dividing by the values used in Equation 5 since specific specimens were being used. These were then used in Equation 13 to find the experimental fracture toughness.

$$G_{IIc} = \left(\frac{P_{cr}^2}{2b}\right)\left(\frac{\partial C}{\partial a}\right) \qquad (13)$$

If simple linear beam theory applied, it would be possible to use the following relationship derived by Russell (13) from theoretical compliance to evaluate the fracture toughness.

$$G_{IIc} = \frac{9P_{cr}^2 a^2}{16b^2 E_{11} h^3} \qquad (14)$$

The fracture toughness values from this theoretical relation and the various compliance-crack length relations are shown in Table X for the room temperature tests, Table XI for 600° F tests, and Table XII for tests done at 1000° F.

The average experimental fracture toughness using the second order curve fits for room temperature was 1.698 lb/in ± 15%, 1.367 lb/in ± 25% for the measured crack length-compliance data for 600° F, and 5.334 lb/in ± 28% for 1000° F. These results indicated that the specimen acted slightly more brittle at 600° F than at room temperature decreasing its fracture toughness 20%. More importantly, the glass ceramic composite more than tripled its fracture toughness at 1000° F. This was a significant increase that could be due to increased ductility blunting the crack tip, fiber bridging (or an entanglement of the fibers) between different layers of the matrix, a chemical change in the matrix or fiber composition, or a combination of all three. The G_{IIc} (1.698 lb/in) from the present study is less than the value (2.17 lb/in) that Vozzola got for his room temperature tests (41). This could be in part due to the differences in the specimen's manufacturing, local variations in composition, and different compliance-crack length relations used. Interestingly, the difference in fracture toughness for the different curve fits for experimental compliance was less than 5% for room temperature, 600° F, and 1000° F. The fracture toughness should be a constant if it is to be considered a material property. Figures 30, 31, 32, and 33 show the fracture toughness derived from Equations 7, 8, 9, and 14, respectively for room temperature. Figures 34, 35, 36, and 37 show

the fracture toughness at 600° F using the same equations. And, Figures 38, 39, 40, and 41 show the fracture toughnesses for Equations 10, 11, and 12, respectively for 1000° F. There is some scatter, but this can be attributed to several factors: 1) Experimental errors in determining the critical load, compliance, etc. ; 2) Local variations in material behavior due to irregularities, fiber bridging, etc.; 3) The small size of the specimen, making it difficult to align and magnifying any position errors, differences in specimen geometry, etc.. The truncated third order curve fit in Figures 32, 36, and 40 appears to have strengthened the fracture toughness for longer cracks and weakened it for shorter cracks. This makes it inappropriate for determining the fracture toughness for this set of data. In contrast, the truncated cubic curve fit for the compliances measured at 1000° F provided the narrowest band of fracture toughnesses (see Figure 42) and therefore the best compliance-crack length relationship for that particular set of data. The fracture toughness derived from the theoretical compliance-crack length relation, Equation 14, shows in Figures 33, 37, and 41, a narrow band width but has as much as a 35% variation from the average, indicating again that the simple linear beam theory is too limited to apply to the fracture toughness testing of small ceramic glass composites.

Table X. Fracture Toughness for Room Temperature Based on Different Compliance-Crack Length Relations

Run		Specimen	(in)	(lbs)	Eq. 7 G_{IIc} (lb/in)	Eq. 8 G_{IIc} (lb/in)	Eq.9 G_{IIc} (lb/in)	Eq.14 G_{IIc} (lb/in)
3	Oct/1725	88C1003A	0.3	351.04	1.447	1.416	1.172	0.387
3	Oct/1834	88C1001A	0.375	305.50	1.727	1.708	1.523	0.503
3	Oct/1803	88C1003A	0.45	274.62	1.656	1.656	1.614	0.533
4	Oct/0850	88C1002A	0.57	231.10	1.704	1.736	1.941	0.641
4	Oct/O920	88C1004A	0.6	241.38	1.774	1.816	2.097	0.692
3	Oct/1821	88C1003A	0.6	241.69	1.880	1.924	2.222	0.734
				Average	1.698	1.709	1.762	0.582

Table XI. Fracture Toughness at 600° Fahrenheit Based on Different Compliance-Crack Length Relations

Run		Specimen	(in)	(lbs)	Eq. 7 G_{IIc} (lb/in)	Eq. 8 G_{IIc} (lb/in)	Eq.9 G_{IIc} (lb/in)	Eq.14 G_{IIc} (lb/in)
22	Oct/1635	88C1008	0.3	248.45	1.025	1.003	0.830	0.274
22	Oct/1741	88C1006	0.3	290.68	1.512	1.480	1.225	0.413
22	Oct/1835	88C1007	0.45	222.36	1.582	1.582	1.541	0.509
22	Oct/2131	88C1008	0.525	206.21	1.628	1.647	1.752	0.579
22	Oct/2038	88C1007	0.6	152.17	1.086	1.111	1.283	0.424
				Average	1.367	1.365	1.326	0.440

Table XII. Fracture Toughness at 1000° Fahrenheit Based on Different Compliance-Crack Length Relations

Run		Specimen	(in)	(lbs)	Eq.10 G_{IIc} (lb/in)	Eq.11 G_{IIc} (lb/in)	Eq.12 G_{IIc} (lb/in)	Eq.14 G_{IIc} (lb/in)
13	Nov/1430	88C1011	0.3	465.83	5.979	5.804	4.977	0.789
13	Nov/2000	88C1011	0.375	427.95	6.832	6.772	6.563	1.041
13	Nov/1630	88C1010	0.45	345.96	5.787	5.869	6.346	1.007
13	Nov/1315	88C1009	0.45	283.85	4.869	4.938	5.340	0.847
13	Nov/1815	88C1012	0.525	273.29	4.295	4.460	5.310	0.842
13	Nov/2120	88C1012	0.6	250.93	4.242	4.510	5.847	0.927
				Average	5.334	5.392	5.731	0.909

Figure 30. Fracture Toughness for Room Temperature Based on a Second Order Curve Fit to the Compliance-Crack Length Relation (Equation 7)

68

Figure 31. Fracture Toughness for Room Temperature Based on a Third Order Curve Fit to the Compliance-Crack Length Relation (Equation 8)

Figure 32. Fracture Toughness for Room Temperature Based on a Truncated Third Order Curve Fit to the Compliance-Crack Length Relation (Equation 9)

Figure 33.   Fracture Toughness for Room Temperature Based on a
Theoretical Compliance-Crack Length Relation (Equation 14)
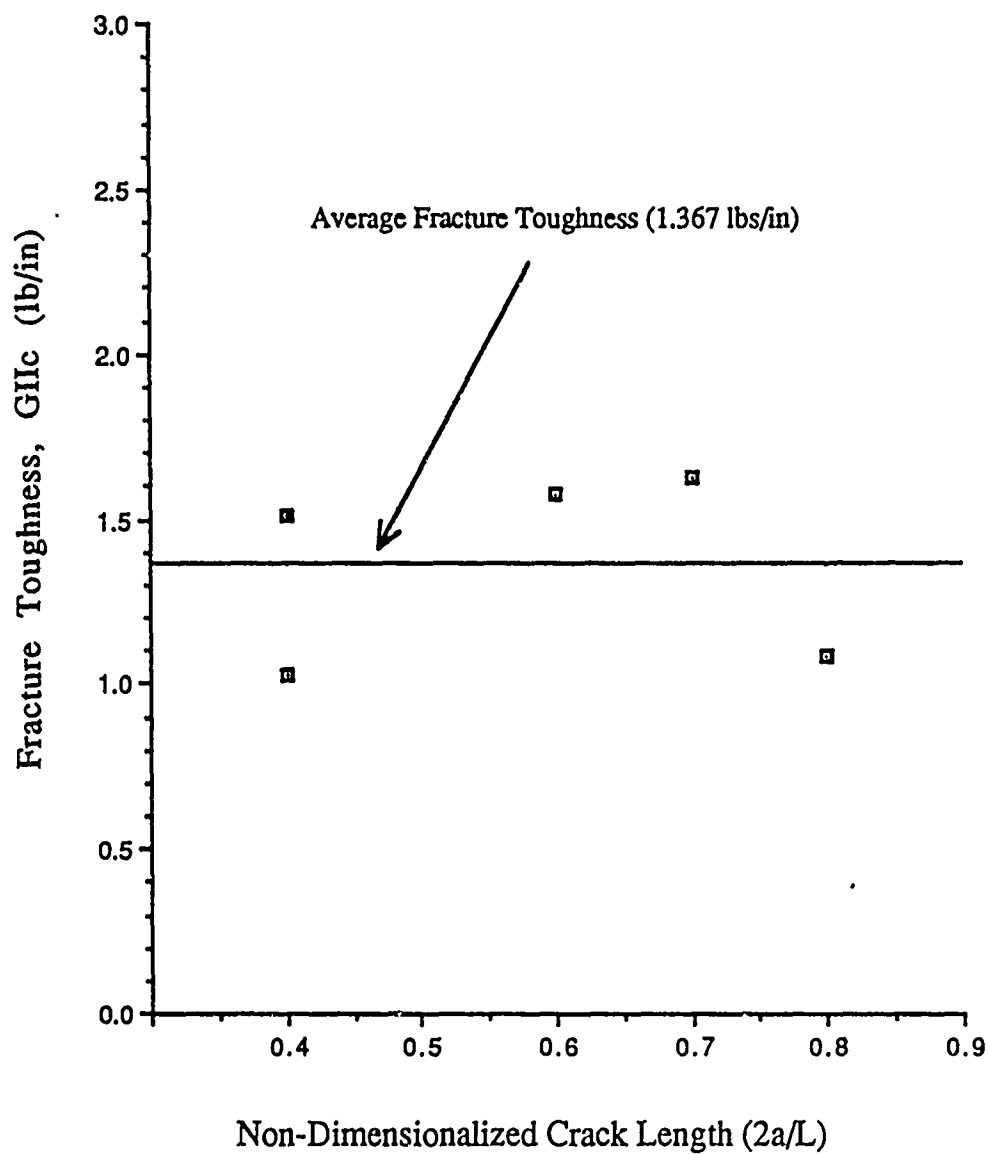
Figure 34. Fracture Toughness for 600° Fahrenheit Based on a
Second Order Curve Fit to the Compliance-Crack Length Relation
(Equation 7)
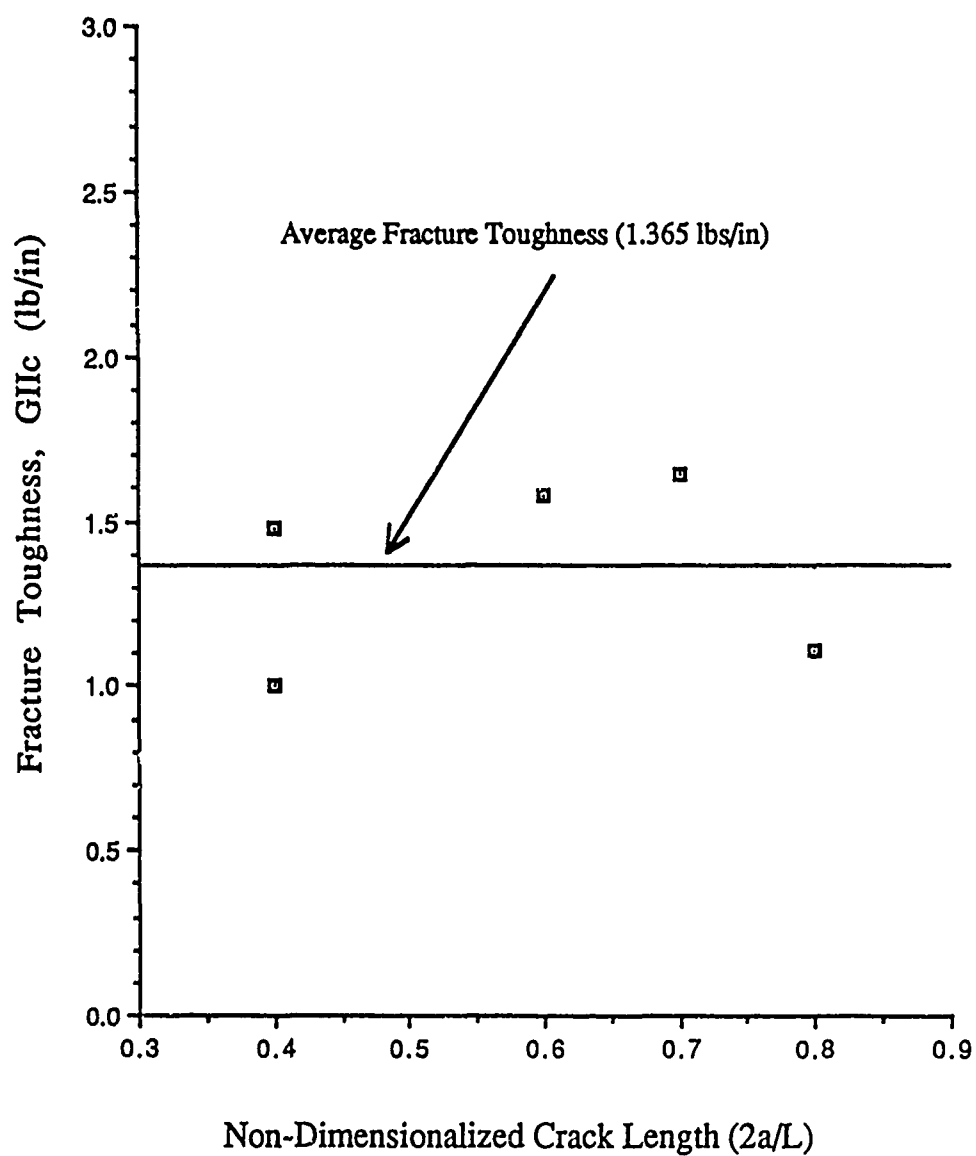
Figure 35. Fracture Toughness for 600° Fahrenheit Based on a Third Order Curve Fit to the Compliance-Crack Length Relation (Equation 8)
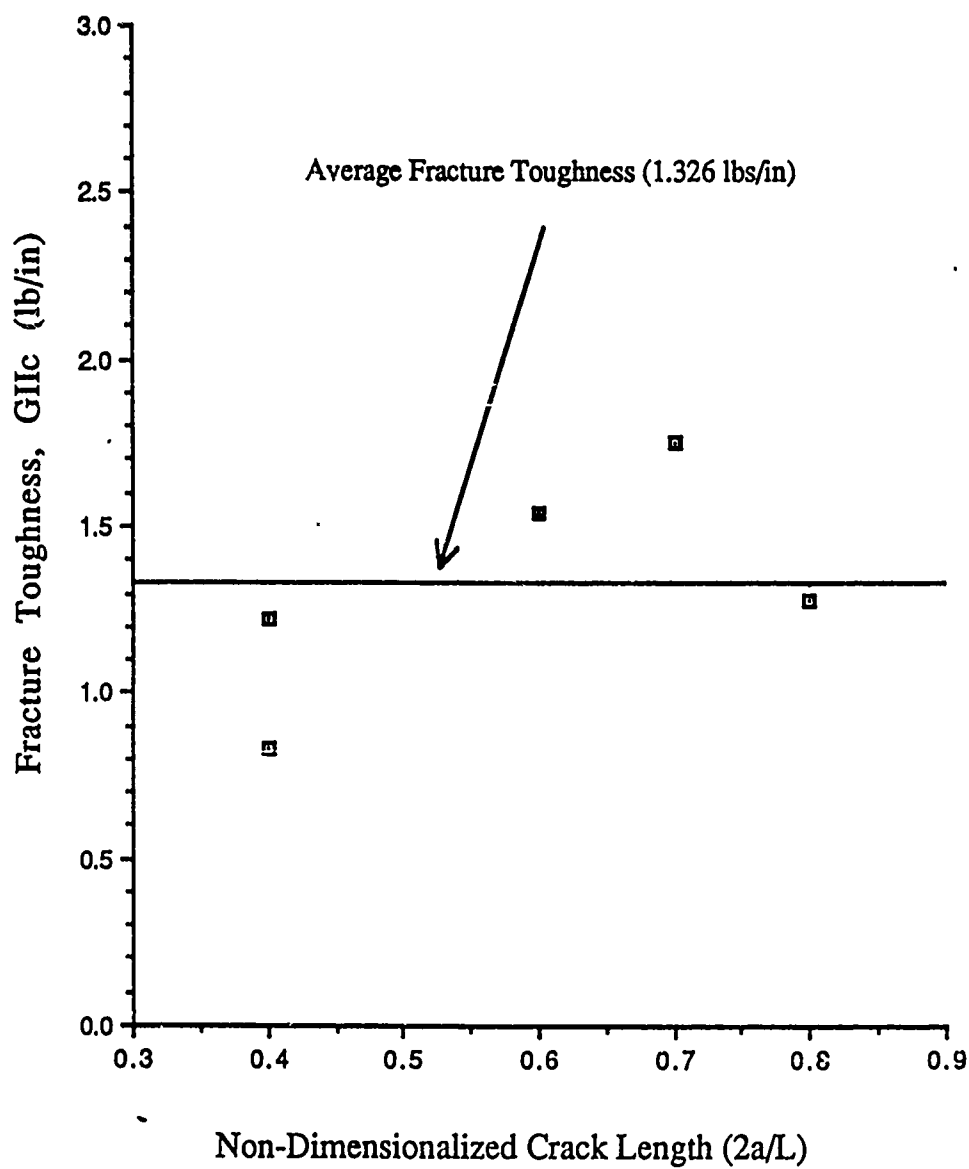
Figure 36. Fracture Toughness for 600° Fahrenheit Based on a
Truncated Third Order Curve Fit to the Compliance-Crack Length
Relation (Equation 9)
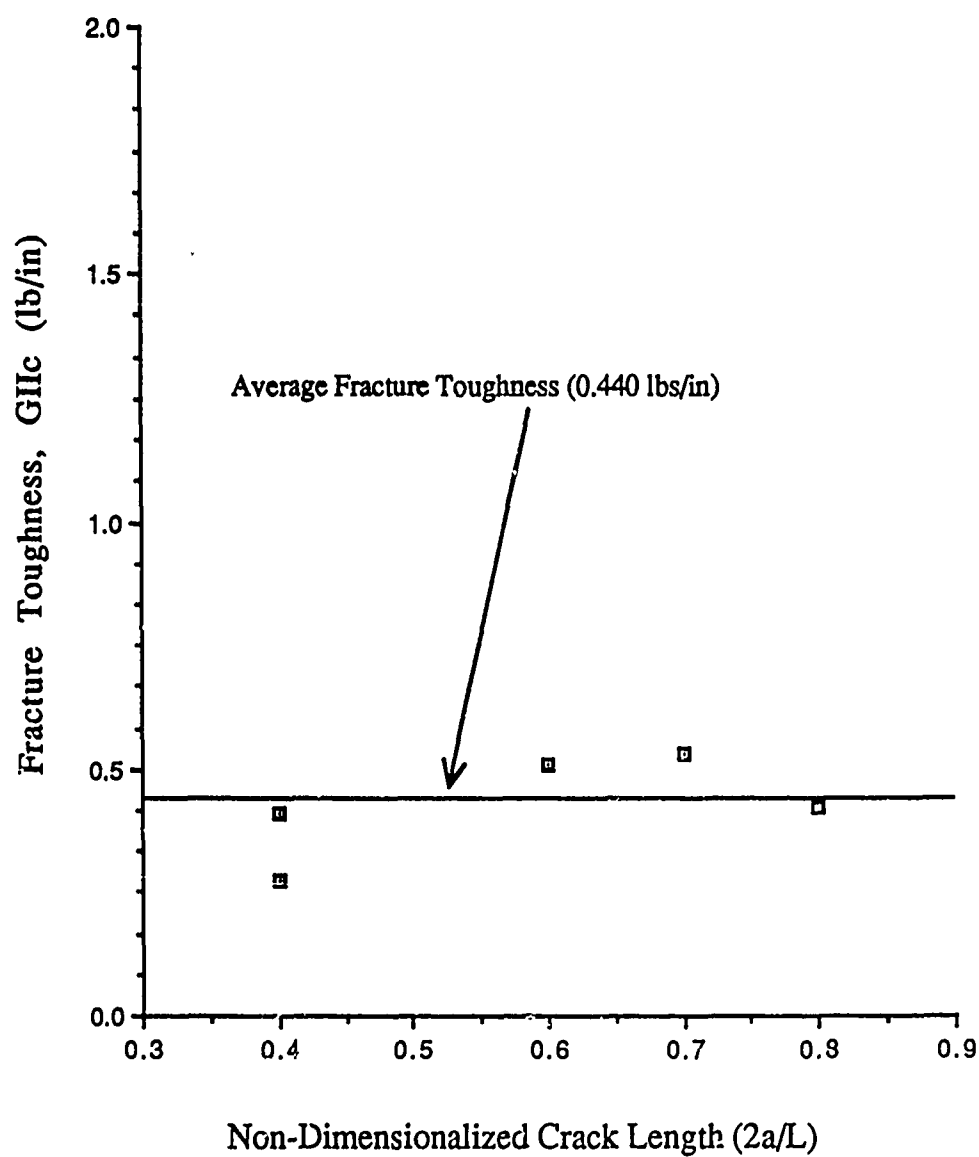
Figure 37. Fracture Toughness for 600° Fahrenheit Based on a
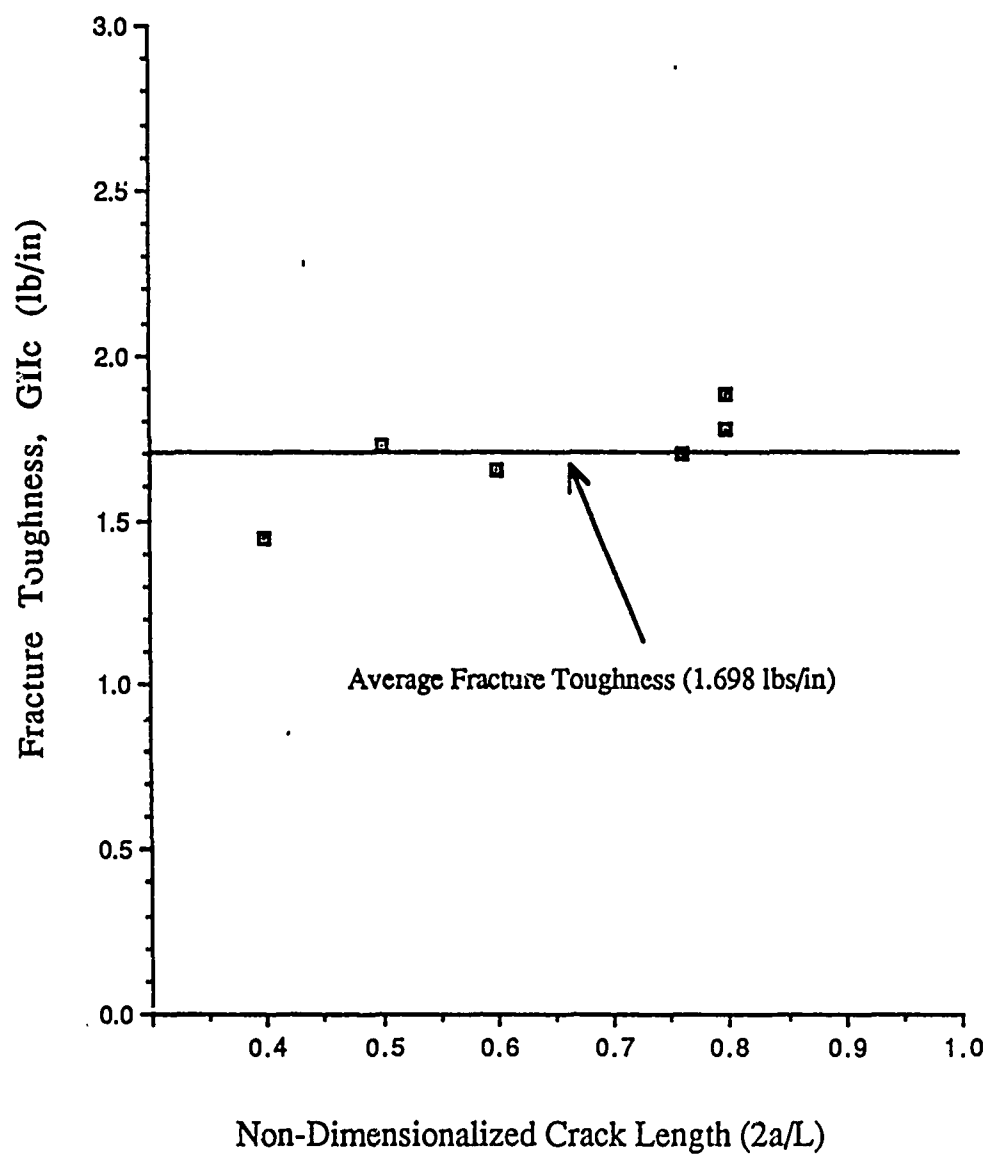Theoretical Compliance-Crack Length Relation (Equation 14)
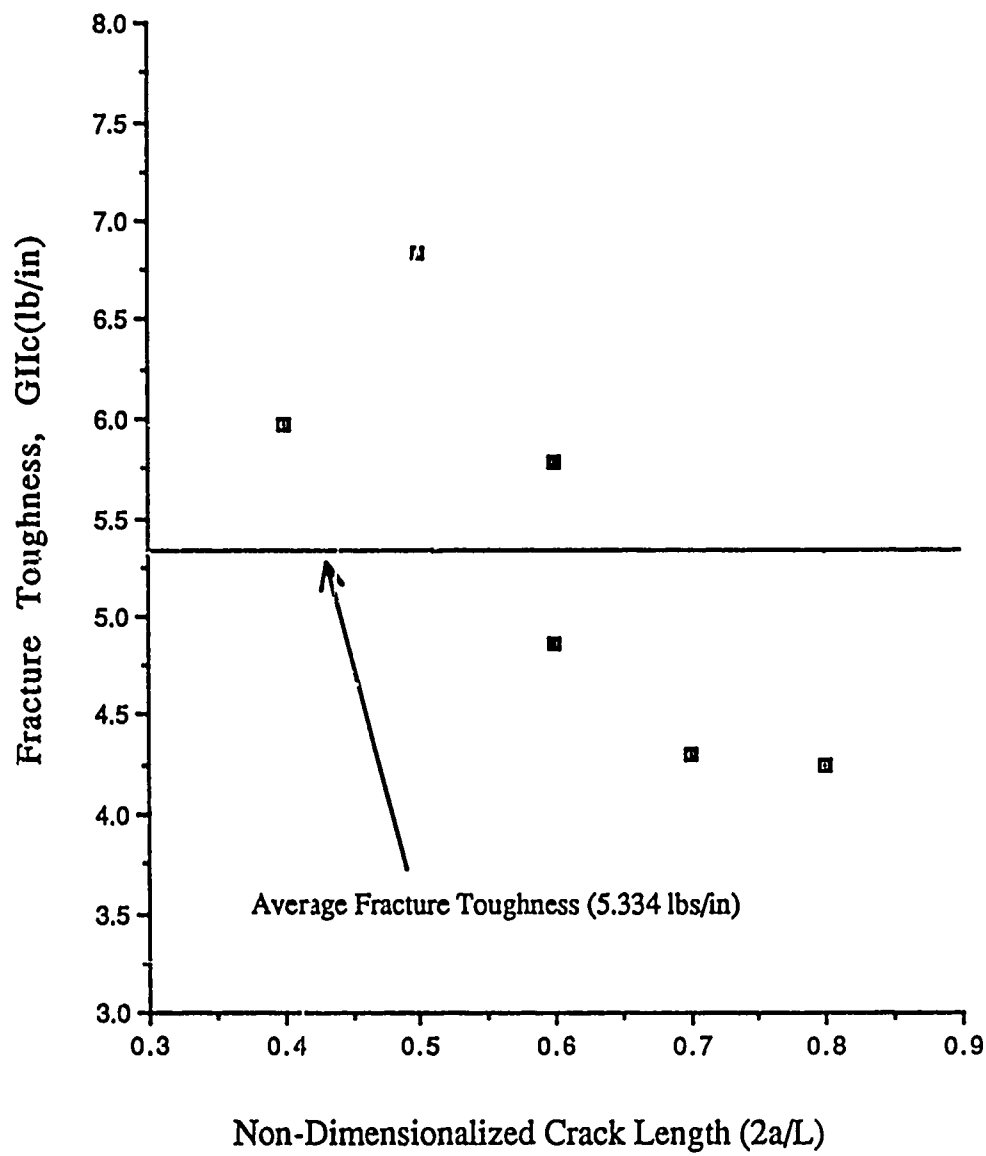
Figure 38. Fracture Toughness for 1000° Fahrenheit Based on a
Second Order Curve Fit to the Compliance-Crack Length Relation
(Equation 10)
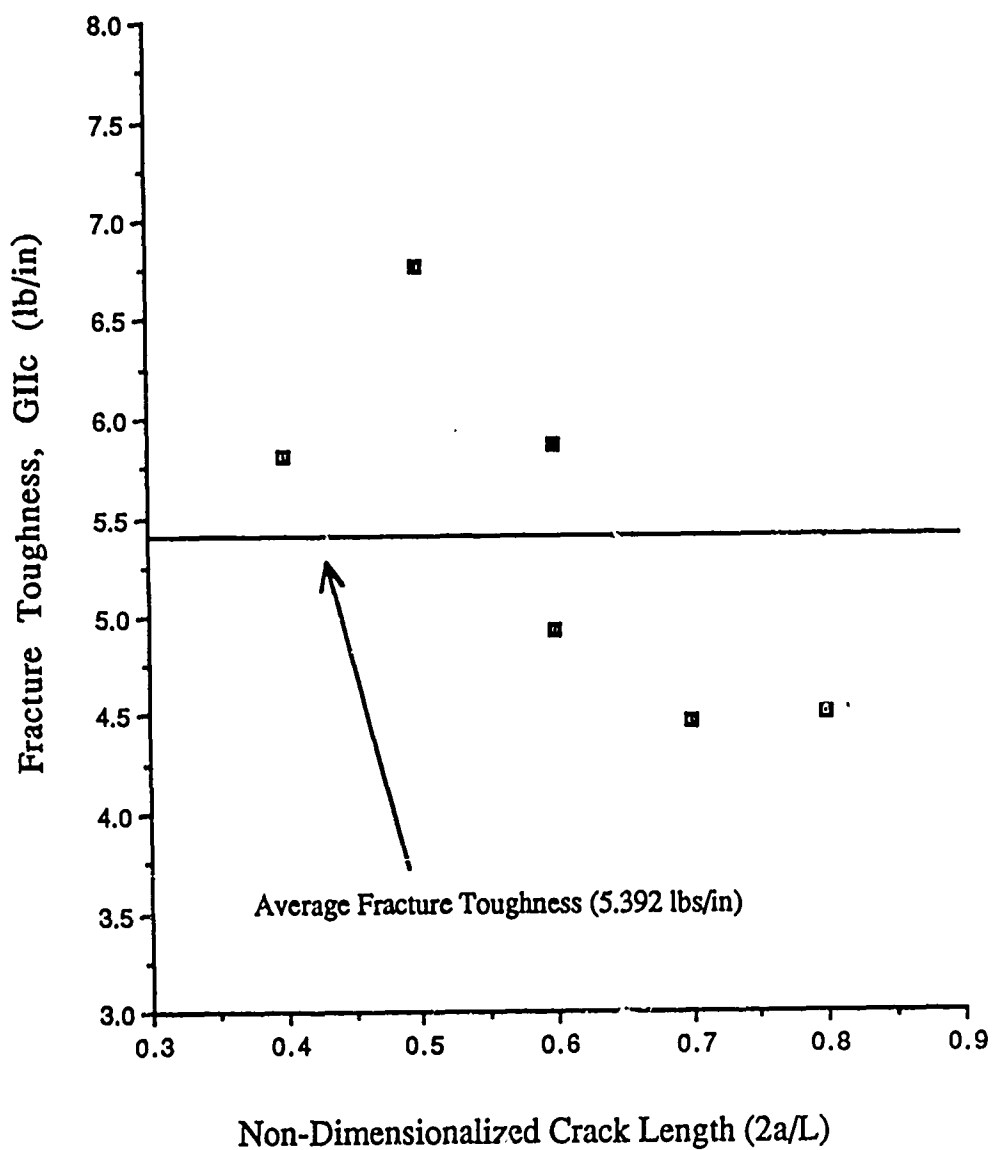
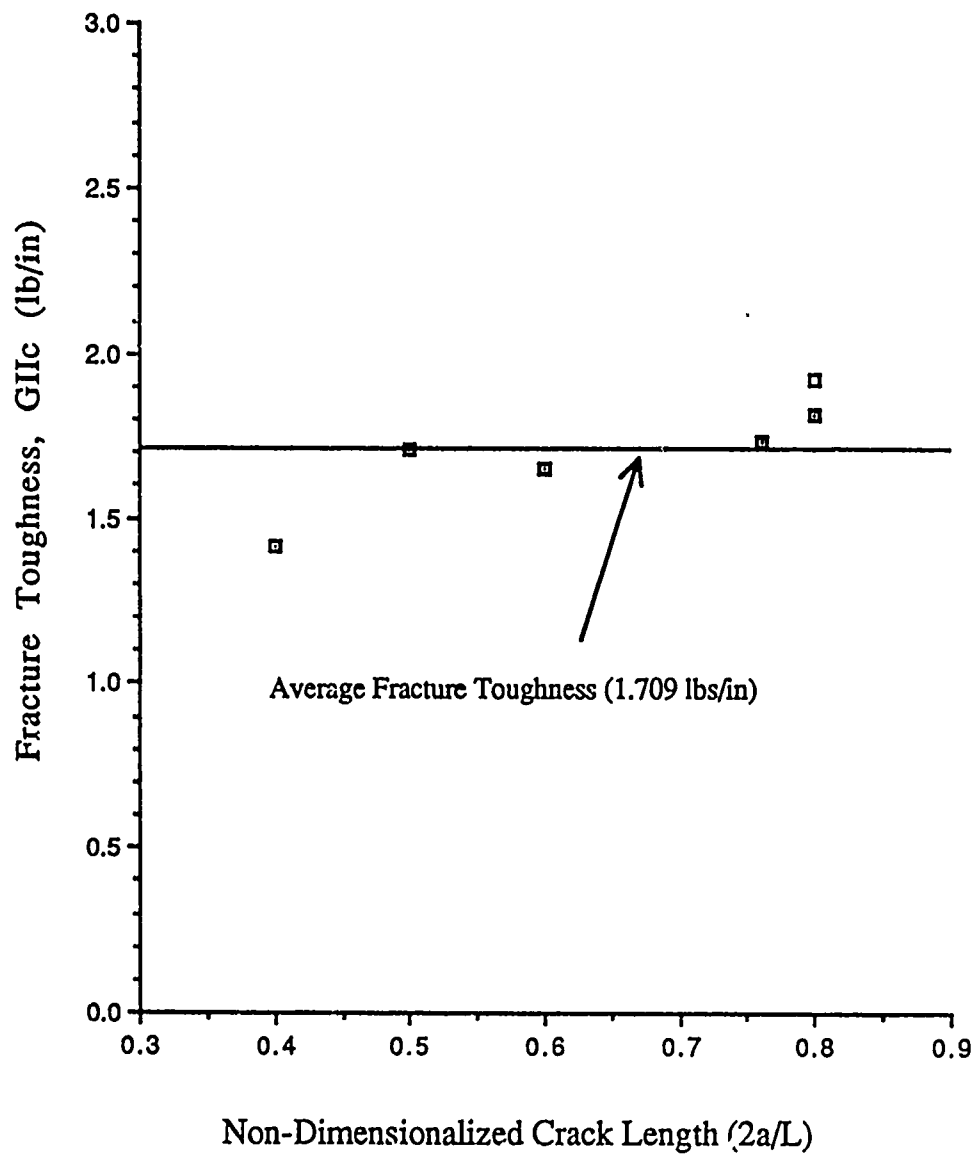Figure 39. Fracture Toughness for 1000° Fahrenheit Based on a
Third Order Curve Fit to the Compliance-Crack Length Relation
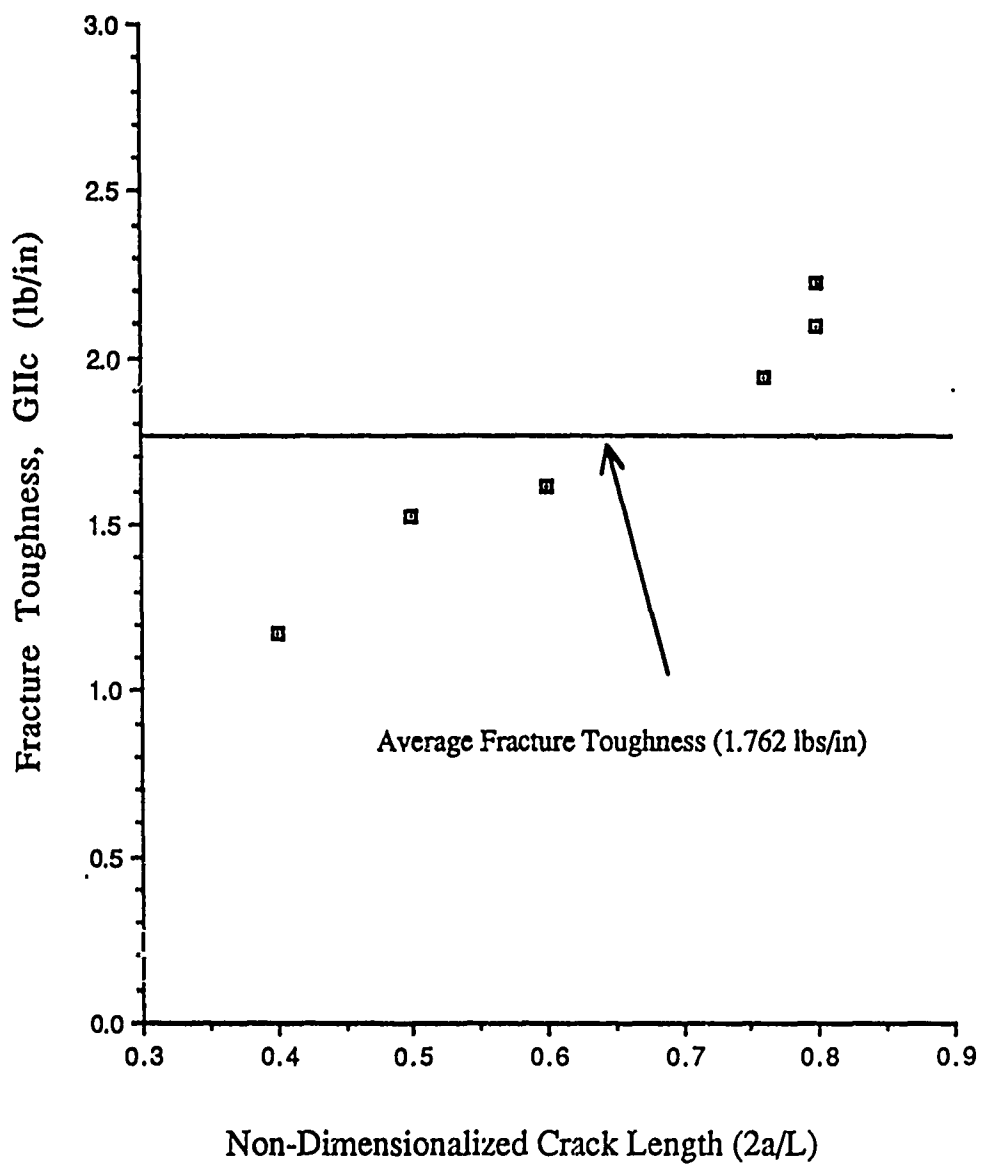(Equation 11)

77
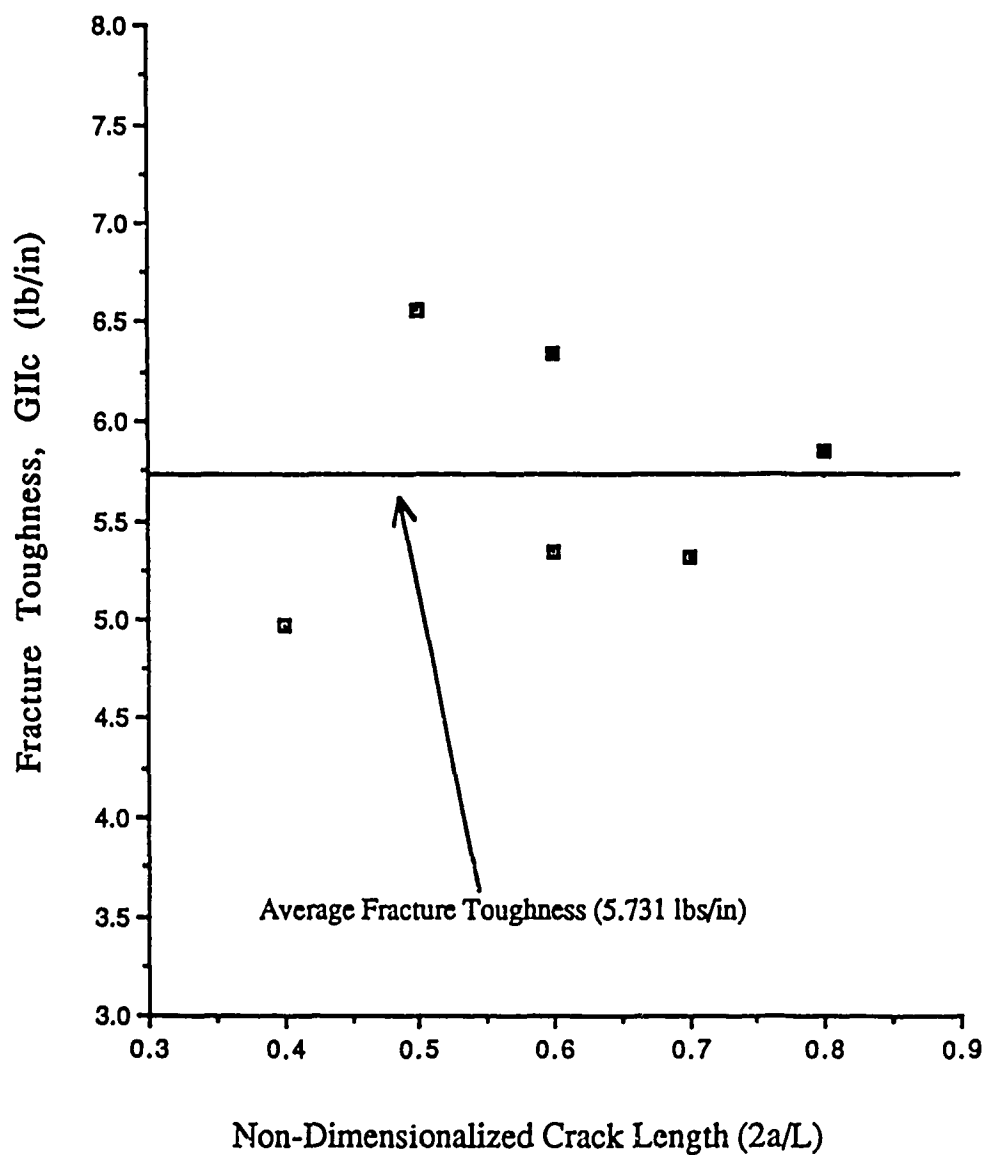
Figure 40.   Fracture Toughness for 1000° Fahrenheit Based on a Truncated Third Order Curve Fit to the Compliance-Crack Length Relation (Equation 12)
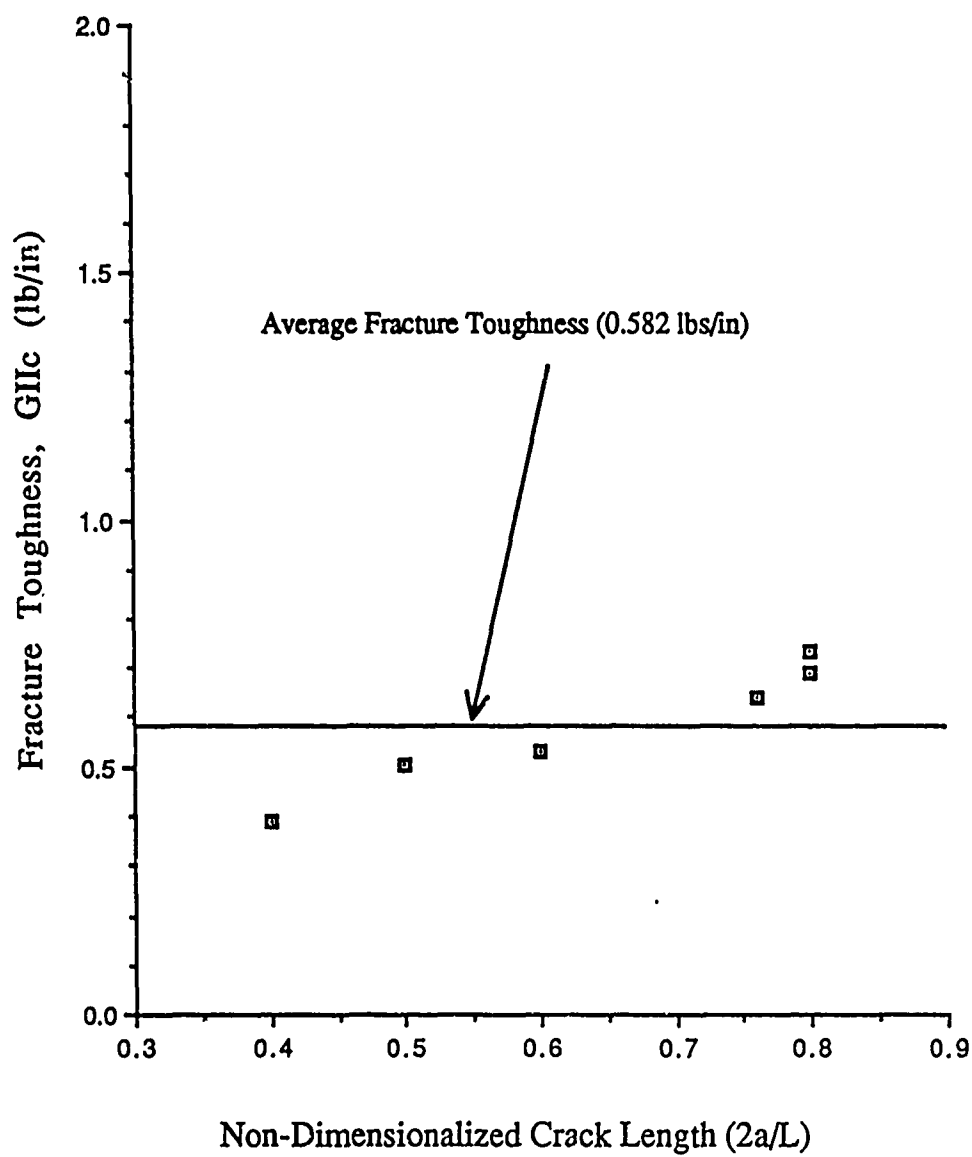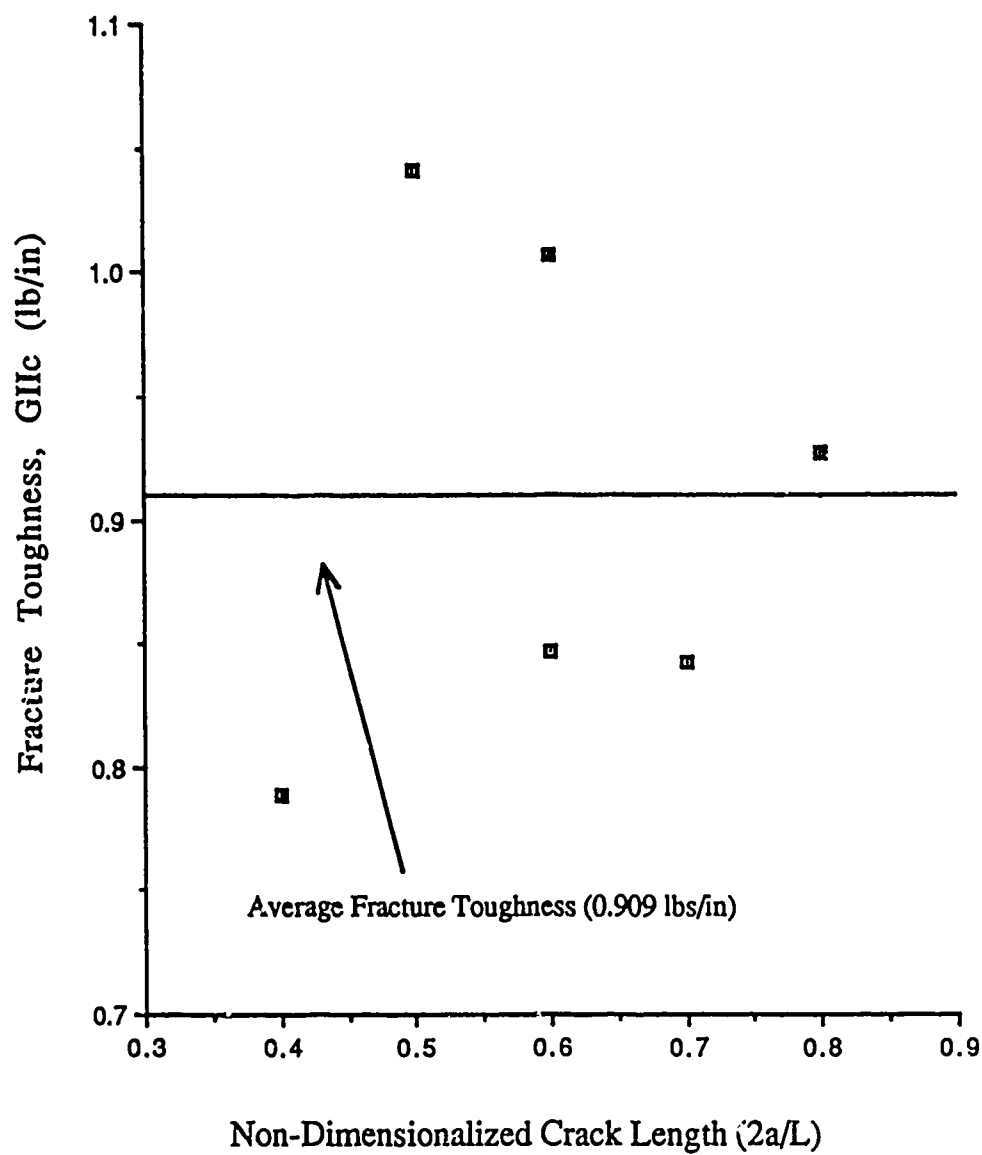
Figure 41. Fracture Toughness for 1000° Fahrenheit Based on a Theoretical Compliance-Crack Length Relation (Equation 14)
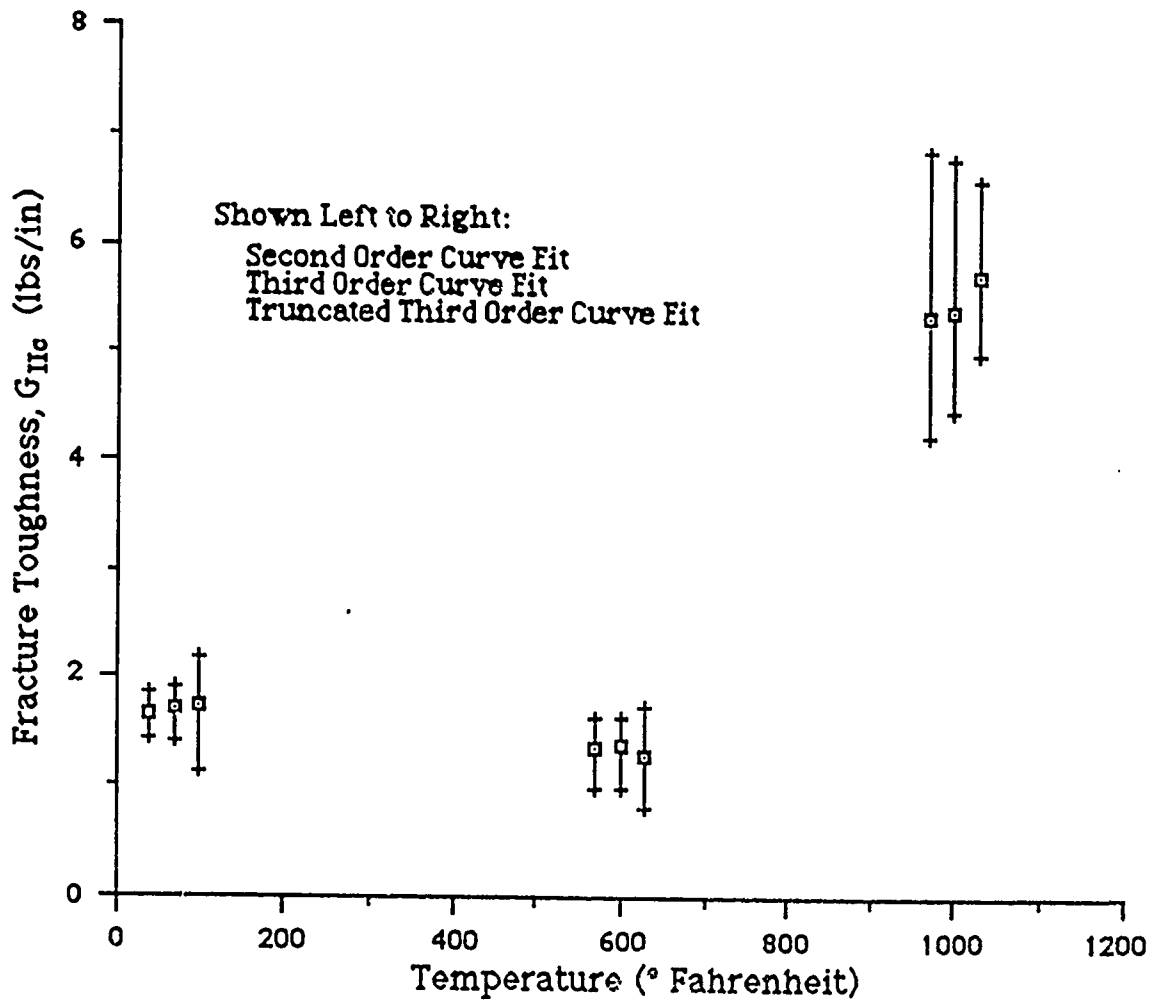
Figure 42. Comparison of Fracture Toughnesses with Change in Temperature

80

Fracture Surfaces

Several specimens, which were cracked to the midpoint during fracture toughness testing, were split open using a Mode I pulling force to examine the fracture surfaces. Since two modes (Mode I and Mode II) of fracture were used to grow the crack (Mode I for pre-cracking and Mode II for determining G_{IIc}), it was hoped that there would be a difference in the fracture surface for the different fracture modes. Figures 43, 44, and 45 show a split open specimen tested at room temperature, 600° F, and 1000° F, respectively. One half of the specimen (the upper portion of the photo in Figures 43 and 44, lower in Figure 45) is laying on its top to expose the fractured surfaces. The notched end of the specimen is on the right. The other half of the specimen is on its side to show the pencil marks
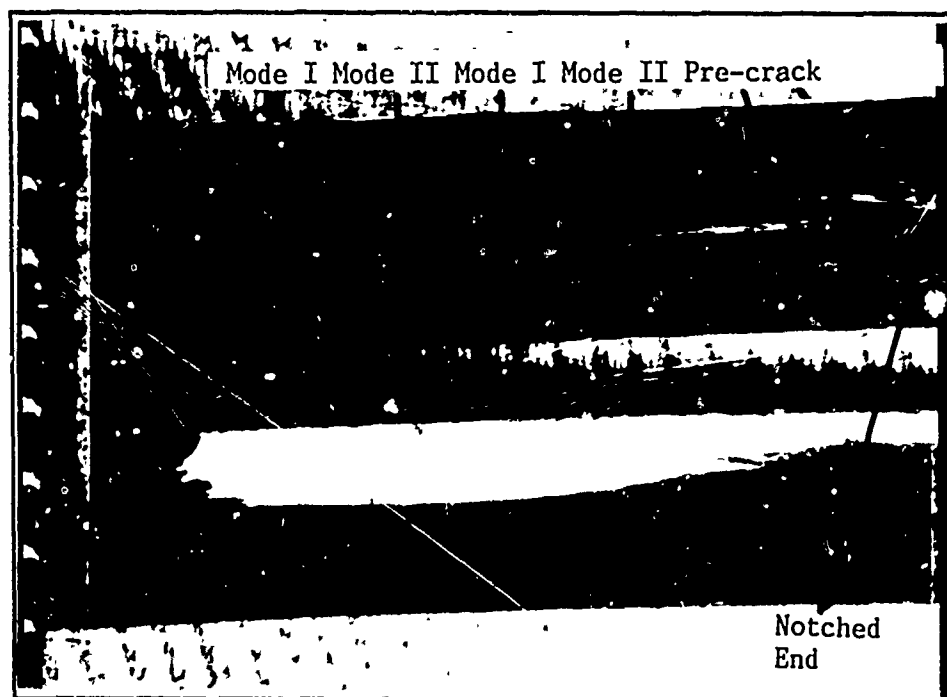
Figure 43. Fracture Surface of Specimen 88C1001A Magnified 6.3X
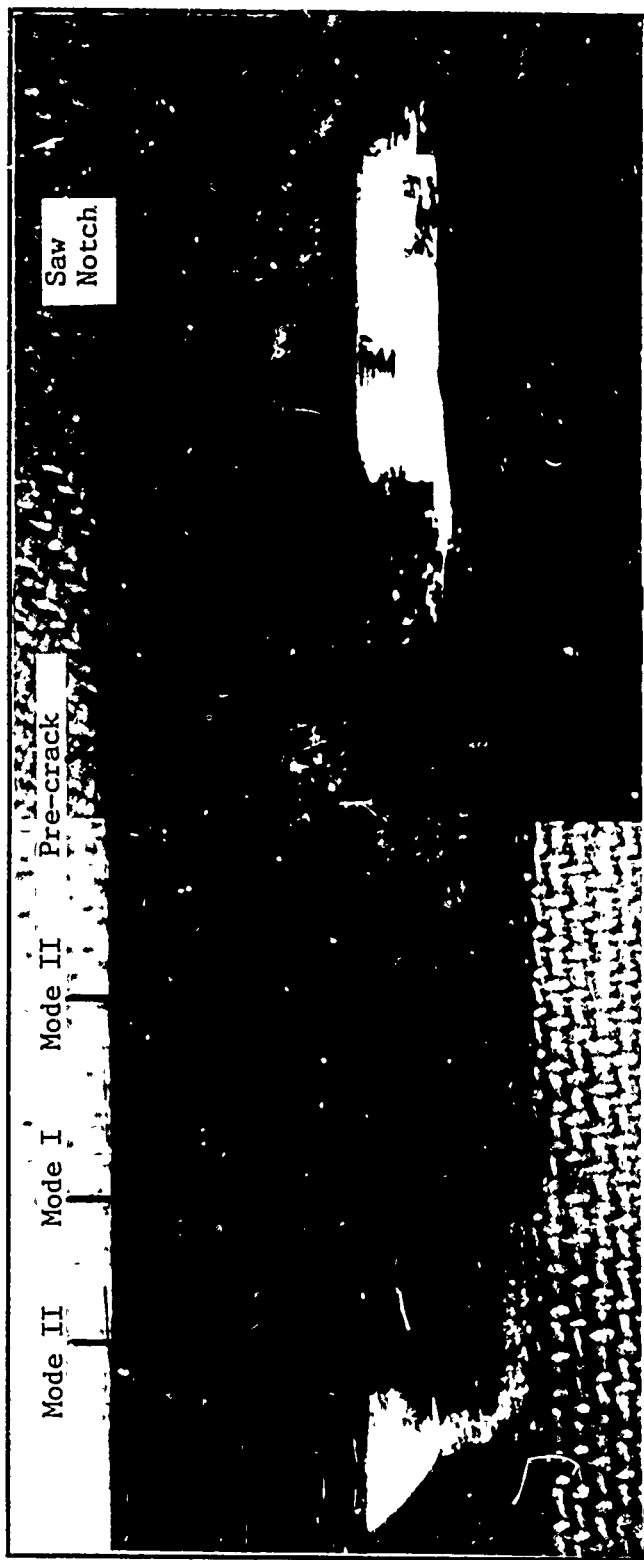
Figure 44. Fracture Surface of Specimen 88C1008 Magnified 6.3X

82
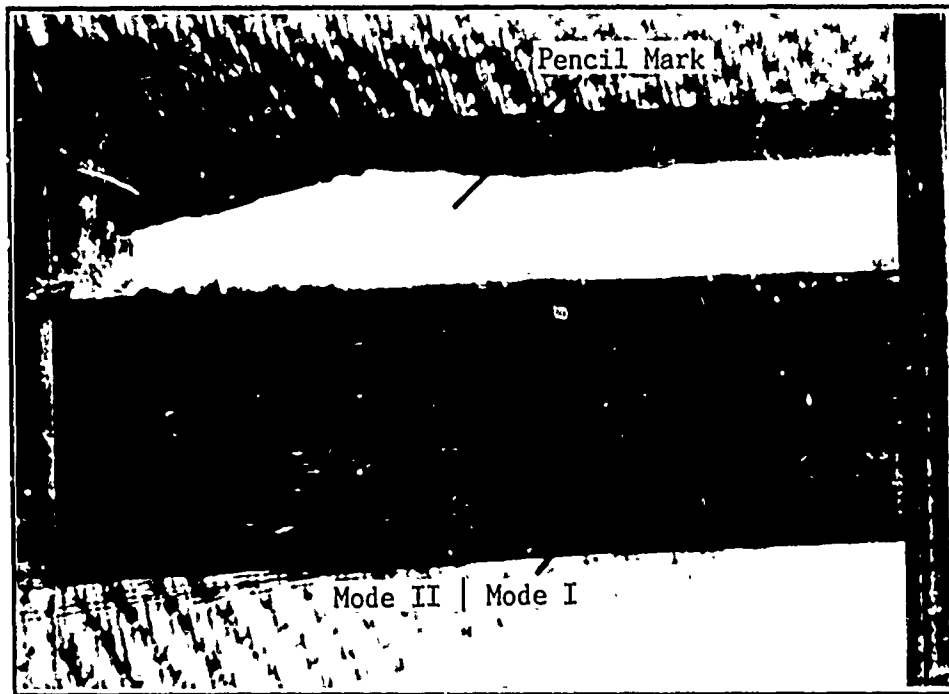
Figure 45. Fracture Surface of Specimen 88C1009 Magnified 6.3X

on the typing correction fluid and to show a side view of how some
of the fibers protrude from the surface. The pencil marks on the
typing correction fluid indicated where the crack tip was thought to
have been when the specimen was marked in the pre-cracking jig.

The pre-crack had a smooth planar surface that blended with
the Mode II fracture surface, indicating a good test. Figure 43 does
not show much difference in coloring or fiber pull-out between Mode
I and Mode II. On the other hand, in Figure 44, light and dark areas
appear on the specimen. They correspond to the pencil marks below
them. The lighter areas indicate Mode I fracture. The lighter areas
are caused by reflection of the photographic lights on the fibers

pulled out of the matrix during Mode I loading. The darker areas indicate Mode II fracture, where there are no fibers pulled out of the matrix because of the brittle behavior and all the fiber failure is in the plane of the fracture surface. Not all specimens showed this distinct difference between modes. This could have been due to the photographic lights not being in as ideal a position to produce the reflection on the pulled out fibers or the pre-crack was not exactly down the neutral axis causing a mixed mode fracture. There would not be a distinct difference in fracture for a mixed mode condition. Figure 46 is a close up of the two failure modes and shows a distinct difference between Modes I and II as discussed above.

Figure 45 shows a different result of the elevated temperature on the specimen. By heating the specimen to 1000° F, the
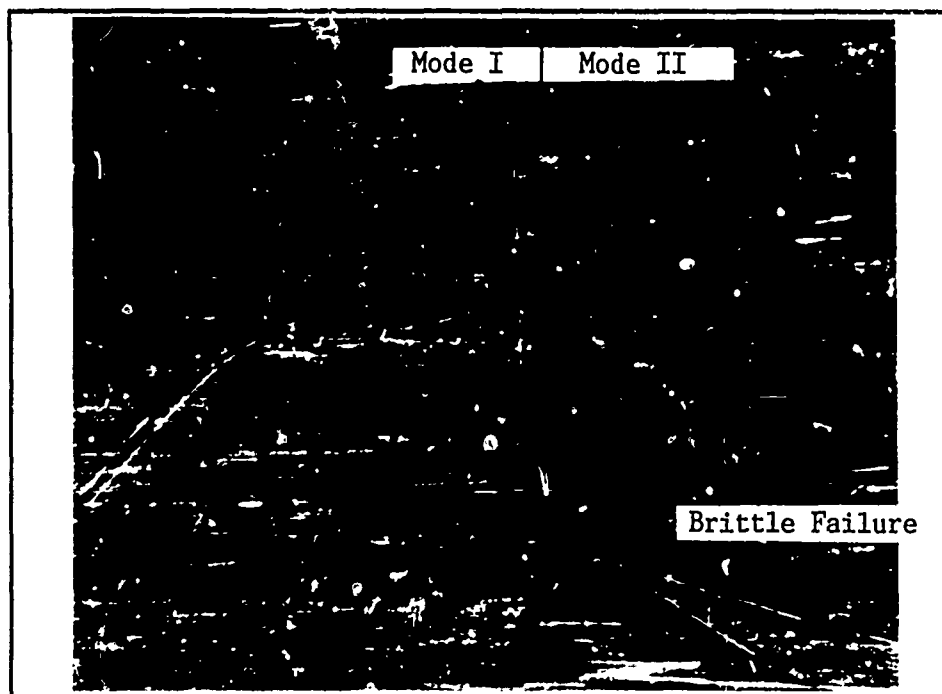
Figure 46. Transition Between Mode I and Mode II Fracture in a Specimen Heated to 600° Fahrenheit (88C1008, Magnified 18X)

Figure 47. Transition Between Mode I and Mode II Fracture in a Specimen Heated to 1000° Fahrenheit (88C1009, Magnified 32X)

composite changed. The increased temperature caused a chemical change in the matrix. This is shown by a change in the color of the specimen from black to a dark shade of gray. Some of this color change can be seen in the Mode I fracture area in Figure 45. Also, the Mode I area is smooth and the Mode II area has much more fiber pull-out. This is exactly the opposite of the 600° F specimen. The smooth Mode I surface was possibly caused at elevated temperature (1000° F) by the matrix "flowing" back over the fibers pulled out during the pre-cracking. The Mode II area shows fiber pull-out that can be explained by matrix failure. The matrix failure allowed fiber bridging, or a layer of fibers mixing with another, which would resist

crack growth, therefore increasing the fracture toughness as experimentally found. Figure 47 shows fragments of failed matrix adhering to the individual fibers in the Mode II area. These fragments were not observed in either the room temperature or 600° F tests (see Figure 48). Figure 49 shows a close up of the Mode I area of the 1000° F specimen, showing the change in color due to the chemical change in the matrix. It appears that the heat has caused crystallization of the matrix, possibly changing the specimen's material properties and causing it to act more ductile during fracture testing.

Figure 48. Blow-up of Mode II Fracture in a Specimen Heated to 600° Fahrenheit (88C1007, Magnified 32X)
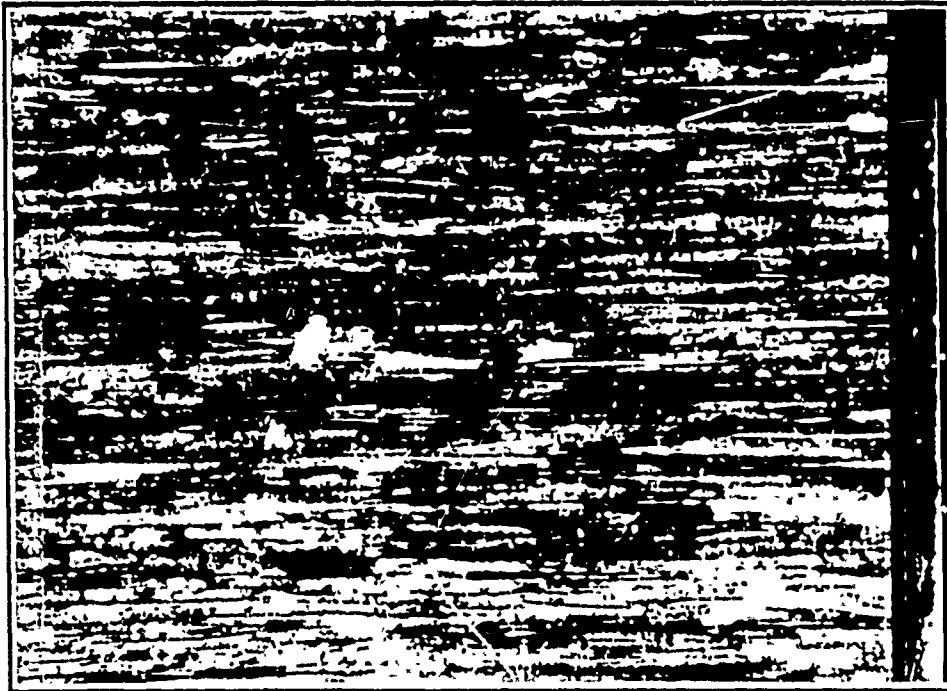
Figure 49. Mode I Fracture in a Specimen Heated to 1000°
Fahrenheit Depicting Color Change in Matrix (88C1009,
Magnified 32X)

To give a larger perspective of the differences between the different specimens, Figures 50 and 51 show the three different temperature specimens side by side. Figure 50 emphasizes the difference in color due to heating of the 1000° F specimen in the middle and the 600° F and room temperature specimen on the left and right, respectively. The small white area at the top of the room temperature specimen on the left is probably due to the shim installed for critical load testing. Figure 51 is of the same three specimens, but at the Mode I/Mode II transition point. Notice the dark area of the 600° F specimen on the left compared to the light area filled with pulled out fibers on the 1000° F specimen both depicting Mode II failure.

Figure 50.   Mode I Fracture in Specimens Heated to 600° F, 1000° F,
and Room Temperature, Left to Right, Respectively.
(88C1007, 88C1009, and 88C1001A Magnified 6.3X)
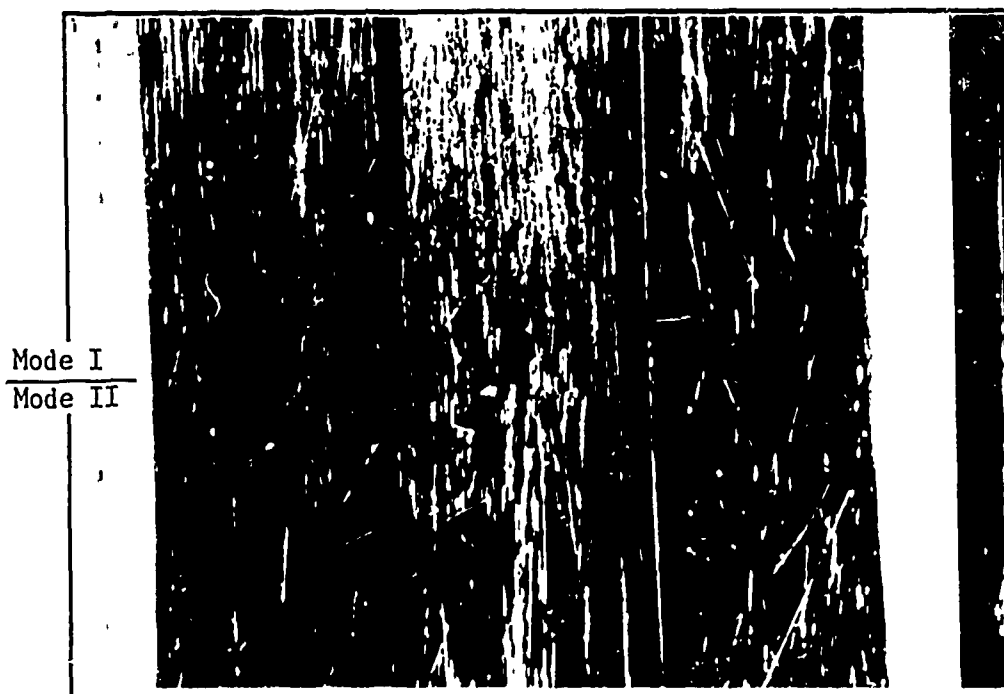
$$\frac{\text{Mode I}}{\text{Mode II}}$$

Figure 51.   Mode I/Mode II Fracture Transition in Specimens Heated
to 600° F, 1000° F, and Room Temperature, Left to Right,
Respectively.(88C1007, 88C1009, and 88C1001A Magnified 6.3X)

Figure 52 shows a specimen where the pre-determined crack tip location is in good agreement with the change in fracture mode inside the specimen. The scale laid next to the specimen is graduated in centimeters, indicating, when converted to inches, a difference of less than 0.004 of an inch or approximately 4% between what was thought to be the cr?   p and where it actually was. This supports the validity of using the typing correction fluid and measuring the pre-crack length under the traveling microscope.
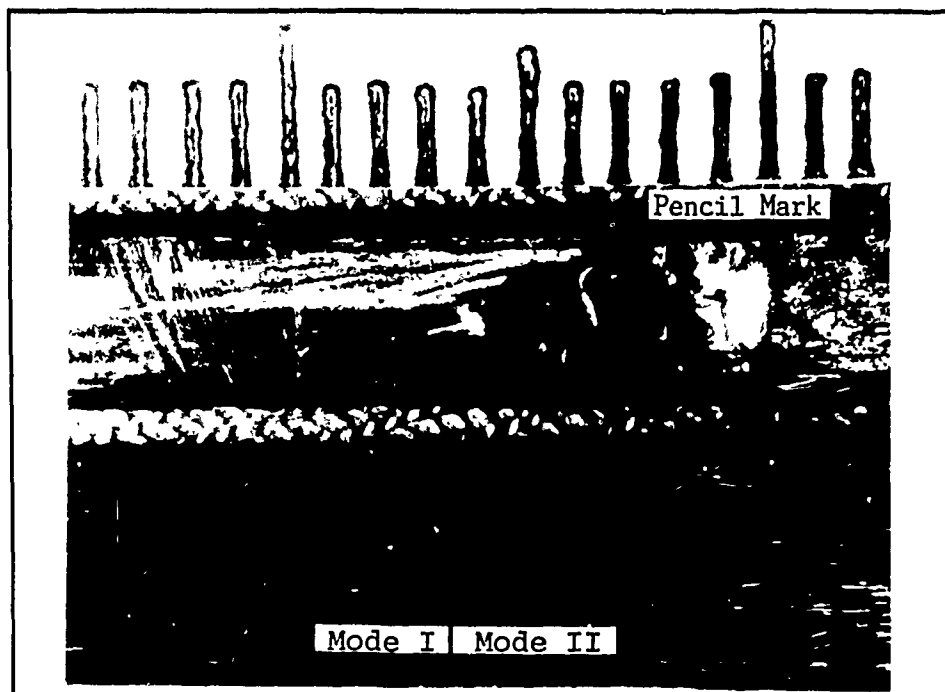
Figure 52. Fracture Surface of Specimen 88C1007 Magnified 6.3X Showing Difference Between Predetermined Crack Length and Actual Crack Length (Small Graduations are Milimeters)

VI. Conclusions and Recommendations

This study's objectives were to design and construct a three point load fixture, develop a technique for finding fracture toughness, and then use that technique to determine the fracture toughness of Corning 1723 ceramic glass matrix composite at temperatures up to 1000° Fahrenheit. Several conclusions and recommendations can be made from the results of this study.

Conclusions

The following conclusions can be made as a result of this study:

1) Three point bend for small end notched flexure specimens is a good test method for determining Mode II fracture toughness.

2) The fracture toughness, or G_{IIc}, of Corning 1723 ceramic glass composite was found for room temperature, 600° F, and 1000° F. The G_{IIc} is lower for 600° F than for room temperature acting more brittle. The G_{IIc} is three times higher for tests run at 1000° F indicating a more ductile behavior of the matrix.

3) Chemical changes, indicated by a change in color and crystal formation, occur at temperatures as low as 1000° F in 1723 Corning Glass Composites.

4) A change in specimen compliance can be used to determine the load where crack growth is first initiated.

5) The analytical expression for compliance when applied to critical strain energy release rate is not suitable for the study of small ceramic glass specimens. Some other expression that more accurately models experimental data needs to be developed.

90

Recommendations

There are several recommendation that can be made as a result of this study. Several components of the experimental setup and load fixture should be changed to increase the reliability, ease of use, and safety of the test setup (see Figure 1). Also, since 1723 Corning Glass Ceramic is a relatively new product, there is a lot of testing that still needs to be done.

1) A computer controlled load machine needs to be used. This would have made testing less painstaking for the present study. It would have eliminated the need to manually take the load off as the specimens were heat soaked. It would also allow the study of specimens under temperature cycling and static or variable loads. Thermal stresses may have a significant affect on ceramic composites.

2) Because of the uncertainties in determining the critical load, a method, such as Vozzola's laser interferometry (41), needs to be developed to work with the thermal equipment. This would require the laser to be shown inside the susceptor or the removal of the susceptor altogether. Crack initiation might be determined by acoustic methods also.

3) The Inconel 718 three point load fixture should be replaced with one constructed of alumina to minimize thermal loading and thermal stress concentrations in the specimen. The fixture should also be articulated to allow for alignment problems or specimen irregularities. Military Standard 1942 (MR) (42) shows an example

of an articulated fixture and Zawada (33) has experience and some suggestions with this kind of fixture.

4) The stainless steel/alumina ram combination should be replaced with a ram entirely made from alumina to minimize thermal loading effects.

5) The alumina ring directly beneath the three point load base should be of a larger diameter so that the load can be distributed to the sides of the stainless steel heat insulator. This would stiffen the load fixture.

6) The LVDT support frame should be modified as in Figure 53. By attaching the LVDT to the top of its support frame and have the LVDT core supported by the spring attached to the LVDT, the effective length of the support frame is shortened making it much stiffer. This will decrease load fixture deflections during testing.
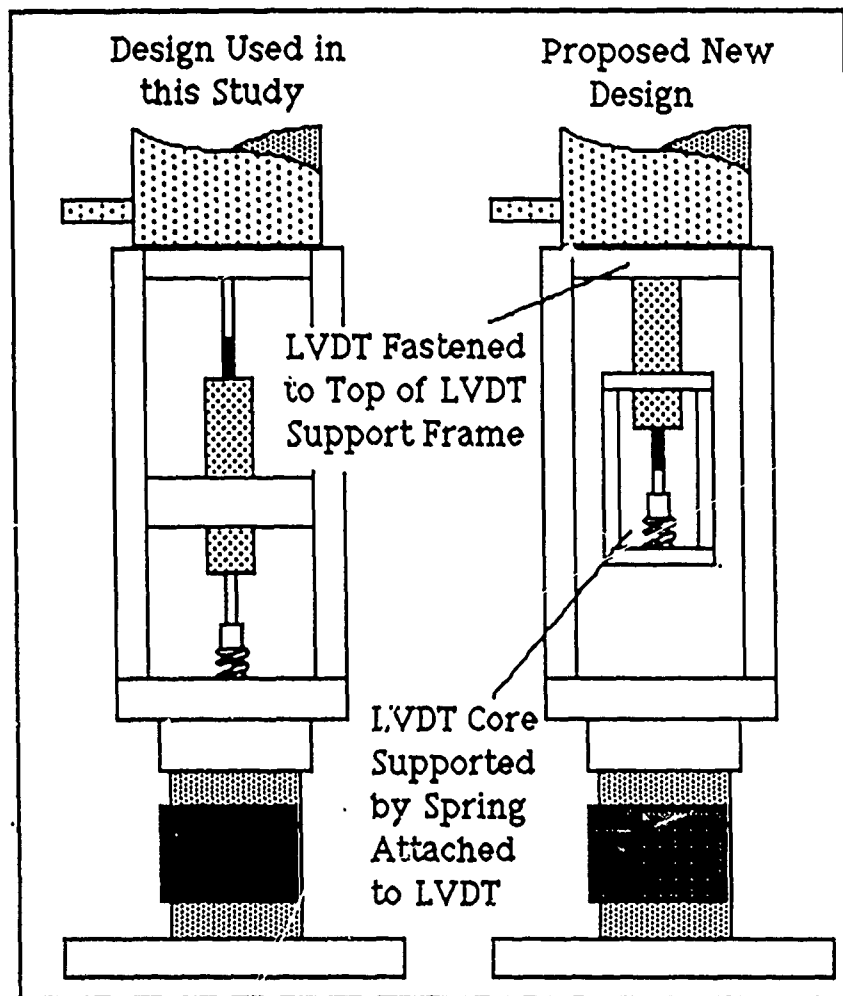
Figure 53. Recommended Changes to LVDT Support Frame to Minimize Measurable Support Frame Flexure

Bibliography

1. "Improved Ceramics Process Opens New Markets," <u>Aviation Week and Space Technology:</u> 71-74 (3 October 1988)

2. Griffith, A.A. "The Theory of Rupture and Flow in Solids," <u>Phil. Trans. Roy. Soc. of London, A221:</u> 163-197 (1921).

3. Griffith, A.A. "The Theory of Rupture," <u>Proc. 1st Int. Congress Appl. Mech., (1924):</u> 55-63. Biezeno and Burgers ed. Waltman, (1925).

4. Irwin, G.R. "Fracture Dynamics," <u>Fracturing of Metals:</u> 147-166, ASM publ. (1948).

5. Broek, David. <u>Elementary Engineering Fracture Mechanics</u> (Fourth Revised Edition): 23-24. The Hague: Martinus Nijhoff Pub. (1984).

6. Jones, Robert M. <u>Mechanics of Composite Materials</u>. New York: Hemisphere Publishing Corporation (1975).

7. Lamicq, P.J., Fernhardt, G.A., Daucher, M.N., Macc, J.G., "SiC/Si Laminar Composite," <u>American Ceramic Society Bulletin, V65:</u> 336-338 (1986).

8. Prewo, Karl M. "The Development of Fiber Reinforced Glass Ceramics," <u>Proceedings of the Conference Tailoring Multipurpose and composite Ceramics,</u> Penn State, July, 1985.

9. Prewo, Karl M., Thompson, E.R. "Research on Graphite Reinforced Glass Matrix Composites," NASA Contractor Report 159312, February, 1980.

10. Prewo, Karl M., Thompson, E.R. Research on Graphite Reinforced Glass Matrix Composites, NASA Contractor Report 165711, May 1981.

11. ASTM Standard E399-78A, "Standard Test Method for Plane-Strain Fracture Toughness of Metallic Materials," *1979 Annual Book of ASTM Standards. Part 10*: 540-561 (1979): Philadelphia.

12. Jenkins, M.G., Kobayashi, A.S., Saka, M., White, K.W., Bradt, R.C. "Fracture Toughness Testing of Ceramics Using a Laser Interferometric Strain Gauge," submitted to the American Ceramic Society Bulletin, June 1986.

13. Russell, A.J. "Factors Affecting the Interlaminar Fracture Energy of Graphite/Epoxy Laminate," *Progress in Science and Engineering of Composites. Proceedings of ICMM-IV*, Tokyo, Japan, 1982, 279-286.

14. Mall, S. and Kochhar, N.K. "Finite-Element Analysis of End-Notched Flexure Specimens." *Journal of Composites Technology & Research. Vol. 8. No.2*, Summer 1986: 54-75.

15. Giare, G.S. "Fracture Toughness of Unidirectional Fiber Reinforced Composites in Mode II," *Engineering Fracture Mechanics. Vol. 20. No. 1*: 11-21 (1984).

16. Jelinek, F.J. "Ceramic Composites," Batelle's Metals and Ceramic Information Center under DOD sponsorship.

17. "Processing Techniques for Fiber-Reinforced Ceramic Matrix Composites," *Ceramic Bulletin. Vol. 65. No. 2*: 297-304 (1986).

18. Rice, R.W. and others, "Refractory-Ceramic-Fiber Composites: Progress, Needs and Opportunities," *Proceedings of the 6th Annual Conference on Composites and Advanced Ceramic Materials*: 698-713. Columbus; The American Ceramic Society (1982).

19. Hasselman, D.P.H. "Elastic Energy at Fracture and Surface Energy as Design Criteria for Thermal Shock," *Journal of the American Ceramic Society. 46* (11): 535-540 (November 1963).

20. Hasselman, D.P.H. "Crack Propagation Under Constant Deformation and Thermal Stress Fracture," *International Journal of Fracture Mechanics, 7* (2): 157-161 (June 1971).

21. Hasselman, D.P.H. "Thermal Stress Resistance Parameters for Brittle Refractory Ceramics: A Compendium," *American Ceramic Society Bulletin, 49* (12): 1033-1037 (December 1970).

22. Kelly, William H., II. *Thermal Shock Resistance of Mullite-Based SiC- Whisker Composites.* MS Thesis, AFIT/GAE/AA/86D-6, School of Engineering, Air Force Institute of Technology (AU), Wright-Patterson AFB OH, December 1986.

23. Valentine, Peter G. *Strength and Thermal Shock Resistance of SiC-BN Composites.* MS Thesis, AFIT/GAE/AA/83D-27, School of Engineering, Air Force Institute of Technology (AU), Wright-Patterson AFB OH, December 1983.

24. Prewo, K.M. "Silicon Carbide Yarn of New Composites," *Composites Review:* 69-71.

25. Prewo, K.M., Brennan, J.J. "Silicon Carbide Fiber Reinforced Glass-Ceramic Matrix Composite Exhibiting High Strength and Toughness," *Journal of Materials Science 17:* 2371-2383 (1982).

26. Prewo, K.M., Brennan, J.J. "Silicon Carbide Yarn Reinforced Glass Matrix Composites" *Journal of Materials Science 17:* 1201-1206 (1982).

27. Prewo, K.M. "A compliant, High Failure Strain, Fiber-Reinforced Glass Matrix Composite," *Journal of Materials Science 17:* 3549-3563 (1982).

28. Strife, J.R., Prewo, K.M. "Silicon Carbide Fiber-Reinforced Resin Matrix Composites," *Journal of Materials Science 17:* 65-72 (1982).

29. Prewo, K.M., Brennan, J.J. "High Strength Silicon Carbide Fiber Reinforced Glass-Matrix Composites," *Journal of Materials Science 15:* 463-468 (1980).

30. Prewo, K.M., Brennan, J.J., Layden, G.K. "Fiber Reinforced Glasses and Glass-Ceramics for High Performance Applications," <u>Ceramic Bulletin, Vol. 65, No. 2:</u> 305-313 (1986).

31. Prewo, K.M. "Fiber Reinforced Metal and Glass Matrix Composites," Presented at the Distinguished Lecture Series "Frontiers in Materials Science," Sandia National Labs, Oct. 1983

32. Prewo, K.M., Minford, E.J. "Graphite Fiber Reinforced Thermoplastic Glass Matrix Composites for Use at 1000°F," <u>Proceedings of the Sixteenth National Sampe Conference,</u> Albequerque, NM, Oct. 1984.

33. Zawada, L.P., Ceramic Engineer, Metals and Ceramic Division. Personal interviews. AFWAL/MLLN, Wright-Patterson AFB, Ohio, 4 Feb.-6 Nov. 1988.

34. ASTM Standard Practice E561-81, "Standard Practice for R-Curve Determination," <u>1982 Annual Book of ASTM Standards,</u> <u>Part 10:</u> 680-699 (1982): Philadelphia.

35. ASTM Standard D790-84a, "Standard Test Methods for Flexure Properties of Unreinforced and Reinforced Plastics and Electrical Insulating Materials," <u>1985 Annual Book of ASTM</u> <u>Standards, Section 8</u>: 397-409 (1985): Philedelphia.

36. Kobayashi, Albert S. <u>Experimental Techniques in Fracture</u> <u>Mechanics</u>. Ames, Iowa: The Iowa State University Press andWestport, Connecticut: Society for Experimental Stress Analysis, 1973.

37. Koboyashi, Albert S. <u>Experimental Techniques in Fracture</u> <u>Mechanics, 2</u>. Ames, Iowa: The Iowa State University Press and Westport, Connecticut: Society for Experimental Stress Analysis, 1975.

38. Wiederhorn, S.M. "Brittle Fracture and Toughening Mechanics in Ceramics," <u>Annual Review of Material Science 14</u>: 373-403 (1984).

39. Lankford, James, Jr. "Characterization of Mechanical Damage Mechanisms in Ceramic Composite Materials," ONR Contract No. N00014-84-C-0213, June 1985.

40. Marshall, D.B. and Evans, A.G. "Failure Mechanisms in Ceramic-Fiber/Ceramic-Matrix Composites," Journal of the American Ceramic Society, Vol. 68, No. 5: 225-231 (1985).

41. Vozzola, Robert P. Fracture Toughness Testing of a Ceramic Matrix Composite. MS Thesis, AFIT/GAE/AA/87D-24, School of Engineering, Air Force Institute of Technology (AU), Wright-Patterson AFB, OH, December.

42. Department of the Army. Flexure Strength of High Performance Ceramics at Ambient Temperatures. Military Standard 1942 (MR), Army Materials and Mechanics Research Center, Watertown, MA: 21 November 1983.

43. Torvik, Peter J., Professor and Head, Department of Aeronautics and Astronautics. Personal interviews. AFIT (AU), Wright-Patterson AFB, Ohio, August, 1988.

44. Vozzola, Robert P., Captain. Personal interviews. Wright-Patterson AFB, Ohio, July, 1988.

45. Chai, H. and Mall, S. "Design Aspects of the End-Notched Adhesive Joint Specimen," International Journal of Fracture 36: R3-R8 (1988).

Appendix A: LVDT Calibration

Because the Linear Variable Differential Transformer (LVDT) and associated equipment used in this study were unproven, it was desirable to calibrate the equipment before and after each day of tests. Observing the voltage output of the LVDT on a multimeter, a slow drift of 40mv/hr after an initial warm-up of 30 minutes was observable. The drift was assumed to be constant since it was so slow. By making this assumption it was possible to interpolate the deflection-voltage output for any given time during the day. Figure 54 shows typical LVDT calibration curve fits for the data taken at the beginning and end of the day. The procedure in Chapter 4 was used for calibration. Voltage output readings were taken every 0.0005 inches, 16 times for a total deflection of 0.008 inches. This was approximately twice as much displacement than would be seen during actual tests. The number next to the data designator was the time the calibration was made. The slope of the curve fit was used as the relationship between displacement and voltage output used in calculating the midpoint deflection for compliance.

In running the room temperature and 600° F tests, a total of 46 calibrations were taken with average slope being 11.089 volts/0.001in and the standard deviation being 0.2824816. For the range of deflection used in this study, that amounts to a 2.6% change in compliance. This is small enough to keep 11.089 volts/0.0001in as the deflection-voltage relation, but calibration should be done prior to testing for the day to ensure that settings were not altered.
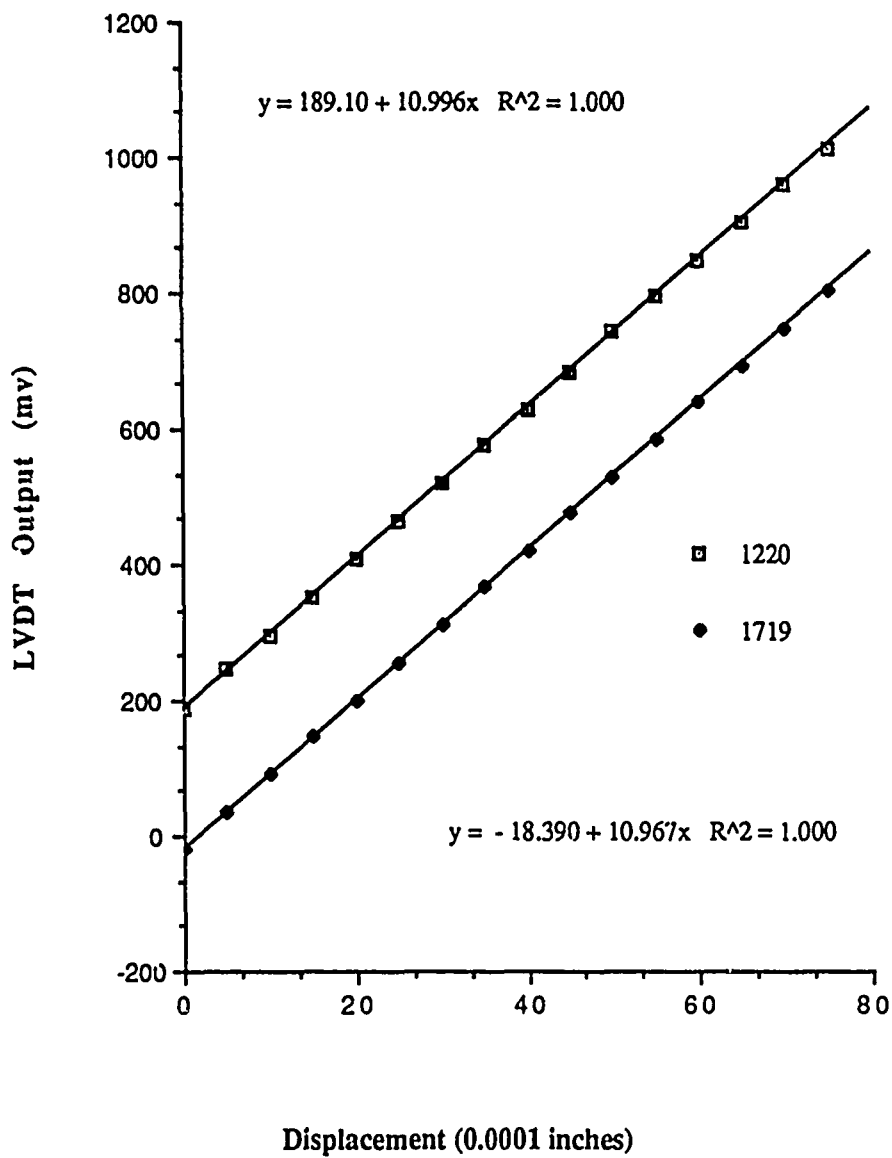
Figure 54. Sample LVDT Calibration Curve Fit

Appendix B: Spreadsheet for Reducing Data

A spreadsheet was used for calculating the repetitive data of this study. Figure 55 shows an example spreadsheet for calculating the compliance of a typical specimen at 1000° Fahrenheit. This appendix will explain each part of the sample spreadsheet.

Heading: Includes the date and type test, i.e. compliance, P critical, etc..

Specimen: Used for identification and determining required dimensions.

Crack Length: Used for identification and calculation of Young's Modulus for 0.0 crack lengths using Equation 6.

Specimen Dimensions: The average of the height and width are used. They normalize the compliance using Equation 5.

LVDT Slope: Start and Final are used for determining displacement as explained in Appendix A.

Load Cell Slope: Calculated by Instron personnel. It is the slope of the load-voltage output relation.

Number of Runs: Used for calculating the average compliance.

Run: The time the run was started. Used in interpolating the LVDT slope for that particular time.

Y and X Axis Scale: The scales set on the X-Y plotter.

Rise & Run: This is the plotted data from the X-Y plotter. Data split into left and right. Procedure for choosing points described in Appendix C.

Compliance: The midpoint displacement divided by the load. Actually, the differences in the left and right run times the

101

interpolated LVDT slope over the differences in the left and right rise times the load cell slope.

Compliance K Corrected: It is the compliance calculated by first subtracting the deflection of the load fixture from both the left and right run. The amount subtracted depends on the curve fit for the temperature of test described in Chapter 3.

Normalized Compliance: This is the compliance that has been corrected for the load fixture compliance and then multiplied by the necessary factor to consider the variation in specimen dimensions using Equation 5.

E_{11}: Only good for the no crack tests. Uses Equation 6 and the normalized compliance to calculate Young's Modulus.

Average E: Average Young's Modulus. Good only for no crack tests.

Average C: Average normalized compliance.

Compliance Calculation , 11 Nov 88, 1000° F		
Specimen	88C1011	
Crack Length	0.3	
Specimen Heights	0.3004	
	0.3005	0.30045
Specimen Widths	0.1778	
	0.1773	0.17755
Start LVDT Slope (v/0.0001in)	10.8815	
Final LVDT Slope (v/0.0001in)	11.0379	
Load Cell Slope (mv/lbs)	1.61	
Number of Runs	1	
Run	2130	
Y axis scale (mv/in)	50	
X axis Scale (mv/in)	20	
Rise (in) Left/Right	2	6.73
Run (in) Left/Right	3.85	14
Compliance (in/lbs)=	1.2521556E-5	
Compliance K Corrected (in/lbs)=	1.1330653E-5	E11
Normalized Compliance (in/lbs)=	1.0104119E-5	1.694853E+07
Run	2028	
Y axis scale (mv/in)	50	
X axis Scale (mv/in)	20	
Rise (in) Left/Right	2	6.67
Run (in) Left/Right	3.31	13
Compliance (in/lbs)=	1.2123033E-5	
Compliance K Corrected (in/lbs)=	1.0927391E-5	E11
Normalized Compliance (in/lbs)=	9.7445108E-6	1.757400E+07
Average E	3.45225E+07	
Average C	1.9848630E-5	

Figure 55.   Sample Spreadsheet for a 1000° Fahrenheit,
0.3 Inch Crack, Compliance Test

103

Appendix C: Typical Compliance Curves

This appendix will describe the method for determining the compliance from the voltage outputs of the LVDT and load cell. A straight line curve fit was required since the compliance is a material property. Figures 56, 57 and 58 show typical outputs from the X-Y plotter reduced 50%. The first example has four room temperature plots on it of compliance measured with an initial 0.075 inch crack. Each curve has a time next to its start. The time is the moment the test was started and is used for identification and for calculating the interpolated displacement-voltage output relationship discussed in Chapter 4 and Appendix A. The first plot was in position 1, the second in position 2, and so forth. The position number relates to Figure 14 in Chapter 4 and indicates the test was made with the specimens notch to the right and pre-crack markings to the front. The scale used on the Y-axis was 50 mv/in and the X-axis was 20 mv/in. The X-Y plotter was "zeroed" to a zero displacement and a 20 mv load which corresponded to the pre-load set on the specimen. Since this example was for compliance, the specimen was loaded to approximately 50% of its critical load which coincided with the end of the graph paper. It was then unloaded. This was done four times and the average taken to acount for the pre-crack not being exactly on the neutral axis and any alignment problems with the load fixture. One can observe how the plots seem to come in pairs, positions 1 and 2, and positions 3 and 4. This justifies using the average of positions 1 and 2 for the compliance, but it was

determined that there was not enough of a difference between positions 1 and 2, and positions 3 and 4 to justify run the latter two. Therefore, all of the elevated temperature tests only used positions 1 and 2 as shown in Figures 57 and 58. The one additional run in Figure 57 was used to prove that a 20 minute heat soak was sufficient. Notice there is little difference between the slope of the first curve that had a 20 minute heat soak and the second curve that had a 50 minute heat soak.

Determining the compliance involved fitting a straight edge to the right two-thirds of the loading slope ignoring the first one-third. This initial non-linearity can be attributed to settling of the specimen on the rollers and settling of the load fixture setup. The rise and run of a left and right point on the straight line fit was recorded for use in calculating the compliance as explained in Appendix B. Points could be measured beyond the limits of the actual load-displacement curve since only the slope was of importance. The hysteresis is due to the load machines changing direction of the cross-head.
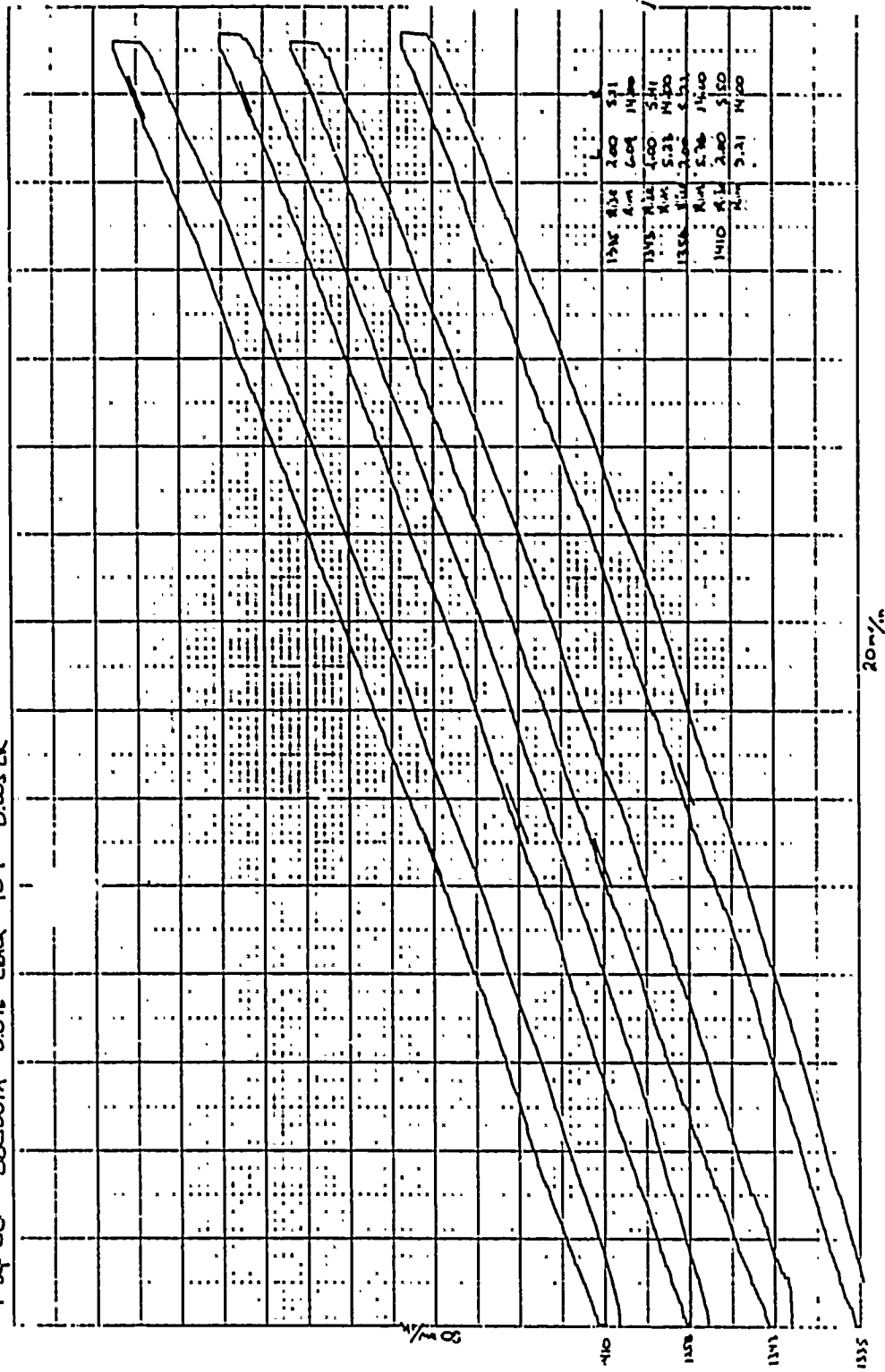
Figure 56. Typical Room Temperature Compliance Curve Plots

106

Figure 57. Typical Compliance Curves for Test at 600° Fahrenheit
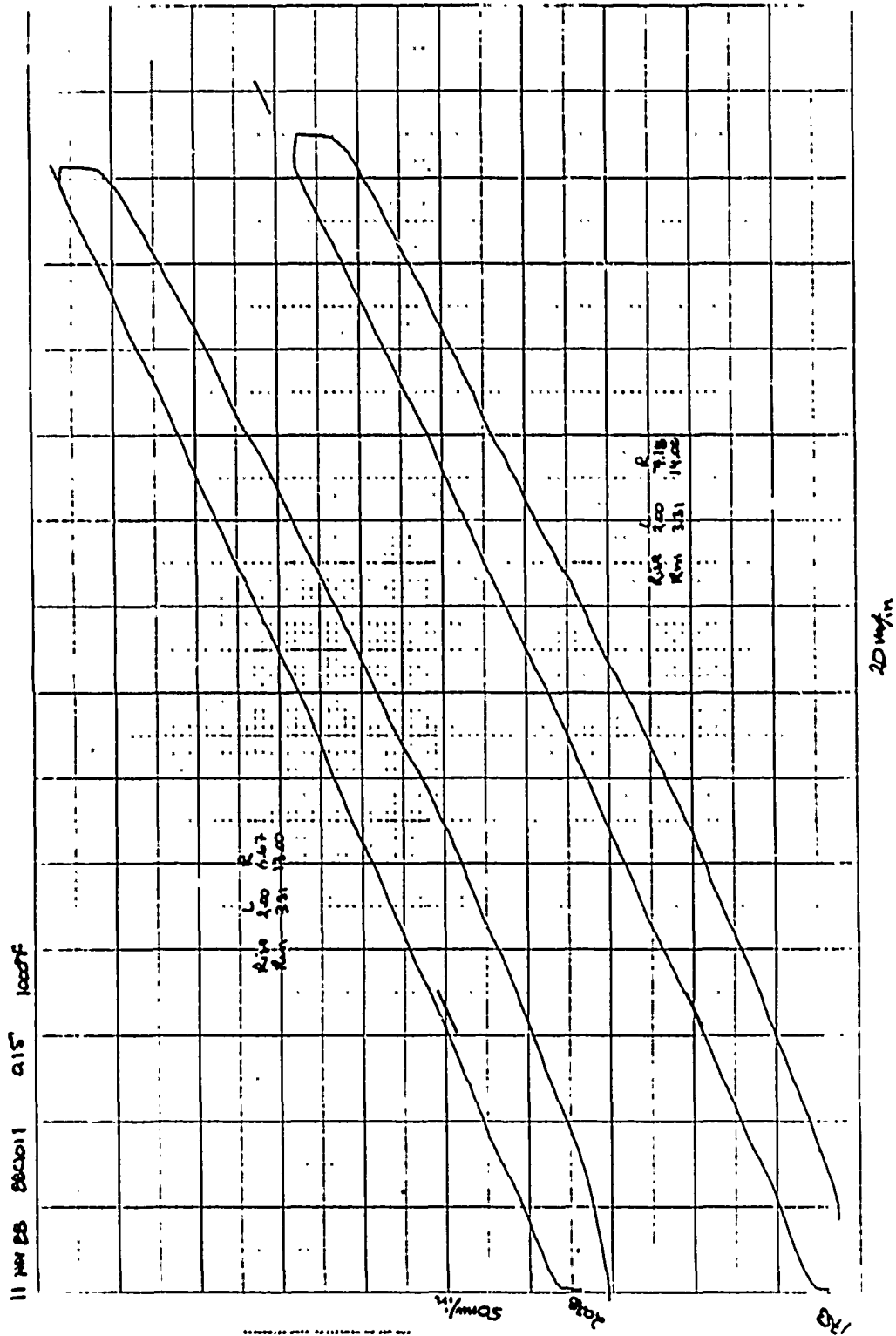
107

Figure 58. Typical Compliance Curves for Test at 1000° Fahrenheit

108

Appendix D: P Critical Curves

Attached are three example curves for determining the critical load for a specimen (Figures 59, 60, and 61). Depending on the scale of the X-Y plotter and the specimen, some critical loads were easy to determine and others were difficult. Figure 59 shows a room temperature test done on a specimen with a long crack (0.6 inches). The X-Y plotter setup was the same as described in Appendix C but the X-axis scale was 50 mv/in rather than 20 mv/in. This allowed for the larger displacements which were anticipated for the critical load test. The curve can be split into thirds. The first third was non-linear and can be attributed to the settling of the specimen and load fixture. The second third is linear. All critical load tests also checked compliance to ensure that the specimen was behaving as before. The last third of the curve shows two definite changes in compliance. The first change in compliance indicates the critical load required for initiating crack growth.

Figure 60 shows the critical load test for a specimen at 600° F with a crack length of 0.45 inches. This curve also has a change in compliance, but due to the scale of the plot which was required due to the expected critical load, it was very difficult to determine precisely were the critical load was. In this case a straight line was fit to the middle of the curve to get the compliance. Then a second curve was fit to the next flat section of the curve. Where the two straight lines intersected was used as the critical load. This curve

shows the need for another method for determining the critical load such as laser interferometry or acoustics.

Figure 61 is of a critical load test at 1000° F of specimen 88C1011 with an effective crack length of 0.375 inches. It too shows the need for a more definitive method for determining the critical load.
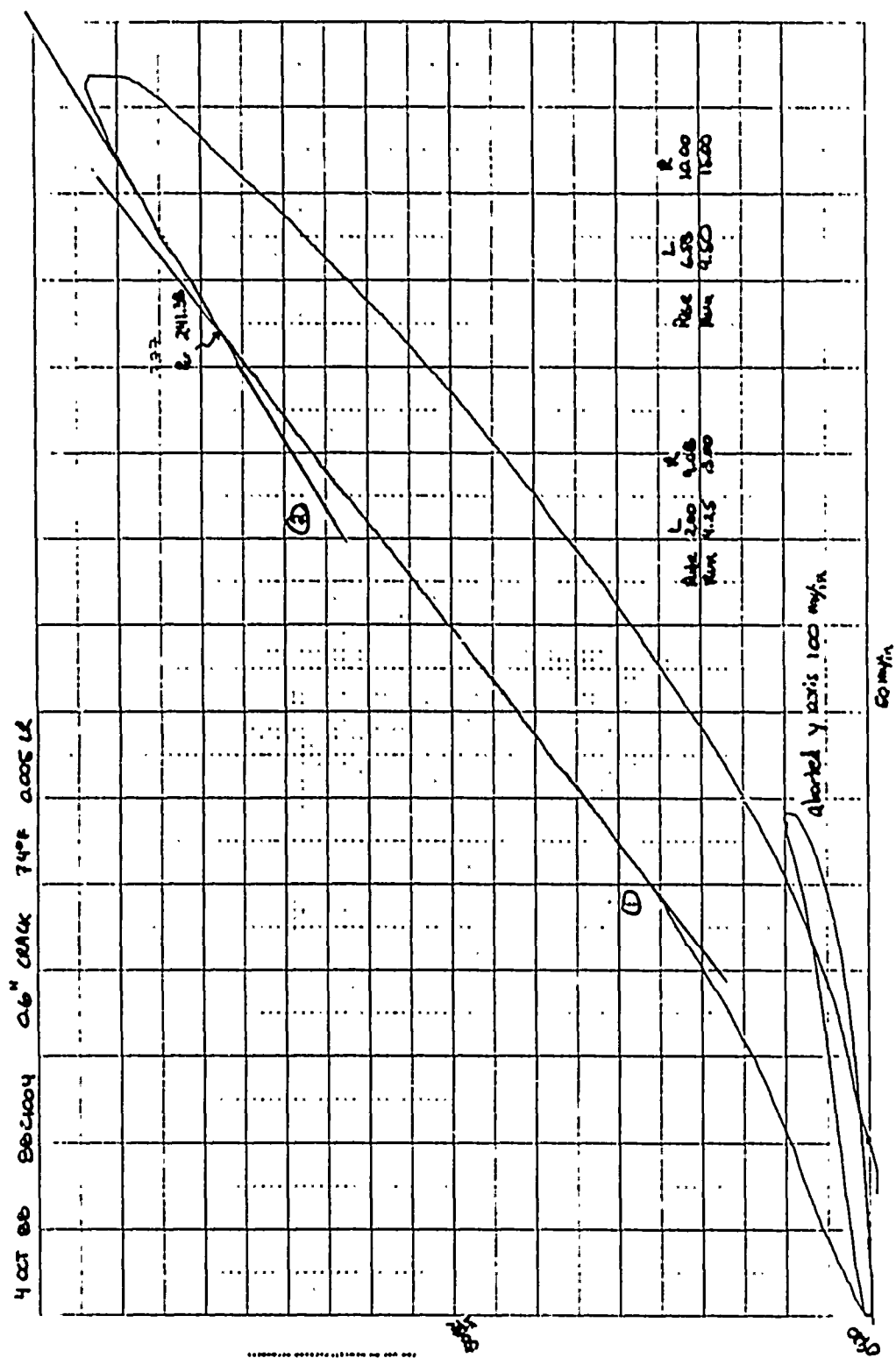
Figure 59. Typical Critical Load Curve for a Specimen at Room Temperature
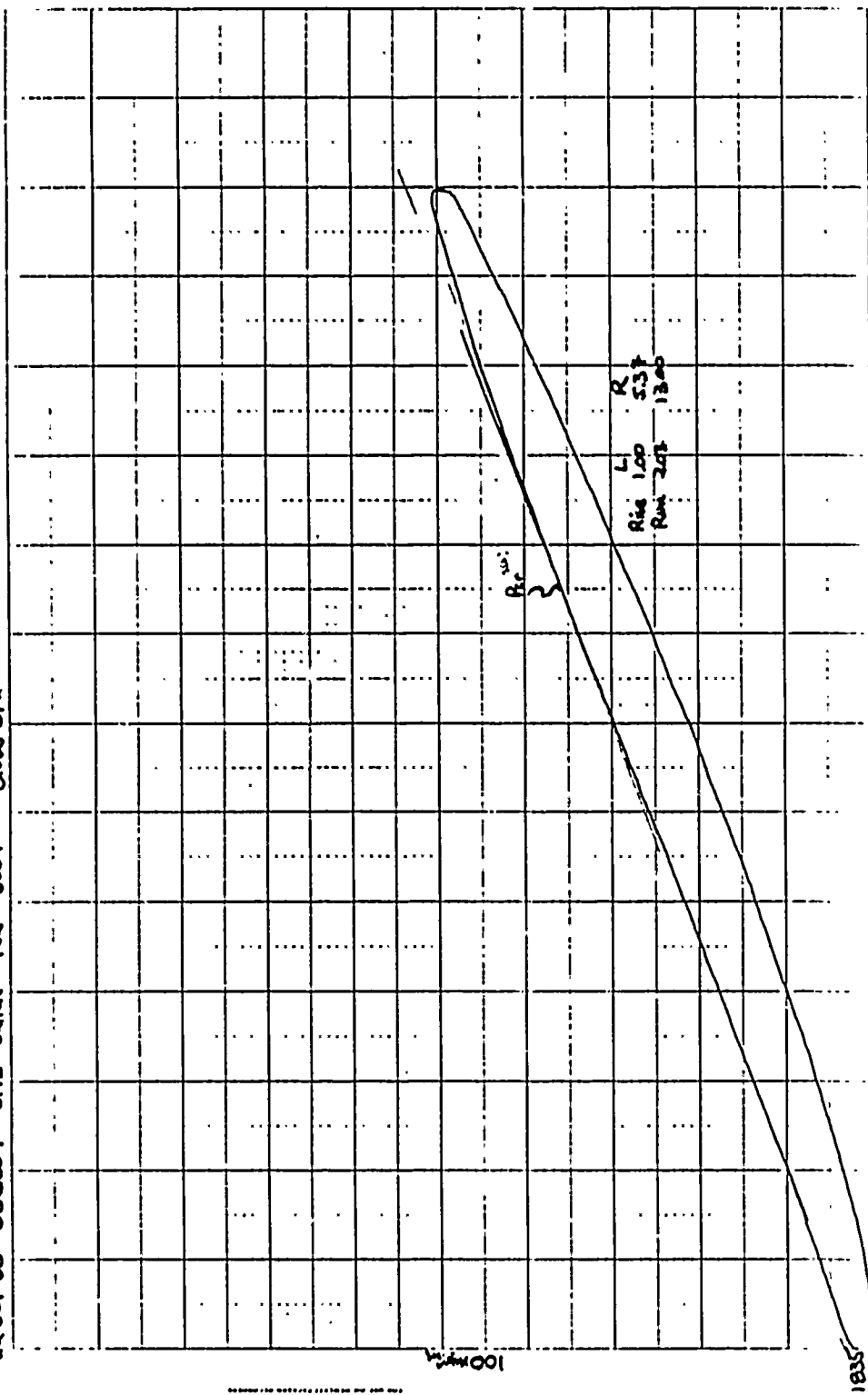
111

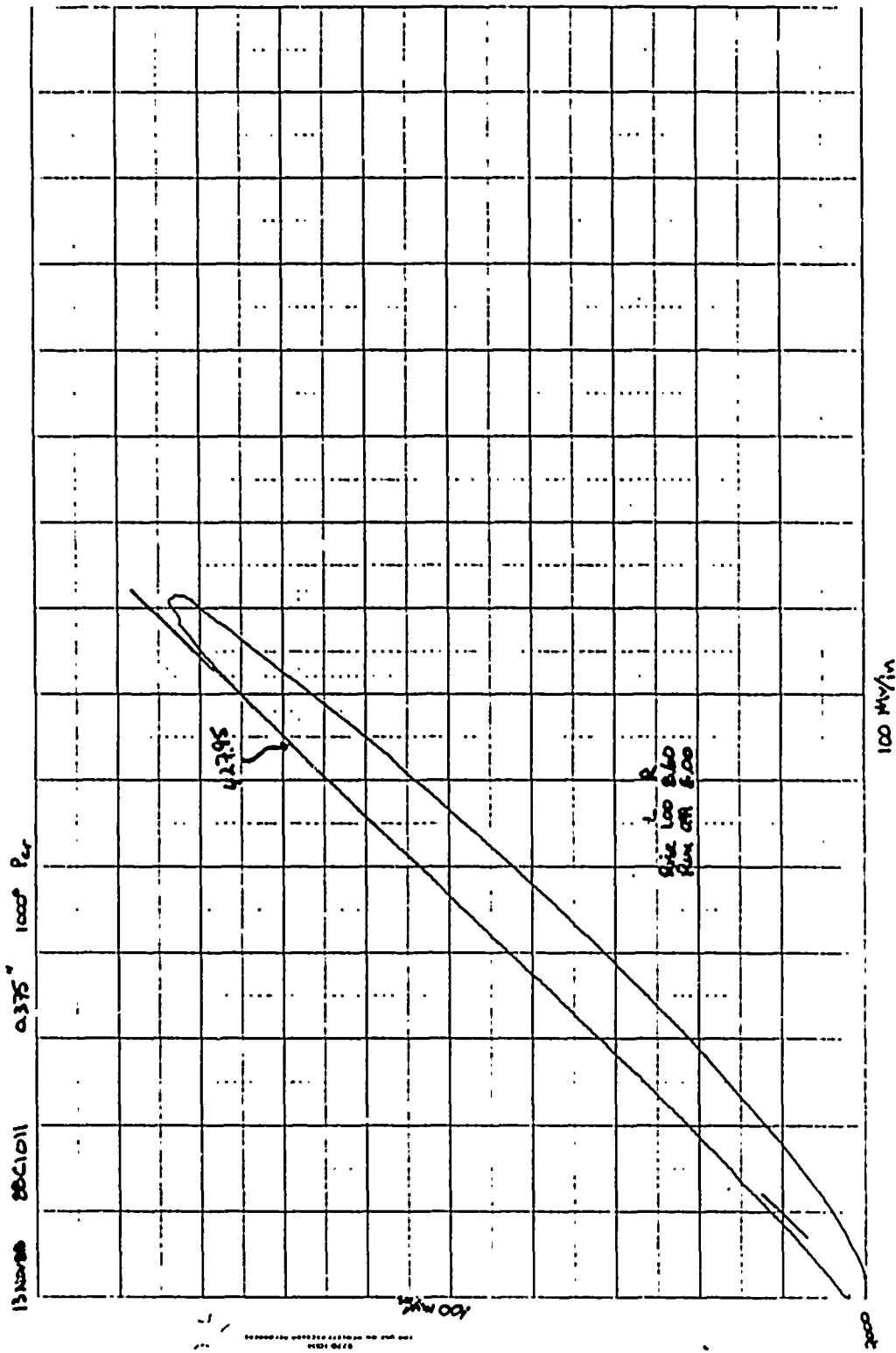Figure 60. Typical Critical Load Curve for a Specimen at 600° Fahrenheit

112

Figure 61. Typical Critical Load Curve for a Specimen at 1000° Fahrenheit

113

Appendix E: Mechanical Drawings

The following figures were used to manufacture parts for the load fixture and experimental setup. These drawings can be copied or modified to simplify and speed construction of new parts Mr. John Brohaus, of the AFIT Fabrication Shop, should be consulted before submitting any final drawings for construction. His years of experience and design and materials knowledge should used to minimize difficulties and maximize results.

Top Piece
FRONT VIEW

1.25in

3/8in

1.25in

2.5in

SIDE VIEW

1.5in

1/2in

Top View of Bottom

Side View of Bottom

centered

1.11"±.001

.305"

doesn't need to be 45 degrees or smooth

needs to be the same thickness and square with the other side

.315"+.005

.810"±.0~ Holes are 0.125" in diameter and are drilled thru

Measurements are from centerline to hole center

.260"+.005

1.01"+.005
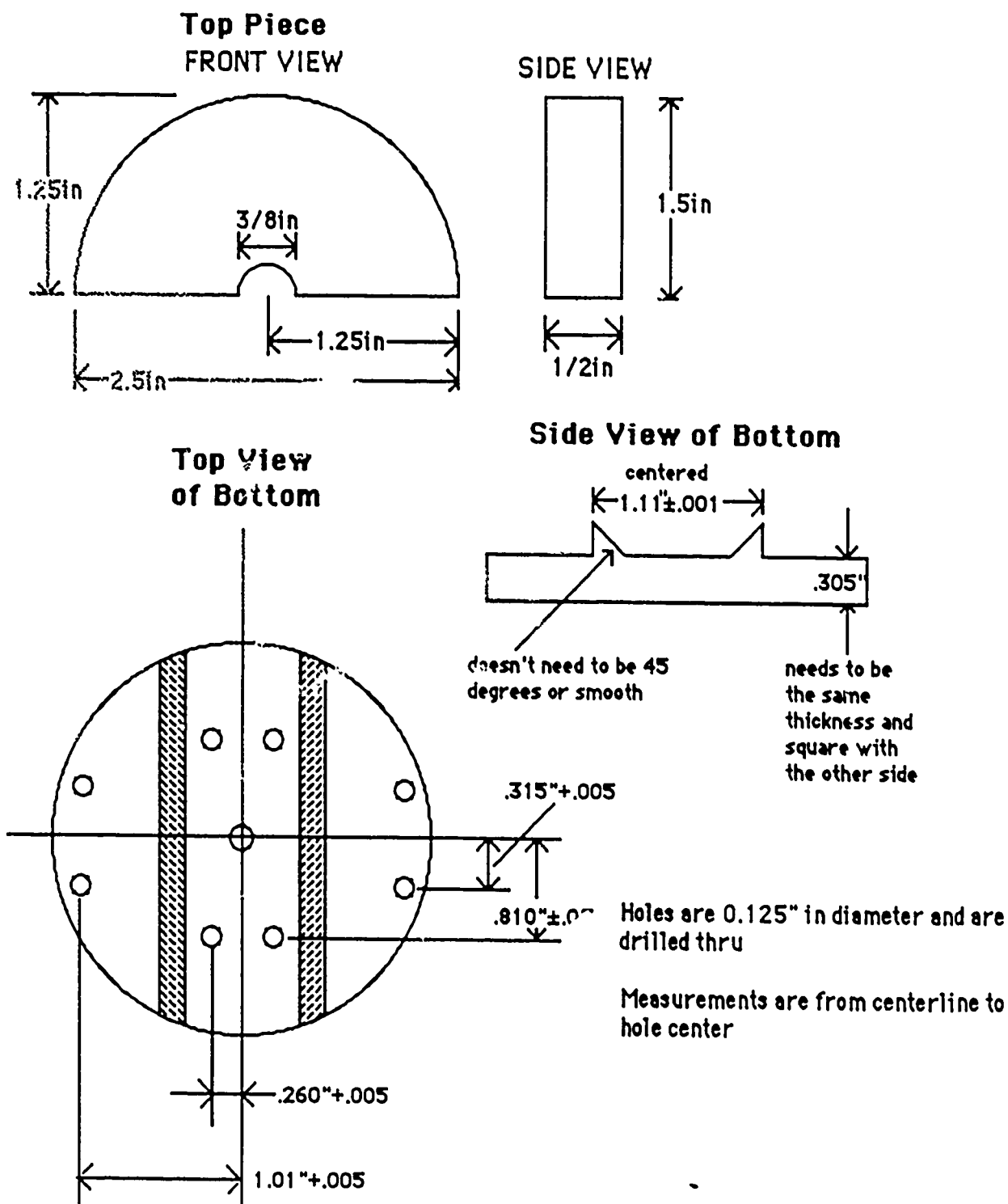
Figure 62. Three Point Bend Fixture

clearance for 1.0" diameter

3.5"

Interior diameter clearance of 2.5"+.1

1/8"x7/8" slot for thermocouple wires

Top

1/2"

1 1/2"

3/8"

Figure 63. Susceptor

3"

Part A

allen head bolt, 10-24

Front View

Assembled

Part C1

Part C2

7 5/8"

Cross-Sectional View

Part D1

Part D2

Part C1

Part C2

Part D1

On centerline

Part B

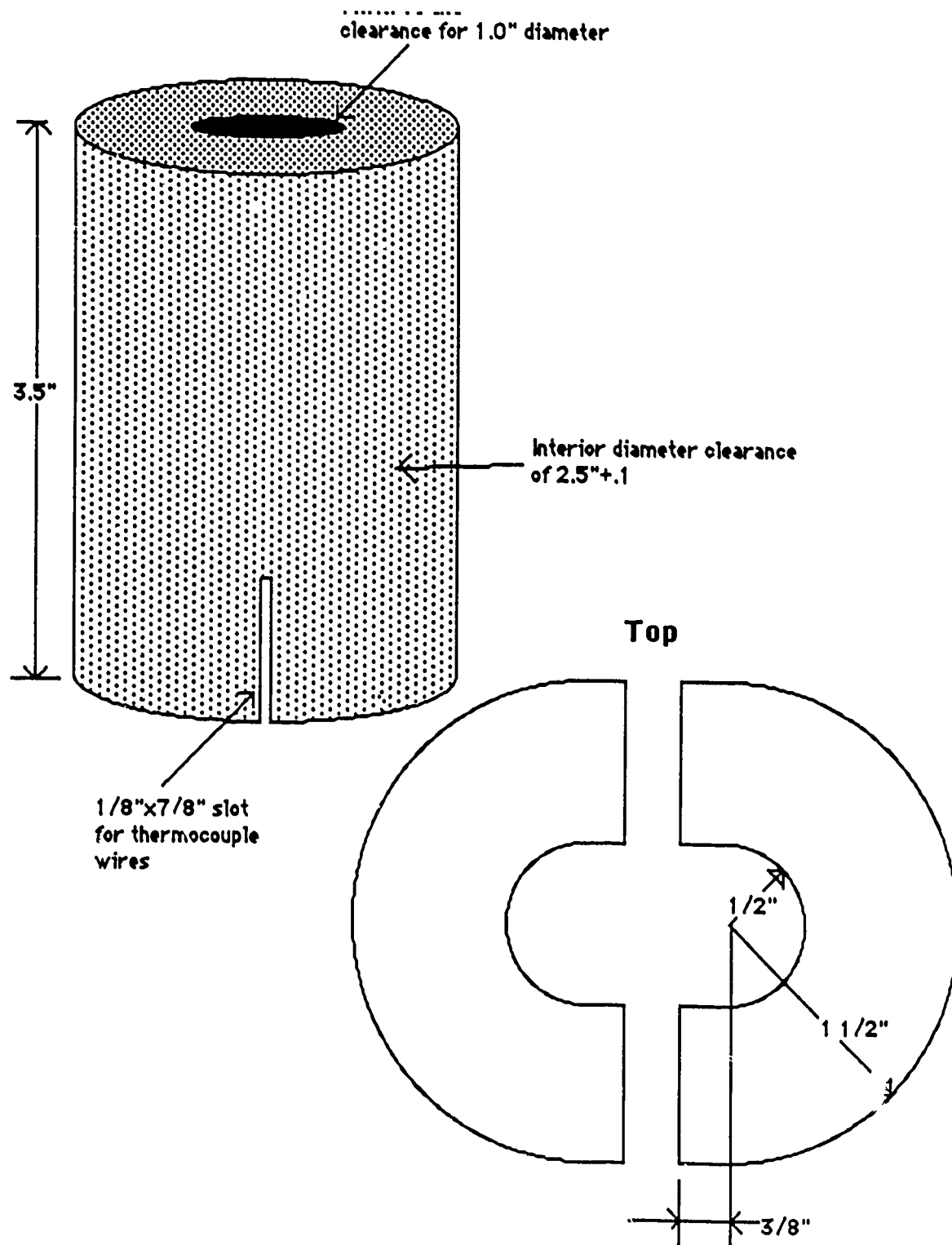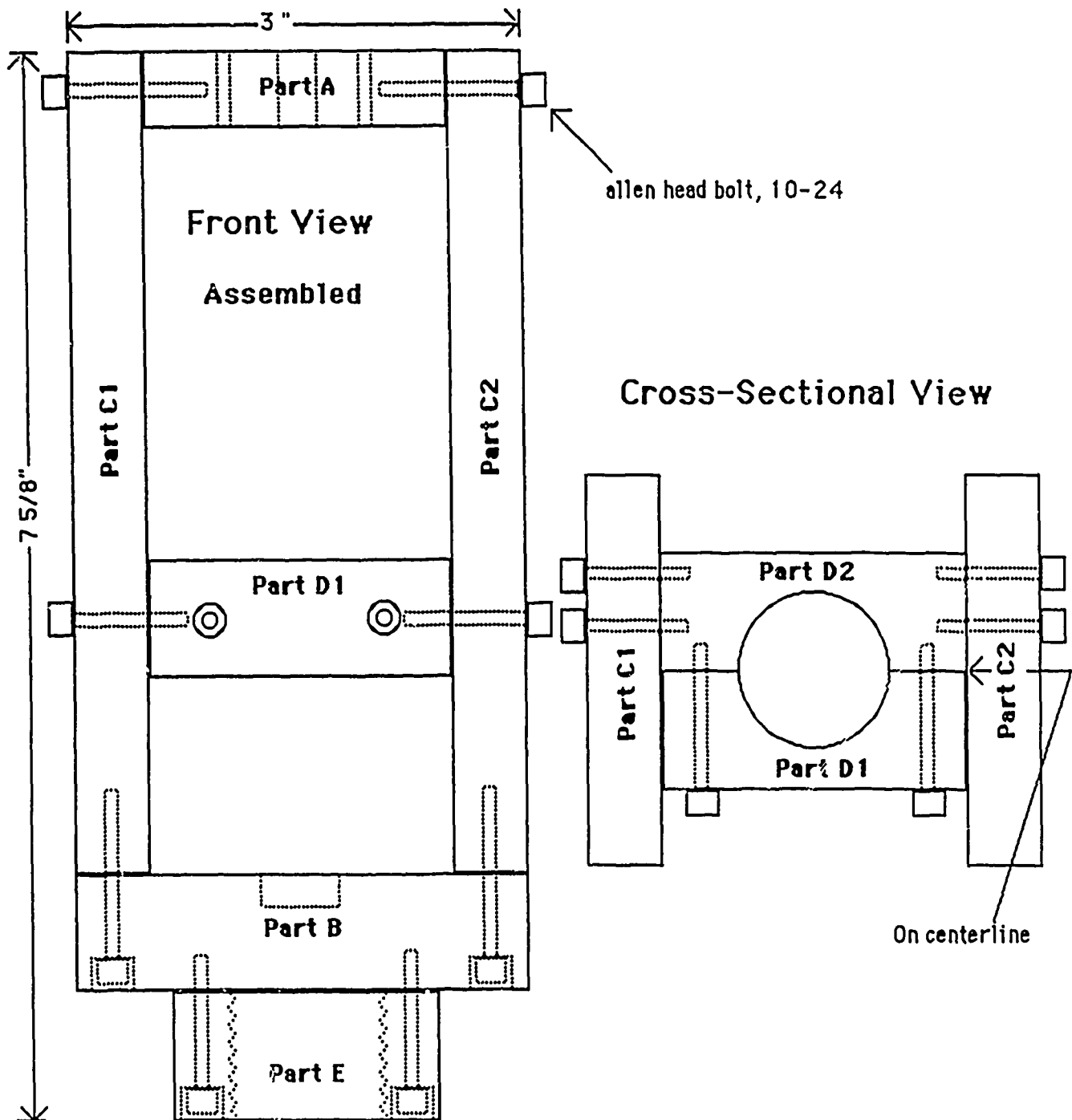Part E

olerances

The assembled load fixture (including the Heat Insulator) must be parallel between top and bottom and the centerline of the threaded portion of Part E must be on centerline both form the front and from the side, +/-.005 inch
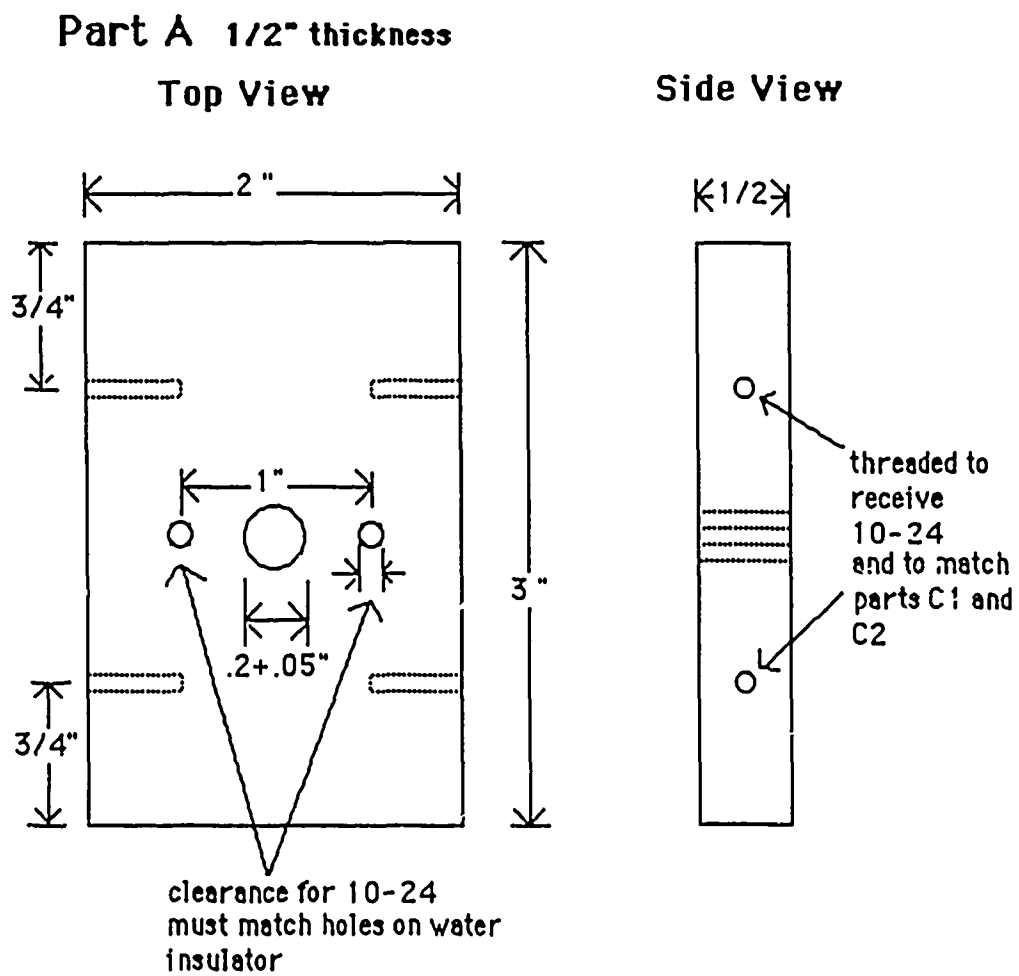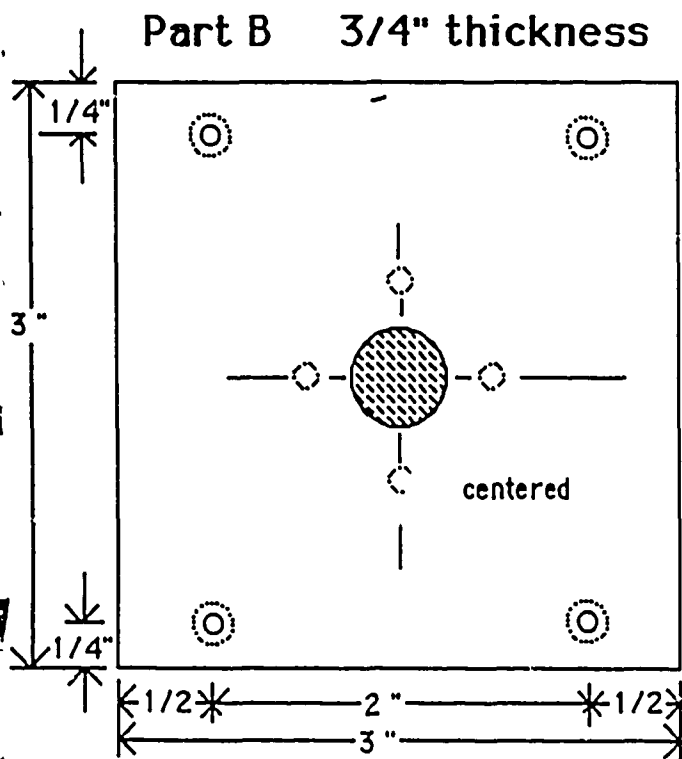
Figure 64.   LVDT Support Frame Assembled

117 •

Part A 1/2" thickness

Top View

Side View

Figure 65. Part A of LVDT Support Frame

Part B   3/4" thickness

Rotated Side View

3/4" diameter cup, 1/4" deep, centered

3/4"

threaded for 10-24 and
drilled to fit Part E

clearance for 10-24, drilled to match Parts
C1 & C2, and counterbored for allen head bolts

1/4"

3"

1/4"

centered

1/2   2"   1/2
3"
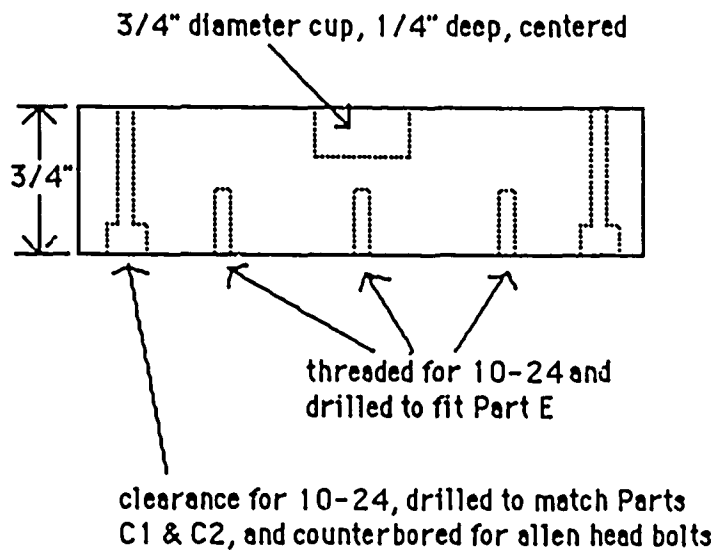
Figure 66. Part B of LVDT Support Frame

119

Parts C1 and C2 1/2" thickness

Side View

Front View

clearance for 10-24
and fit for part A
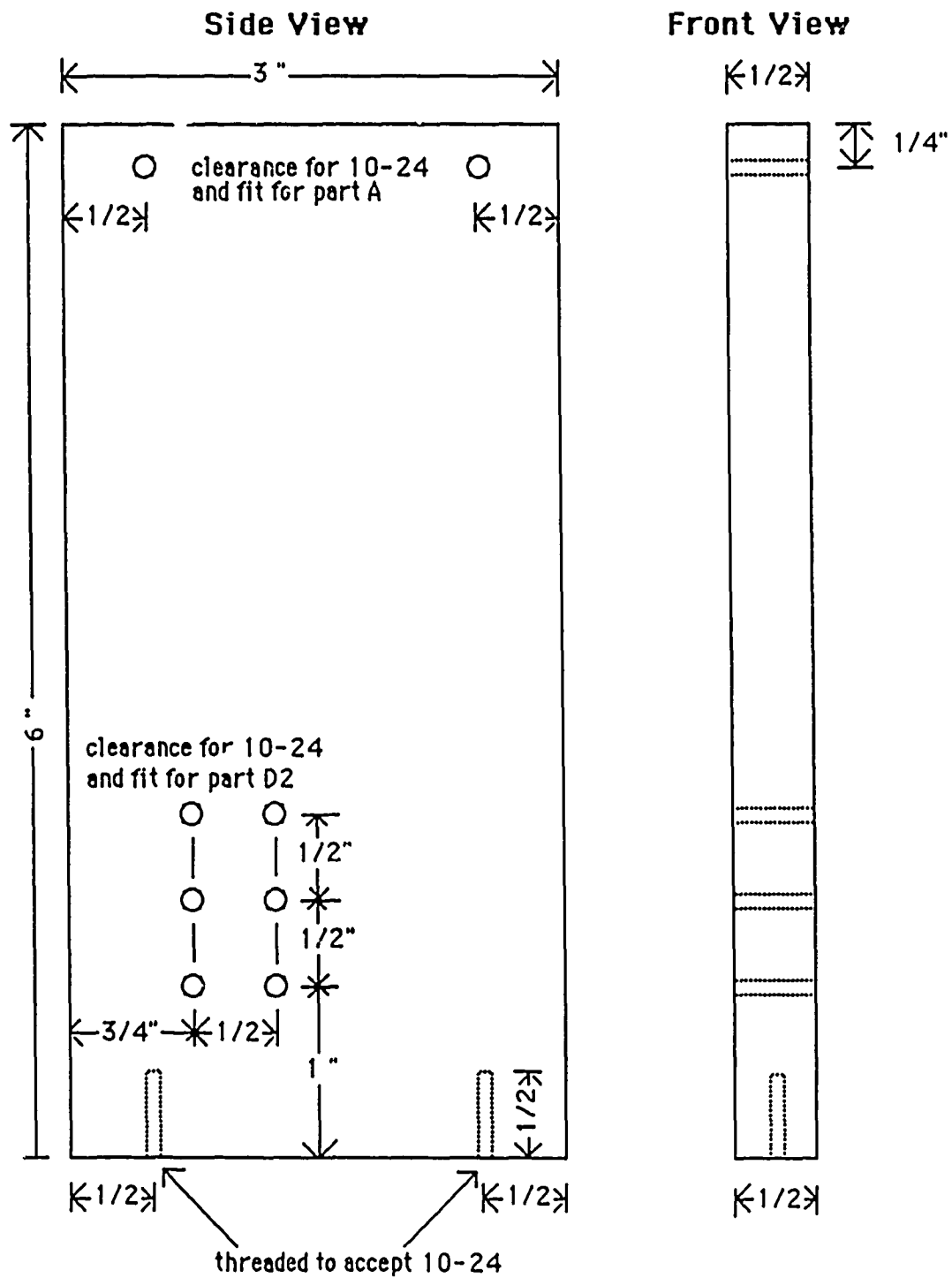
clearance for 10-24
and fit for part D2

threaded to accept 10-24

Figure 67.   Parts C1 and C2 of LVDT Support Frame

Part D1

Top View

7/16" radius
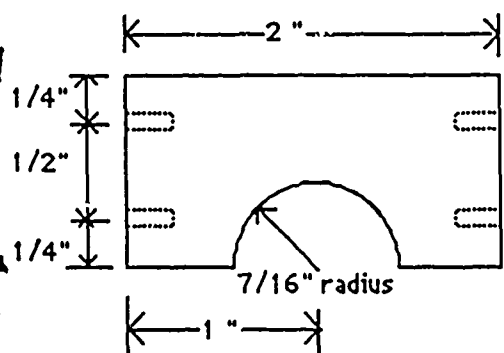
.05"

Back View

1/2"

1/4"

clearance for 10-24
drilled to match Part D2

Part D2
Top View

2 "

1/4"

1/2"

1/4"

7/16" radius

1 "

1/2"

1/4"
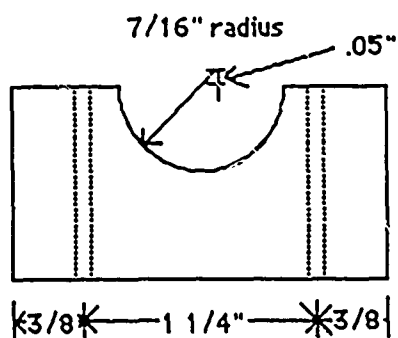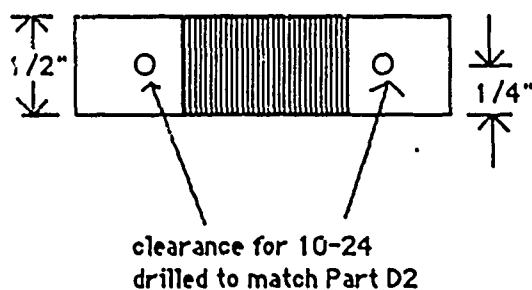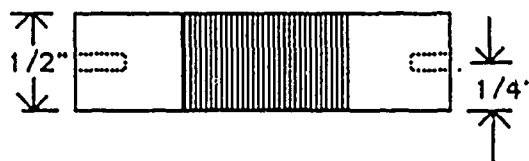
threaded to accept 10-24

Figure 68. Parts D1 and D2 of the LVDT Support Frame

121

Front View

1/8" thick, 1/4" wide ring welded

1/4"

1/4"

1/2"

3"

1/16" thick

3/16" thick

3/8" pipe

3/8"

Groove for nylon tie

Drilled and threaded for 10-24 bolt
Do not break through

3/8"

1"

Top View

1/4"

2 1/2"

3"
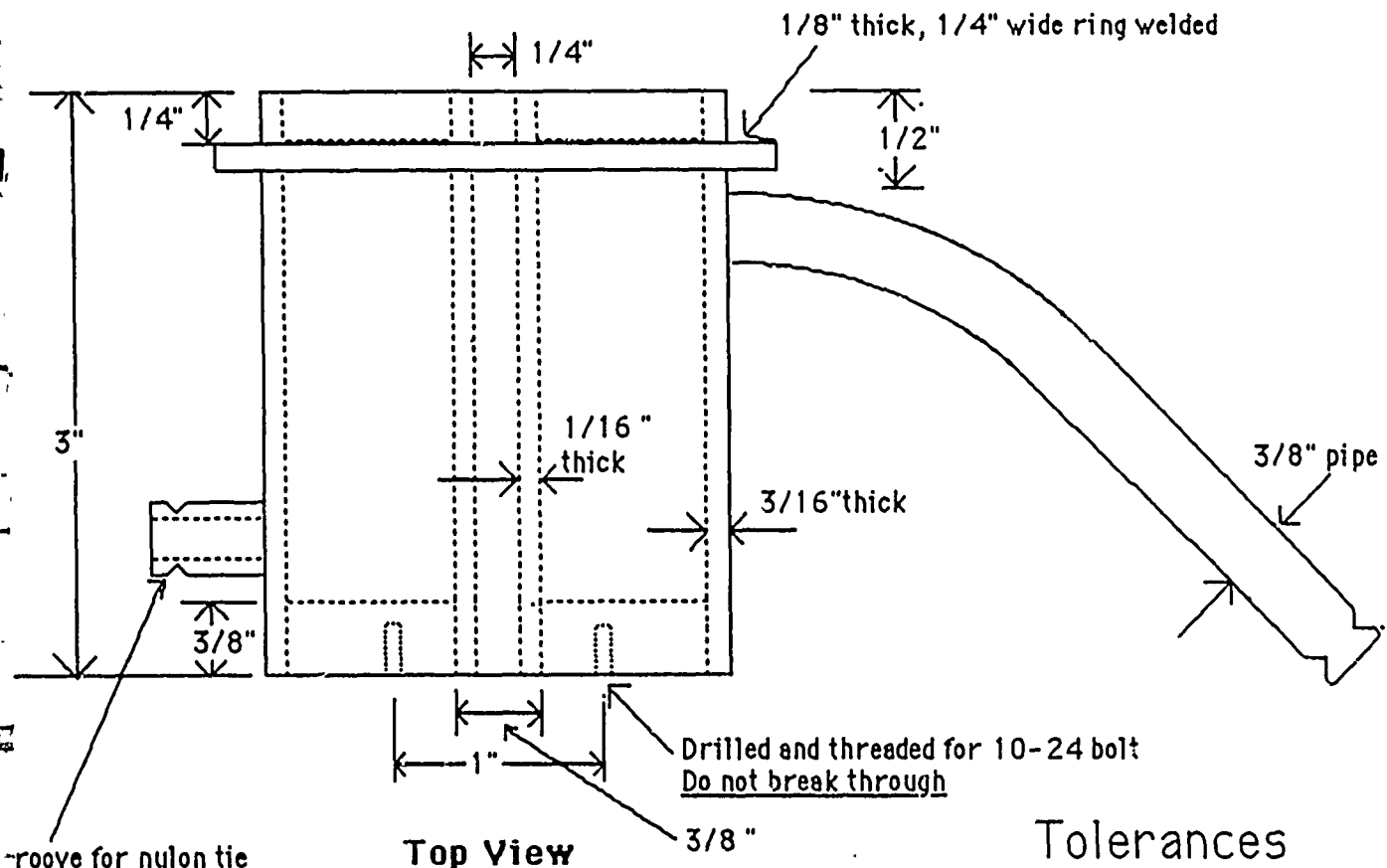
Tolerances

Center thru hole can not
be less than .2 inches
Top and bottom must be
parallel
Holes drilled for 10-24
bolt must match those
of Part A, Load fixture

Figure 69.   Heat Insulator

Side View

Thread number and taper
to match provided sample

Beveled tip

|←—1/2"—→|←—1/2"—→|← →|← 1 :"—→|← →|

|←—————2 1/2"—————→|

1/4"

1/8"

1/8"

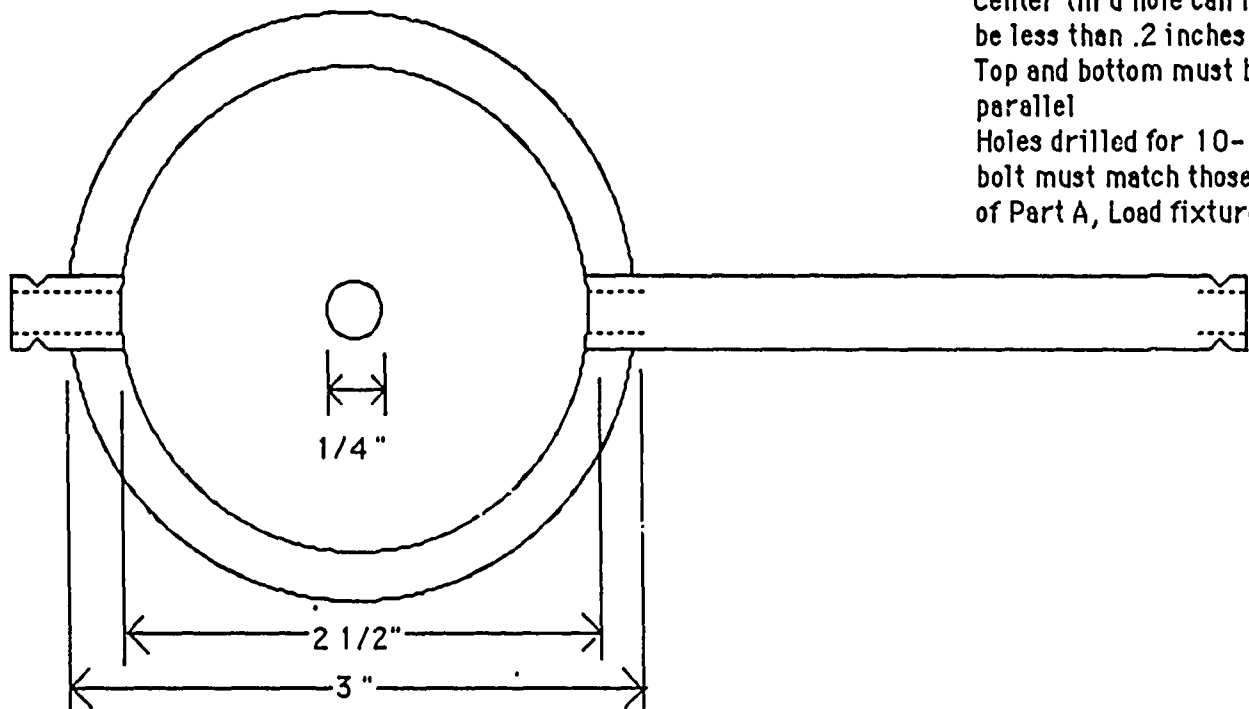## End View

11/16"

|←1/4"→|

|←3/8"→|
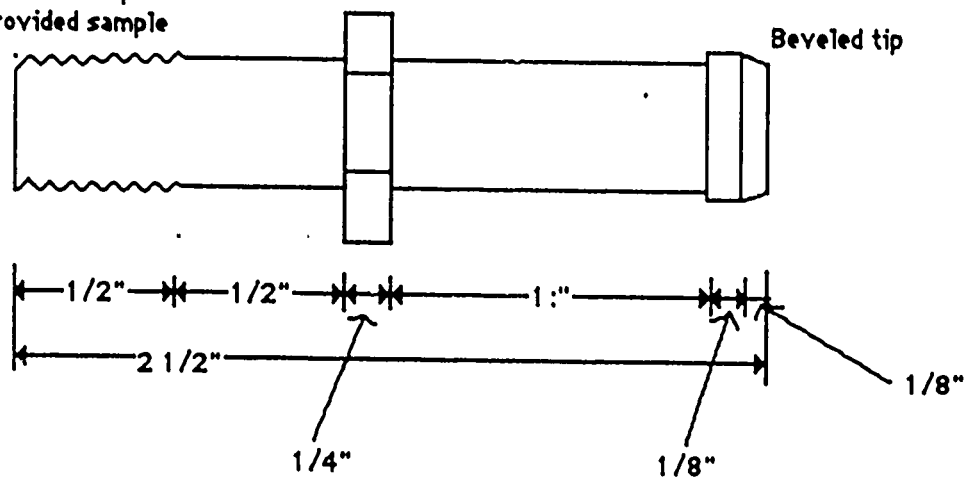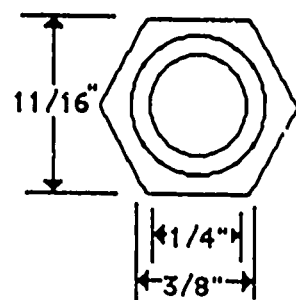
Figure 70. Water Nozzle for Heat Lamps

123

3/4" 1/2" 1/2" 3/4" 2 1/2" 3/4"

5"

1"

Top (xray) View

Top and bottom tubes have 1/2" OD and are flared

All side tubes have 3/8" OD and are flared

1/2" diameter hole with allen set screw for mounting on 1/2" diameter rod
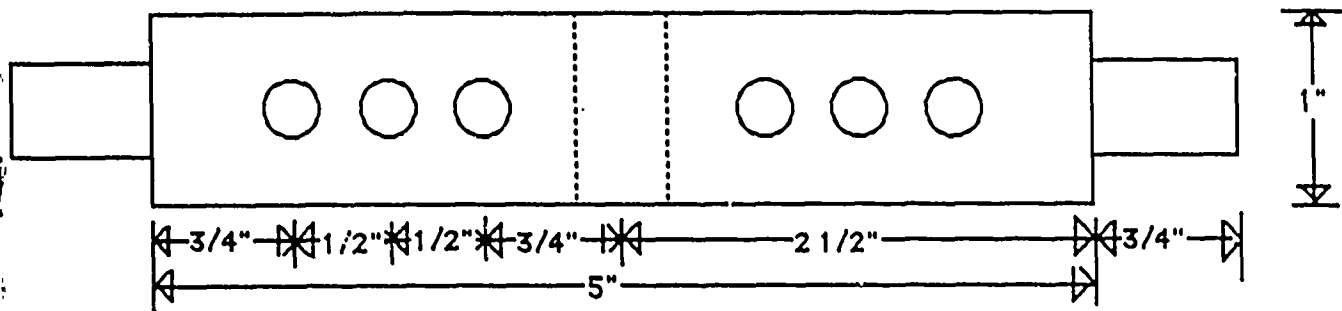
End View

Figure 71. Water Manifold (for Distributing Cooling Water)

Vita

Major John H. Mol,

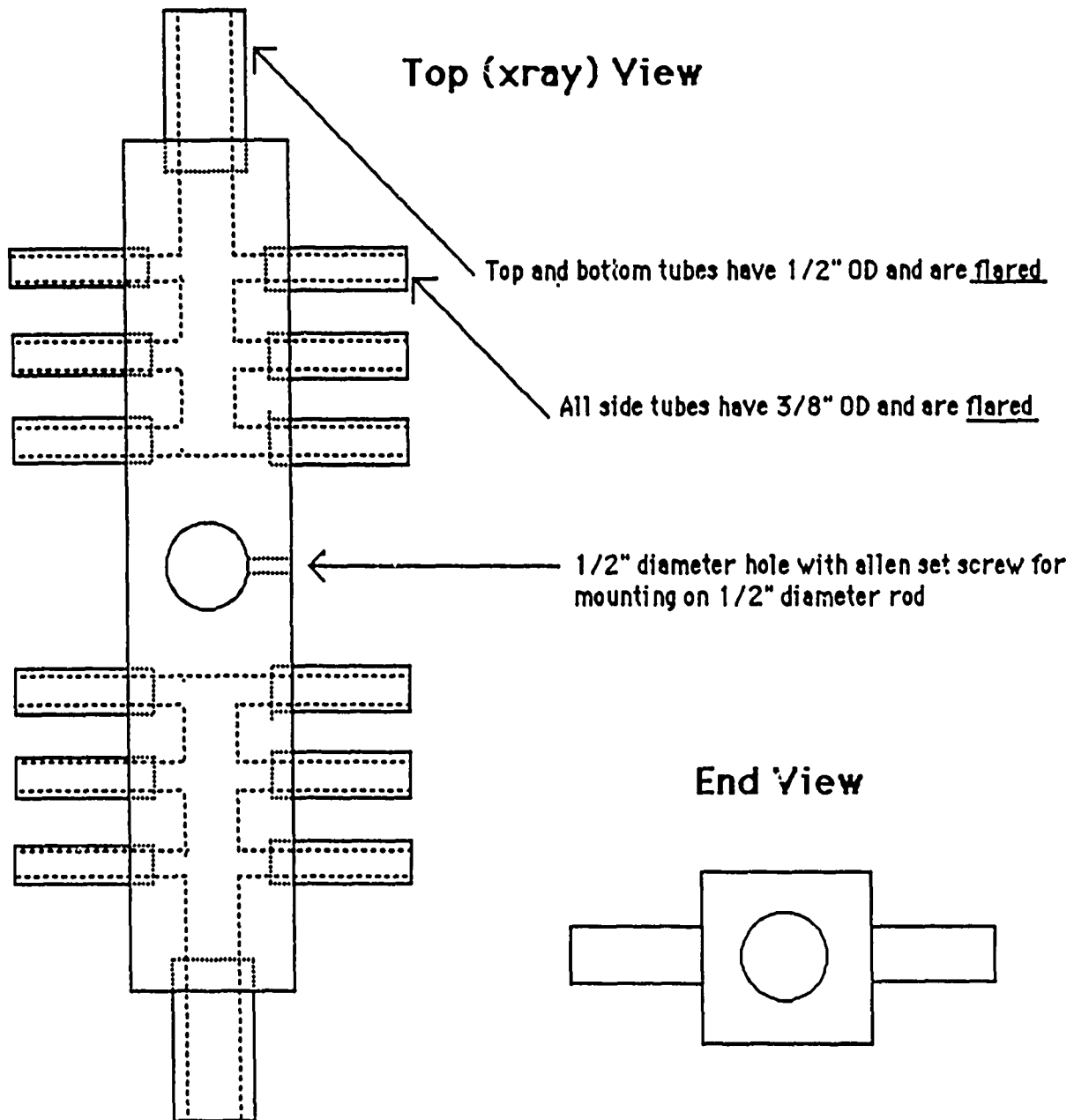He attended the University of Wisconsin, Eau Claire for a year, before accepting an appointment to the United States Air Force Academy. There he received a Bachelor of Science degree in Engineering Mechanics and a commission as a 2nd Lieutenant in the USAF. After a year of Undergraduate Pilot Training at Williams AFB, Arizona he flew C-130's as a copilot at Dyess AFB, Texas until January of 1982. He was then assigned to the 7th Special Operations Squadron, Rhein Main AB, West Germany where he commanded Crew 5 and became an instructor pilot. In June of 1985 he moved to the 8th Special Operations Squadron where he instructed in the Combat Talon School and later became a flight evaluator. Just prior to entering the School of Engineering, Air Force Institute of Technology in June of 1987, he commanded the crew representing 23rd Air Force at the Military Airlift Command's world wide competition, Airlift Rodeo.

REPORT DOCUMENTATION PAGE		Form Approved OMB No. 0704-0188

1a. REPORT SECURITY CLASSIFICATION UNCLASSIFIED	1b. RESTRICTIVE MARKINGS
2a. SECURITY CLASSIFICATION AUTHORITY	3. DISTRIBUTION/AVAILABILITY OF REPORT Approved for public release; distribution unlimited
2b. DECLASSIFICATION/DOWNGRADING SCHEDULE	

4. PERFORMING ORGANIZATION REPORT NUMBER(S) AFIT/GAE/AA/88D-26	5. MONITORING ORGANIZATION REPORT NUMBER(S)

6a. NAME OF PERFORMING ORGANIZATION School of Engineering	6b. OFFICE SYMBOL (If applicable) AFIT/ENY	7a. NAME OF MONITORING ORGANIZATION

6c. ADDRESS (City, State, and ZIP Code) Air Force Institue of Technology Wright-Patterson AFB OH 45433-5000	7b. ADDRESS (City, State, and ZIP Code)

8a. NAME OF FUNDING/SPONSORING ORGANIZATION AFWAL	8b. OFFICE SYMBOL (If applicable) AFWAL/MLLN	9. PROCUREMENT INSTRUMENT IDENTIFICATION NUMBER

8c. ADDRESS (City, State, and ZIP Code) Air Force Wright Aeronautical Lab. Wright-Patterson AFB OH 45433-5000	10. SOURCE OF FUNDING NUMBERS			
	PROGRAM ELEMENT NO.	PROJECT NO.	TASK NO.	WORK UNIT ACCESSION NO.

11. TITLE (Include Security Classification)
FRACTURE TOUGHNESS TESTING OF A CERAMIC MATRIX COMPOSITE AT ELEVATED TEMPERATURES

12. PERSONAL AUTHOR(S)
John H. Mol, B.S., Major, USAF

13a. TYPE OF REPORT MS Thesis	13b. TIME COVERED FROM _____ TO _____	14. DATE OF REPORT (Year, Month, Day) 1988 December	15. PAGE COUNT 140

16. SUPPLEMENTARY NOTATION

17.	COSATI CODES		18. SUBJECT TERMS (Continue on reverse if necessary and identify by block number)
FIELD	GROUP	SUB-GROUP	Fiber Reinforced Ceramic Composites
11	04		Mode II Fracture Toughness

19. ABSTRACT (Continue on reverse if necessary and identify by block number)

Thesis Advisor: Shankar Mall
Professor
Department of Aeronautics and Astronautics

Approved for public release: IAW AFR 190-1

JS Prennienela
12 Jan 1989

20. DISTRIBUTION/AVAILABILITY OF ABSTRACT ☒ UNCLASSIFIED/UNLIMITED ☐ SAME AS RPT. ☐ DTIC USERS	21. ABSTRACT SECURITY CLASSIFICATION UNCLASSIFIED
22a. NAME OF RESPONSIBLE INDIVIDUAL Shankar Mall, Professor	22b. TELEPHONE (Include Area Code) (513) 255-2998	22c. OFFICE SYMBOL AFIT/ENY

DD Form 1473, JUN 86   Previous editions are obsolete.   SECURITY CLASSIFICATION OF THIS PAGE

The need for a load fixture and technique for determining the fracture toughness in fiber reinforced ceramic composites at elevated temperatures was identified. A three point bend load fixture capable of withstanding temperatures up to 1000 degrees Fahrenheit was designed and constructed. A test procedure for finding compliance and critical load at room and elevated temperatures was developed. Specimens were tested at varying crack lengths at room temperature, 600, and 1000 degrees Fahrenheit.

Second order, third order and truncated third order curves were fitted to the compliance data to determine the best compliance-crack length relationship and compared with the results from a theoretical compliance-crack length relationship. Finally, the Mode II critical strain energy release rate, or fracture toughness, was calculated at each temperature. The fracture toughness for room temperature was slightly higher than the fracture toughness for 600° F. The fracture toughness for 1000° F was more than three times that for room temperature.

Postmortem examination was done on specimens for each temperature. Specimens tested at 600° F had smoother Mode II fracture surfaces than the room temperature specimens indicating a more brittle fracture and supporting the experimental results. The specimens tested at 1000° F had a rougher Mode II fracture surface with fiber pull-out and small matrix fragments attached to the fibers, indicating a more ductile failure and therefore increasing the fracture toughness. A color change from black to dark gray and the presence of crystals on the Mode I fracture surface of the 1000° F specimens indicated a chemical change in the specimens. The apparent chemical change and significantly higher fracture toughness in the 1000° F specimens indicates that much more study is required of this material at elevated temperatures.

Keywords: military theses; fracture mechanics; crack propagation; (??, ???)